1-5-2017

Development, Validation, and Clinical Application of a Numerical Model for Pulse Wave Velocity Propagation in a Cardiovascular System with Application to Noninvasive Blood Pressure Measurements

Jeffrey S. Lillie
jsliee@rit.edu

Development, Validation, and Clinical Application of a Numerical Model for Pulse Wave Velocity Propagation in a Cardiovascular System with Application to Noninvasive Blood Pressure Measurements

A DISSERTATION
SUBMITTED TO THE DEPARTMENT OF
MICROSYSTEMS ENGINEERING
AND THE COMMITTEE ON GRADUATE STUDIES
OF ROCHESTER INSTITUTE OF TECHNOLOGY
IN PARTIAL FULFILLMENT OF THE REQUIREMENTS
FOR THE DEGREE OF DOCTOR OF PHILOSOPHY

Jeffrey S. Lillie

January 5, 2017

Development, Validation, and Clinical Application of a Numerical Model for Pulse Wave Velocity Propagation in a Cardiovascular System with Application to Non-invasive Blood Pressure Measurements

by

Jeffrey S. Lillie

Committee Approval:

We, the undersigned committee members, certify that we have advised and/or supervised the candidate on the work described in this dissertation. We further certify that we have reviewed the dissertation manuscript and approve it in partial fulfillment of the requirements of the degree of Doctor of Philosophy in Microsystems Engineering.

_____

Dr. David A. Borkholder Date
Bausch and Lomb Professor, Microsystems Engineering

_____

Dr. Alexander S. Liberson Date
Associate Professor, Mechanical Engineering

_____

Dr. Daniel B. Phillips Date
Associate Professor, Effective Access Technology Research & Development

_____

Dr. Steven W. Day Date
Department Head-Biomedical Engineering, Associate Professor

_____

Dr. Gill R. Tsouri Date
Associate Professor, Electrical and Microelectronic Engineering

Certified by:

_____

Dr. Bruce W. Smith Date
Director, Microsystems Engineering

_____

Dr. Doreen D. Edwards Date
Dean, Kate Gleason College of Engineering

Abstract

Kate Gleason College of Engineering
Rochester Institute of Technology

Degree: Doctor of Philosophy **Program**: Microsystems Engineering
Author: Jeffrey S. Lillie
Advisor: David A. Borkholder
Co-Advisor: Alexander S. Liberson

Dissertation Title: Development, Validation, and Clinical Application of a Numerical Model for Pulse Wave Velocity Propagation in a Cardiovascular System with Application to Non-invasive Blood Pressure Measurements

High blood pressure blood pressure is an important risk factor for cardiovascular disease and affects almost one-third of the U.S. adult population. Historical cuff-less non-invasive techniques used to monitor blood pressure are not accurate and highlight the need for first principal models. The first model is a one-dimensional model for pulse wave velocity (PWV) propagation in compliant arteries that accounts for nonlinear fluids in a linear elastic thin walled vessel. The results indicate an inverse quadratic relationship ($R^2 = .99$) between ejection time and PWV, with ejection time dominating the PWV shifts (12%). The second model predicts the general relationship between PWV and blood pressure with a rigorous account of nonlinearities in the fluid dynamics, blood vessel elasticity, and finite dynamic deformation of a membrane type thin anisotropic wall. The nonlinear model achieves the best match with the experimental data. To retrieve individual vascular information of a patient, the inverse problem of hemodynamics is presented, calculating local orthotropic hyperelastic properties of the arterial wall. The final model examines the impact of the thick arterial wall with different material properties in the radial direction. For a hypertensive subject the thick wall model provides improved accuracy up to 8.4% in PWV prediction over its thin wall counterpart. This translates to nearly 20% improvement in blood pressure prediction based on a PWV measure. The models highlight flow velocity is additive to the classic pressure wave, suggesting flow velocity correction may be important for cuff-less, non-invasive blood pressure measures. Systolic flow correction of the measured PWV improves the R^2 correlation to systolic blood pressure from 0.81 to 0.92 for the mongrel dog study, and 0.34 to 0.88 for the human subjects study. The algorithms and insight resulting from this work can enable the development of an integrated microsystem for cuff-less, non-invasive blood pressure monitoring.

Contents

Figures

Tables

ACKNOWLEDGEMENTS

As iron sharpens iron, so one person sharpens another. - Proverbs 27:17

This work would not have been possible without funding provided by National Semiconductor and Google Incorporated. I would also like to acknowledge my employer Synaptics, which allowed me to have a flexible work schedule to accomplish this body of work.

Finishing my Ph.D. is the completion of a journey that started approximately seven years ago. In retrospect, it has been a very rewarding process that has enabled me to grow as an engineer and a person in ways I did not realize possible at the start. It has been a humbling process whereby people from all disciplines have tirelessly offered me their guidance, consultation, and friendship to aid in the creation of this work. If I neglect to mention your name, you know who you are and how you have helped me through this process; I thank you.

First, I would like to thank my advisor David A. Borkholder. I like the quote from Proverbs that states, “As iron sharpens iron, so one person sharpens another.” He has consistently been that person throughout this rewarding process. His attention to detail has made me a more disciplined engineer, and his sharp insight has improved my ability to think critically. This work would not have been possible without his guidance and support. Early on, I learned from Dave that initial results often fail, but with continuous iteration and refinement, success can be achieved. Beyond providing his guidance, he has also taken the time to be a friend. I have enjoyed our discussions and

the time on his deck at the lake. I hope we continue to collaborate on interesting projects in the future.

I was fortunate enough to also have a co-advisor, Alexander S. Liberson. I have learned a lot from his humble, patient approach to working on teams and solving difficult problems. He has the ability to look at a physical system and describe it with mathematics in an elegant form. I feel fortunate that he has shared some of his techniques and thought processes. His constant encouragement and friendship has made this an enjoyable journey. I appreciate all the discussions over tea or by phone on topics relating to our research or just life. I hope we continue to work together going forward.

We are fortunate at RIT to have both Rochester General Hospital and the University of Rochester to collaborate with and conduct clinical research. At RGH, I would like to thank Sreedevi Chennupati for her patient guidance during my first IRB study in the catheter lab. At the University of Rochester, I have been fortunate to collaborate with Ankur Chandra and Karl Schwartz. They both allowed me to work in their labs and answered a myriad of clinical questions. Ankur encouraged me to submit my first conference paper to Arteriosclerosis, Thrombosis and Vascular Biology. Karl has spent many hours explaining what is possible with ultrasound and has often spent his free time helping to extract important clinical information. Doran Mix spent countless hours working with me on a hemodynamic simulator, to help understand pressure wave velocity. He patiently helped me work through many issues to develop a repeatable and

controllable platform. His passion for research and thought experiments helped to inspire me. I hope we continue to collaborate as we both progress in our careers.

I'd like to thank Daniel B. Phillips, who has been supportive at different times throughout my research and writing of journal papers. His patient tips on writing style have been appreciated. I'd like to thank Steven W. Day, who helped answer my questions early on about fluid dynamics. He was also supportive throughout the writing of my first journal paper and one of our patents. Dan and Steven both had the insight to develop the initial version of the hemodynamic simulator that provided the early measures to develop our first model. I'd also like to thank Gill Tsouri, who is also on my committee and has provided feedback on my thesis even while traveling overseas.

I would like to thank Clyde Washburn, with whom I was fortunate enough to work at National Semiconductor. During a late-night discussion, we both thought continuous non-invasive blood pressure would be an interesting focus for a Ph.D. thesis. Clyde always taught me to tackle hard problems, because that is where the important findings occur. He has patiently helped guide parts of my research and taught me how he approaches difficult problems.

My wife Debbie has been there for me throughout this journey. She has patiently allowed me to miss many activities to allow me the freedom to pursue my goals. She has also been the person with whom I have shared all my successes and failures along the way. It's nice because it brings meaning to the work. Finally, her relaxed outlook on life reminds me what is ultimately important. The other important person in my immediate family is my daughter Brittany. She helped me understand different

physiology questions and challenged my work in positive ways. Most importantly, though, she took the time to take me surfing, biking, kite surfing, hiking, and running to relax and enjoy life.

Finally, I would like to thank my parents for their constant encouragement and support. My dad has always taught me the importance of hard work, honesty, integrity, and a humble approach. He also helped me understand the importance of a logical thought process as we worked together on many projects over the years. He was certainly the first engineer I knew, and he helped guide me down this career path. My mom has always liked the clinical side and enjoyed helping people. It is the blend of these lessons, encouragement, and skills that helped me to pursue this journey. My parents have both helped to allow me to finish my doctorate today.

Chapter 1: Introduction

A wave may seem like a simple thing, but in fact it is the most complicated form in nature. - Susan Casey

1.1. Abstract

This chapter motivates the importance of continuous noninvasive monitoring of blood pressure and arterial compliance. It reviews historical techniques used or attempted to date. The review highlights the need for first principle models to gain the insight required to improve continuous blood pressure monitoring. The goals of this work are to develop the models, understand the fundamental nature of pulse wave propagation in arteries, and enable the development of an integrated microsystem for continuous noninvasive blood pressure monitoring.

1.2. Nomenclature

c_{MK}	Moens-Korteweg speed of propagation (m/s)
E	Modulus of elasticity (Pa)
h_0, h	Thickness of the wall in zero-stress and deformable conditions, respectively (m)
H	Ratio of the wall deflection to r_0
L	1D final length (m)
r	Radius (m)
r_0	Radii in a zero-stress condition (m)
p	Pressure (Pa)
ρ	Density of incompressible fluid (kg/m^3)
PTT	Pulse transit time (s)
PWV	Pressure wave velocity (m/s)
ν	Poisson's coefficient

Subscripts

0	Initial

1.3. Introduction

Hypertension, or high blood pressure, is an important risk factor for cardiovascular disease and affects almost one-third of the U.S. adult population [1]. In 2009-2010, nearly 82% of adults with hypertension were aware of their status, and nearly 76% were taking medication [2]. Despite considerable improvement in increasing the awareness, treatment, and control of hypertension, undiagnosed and uncontrolled hypertension among minority groups remains a challenge [3,4,5]. During 2011-2012, among adults with hypertension, 82.7% were aware of their hypertension, 75.6% reported currently taking prescribed medication to lower their blood pressure, and 51.8% had their blood pressure controlled. The prevalence of hypertension increased with age, from 7.3% among those aged 18-39, to 32.4% among those 40-59, to 65% among those 60 and over [6]. The ability to create a continuous noninvasive microsystem to improve awareness, treatment, and control of hypertension is the long-term goal of this work.

Research conducted in 1955 by Thomas et al. [7], tried to use the arterial pulse wave to measure blood pressure. The pulse wave, generated by left ventricular ejection, propagates at a velocity that has been identified as an important marker of atherosclerosis and cardiovascular risk [8-16]. Cardiovascular disease affects 37% of the United States population and is the leading cause of death [8]. Increased pulse wave velocity (PWV) indicates an increased risk of stroke and coronary heart disease [9]. This velocity is considered a surrogate marker for arterial compliance [10], is highly reproducible [10], and is widely used to assess the elastic properties of the arterial tree [11]. Research shows that aortic compliance measurement using PWV could allow for

early identification of patients at risk for cardiovascular disease [8,10,14]. The ability to identify these patients would lead to better risk stratification and earlier, more cost-effective preventative health intervention [12].

Pulse transit time or PWV has also been measured in various research studies as a method to continuously monitor blood pressure [21-23]. Hypertension is defined as a chronic condition in which blood pressure is above 140 mmHg/90 mmHg (systolic/diastolic) [13]. Hypertension increases the risk for stroke, coronary heart disease, congestive heart failure, and renal disease [11,17]. Blood pressure has been shown to vary up to 20% in a 24-hour period due to circadian rhythms [14]. It is also variable in the clinic where “white coat” and “masked” hypertension can lead to misdiagnosis of high blood pressure [15]. This variation highlights the need for continuous blood pressure monitoring, which is not achieved with occasional measurement that occurs with “at-home cuff”-based oscillometric monitors. If a continuous noninvasive blood pressure monitor were available, it would be possible to track long-term trends and allow for lifestyle and/or medication adjustments.

1.4. History of PWV used for Continuous Noninvasive Blood Pressure

The Moens-Korteweg (c_{MK}) equation (1.1) was derived in 1878 from the wave equation for the velocity of propagation in meters per second of a pressure impulse within a thin-walled, perfectly elastic (v=0.5), cylindrical tube [27,28].

$$c = c_{MK} = \sqrt{\frac{\overline{E}h}{2r_0\rho}} \tag{1.1}$$

E is the elastic modulus for the wall, $\bar{E} = E/(1-\nu^2)$, ν is Poisson's coefficient, h is the constant thickness of the wall, and r_0 is the cross-sectional radius of the unstressed cylindrical vessel at zero pressure $(p = 0)$. Details of the derivation were reviewed by Hardung [16]. Young's modulus in this equation is the static modulus of elasticity at zero pressure. Experimental research has proven that the modulus of elasticity does, in fact, change dynamically; therefore, Hughes et al. empirically modified the c_{MK} equation to reflect this observation [21,28]. Hughes et al. [17] defined the dynamic Young's modulus as:

$$E = \overline{E}e^{\alpha p} \tag{1.2}$$

where: α is a vessel coefficient, and p is pressure (Pa). The vessel coefficient was selected to match a specific canine's excised aorta based on a single plot of static pressure versus Young's modulus. Chen et al. [18] extended this work to derive an equation for pressure, as shown in equation (1.3).

$$p = \frac{1}{\propto}\left[ln\left(\frac{\rho 2rL^2}{hE_0}\right) - 2lnTT\right] \quad (1.3)$$

where: ρ is the density of blood, r is the radius of the artery at a respective pressure, L is the length between the two pulse measurement points, and TT is the true transit time for the pulse to propagate between the two measurement points. While this provides more accurate results than using a static Young's modulus, it is not derived from first principles, and it misses important variables that influence blood pressure. In addition, the parameters required (E_0, h, r) are difficult to measure.

Several studies have shown the influence of blood pressure [8,19,20,30] and left ventricular ejection time (LVET) [11, 19] on PWV. Nurnberger et al. [11] used myocardial stimulation to modulate ejection time and measure the associated change in PWV that was found to correlate only with LVET ($R^2 = 0.52$, $p = 0.0325$). In their study, a change in ejection time of ~40 ms caused a change of PWV of ~1 m/s. Salvi et al. [19] performed a large population study to explore the link between PWV and LVET. An inverse association was found between PWV and LVET at all ages ($<R^2 = 0.43$; $p < 0.001$). In both studies, it was not possible *in vivo* to control LVET, systemic vascular resistance (SVR), and ejection volume, which likely decreased their observed correlation. The clinical relationship between PWV and arterial stiffness is often based on classic linear models [32,33] or the combination of the linear models and measured results with an incorporated correction factor [21,28,35]. Whereas linear models predict PWV as a function only of the geometric and physical properties of the fluid and the wall, there is strong evidence that PWV is also correlated with pressure [19,20,30] and ejection time [14,19].

1.5. Objectives and Goals of the Work

While both pressure and LVET are clinically shown to affect PWV, a predictive model that provides mechanistic insight and incorporates peak pressure, ejection time, ejection volume, and modulus of elasticity has yet to be developed. The aim of this work is to develop and validate a model to provide this missing insight. The approach used is based on a one-dimensional nonlinear model for pressure wave propagation in a compliant tube with a linear elastic wall filled with an incompressible fluid. The model incorporates the classical solitary wave-based solution, connecting speed of propagation to the ejection time, ejection volume, and peak pressure, accounting for nonlinear wave propagation effects, elastic deformable vessels, and the inertia of the distensible vessel walls. The model is validated using a physiologically based electromechanical hemodynamic simulator.

A number of researchers have used pulse arrival time (rPTT) or true transit time (TT) to try to estimate systolic blood pressure (SBP) and diastolic blood pressure (DBP). The results have not met the accepted Association for the Advancement of Medical Instrumentation (AAMI) standards for accuracy using the standard cuff-based approach. These results have even caused some researchers to conclude that pulse transit time measured from the ECG is an unreliable marker of beat-to-beat blood pressure [20]. Existing systems fail to measure blood pressure accurately across population and activity level. The second aim of this work is to develop a model that predicts the general relationship between PWV and blood pressure (BP) with a rigorous account of nonlinearities in the fluid dynamics model, blood vessel elasticity, and finite dynamic deformation of a membrane-type thin anisotropic wall. Using this model, we aim to

develop a per patient calibration (4-point) using parametric optimization and Nelder-Mead optimization. This model is validated using existing clinical studies. Finally, the model is used to predict SBP/DBP after an initial per patient calibration.

This work focused on understanding the fundamental nature of pulse wave propagation in arteries that can be integrated into wearable microsystems technologies. PWV and ECG are two of the physiological signals required. While today's wearables have integrated photoplethysmography as a way to measure heart rate, they have yet to extend and combine the necessary measures to extract PWV. Companies like AlivCor have created smartphone sensors that enable ECG measurement; however, the sensors are not yet in a wearable form. In addition to these measures, a measure of pre-ejection period and flow are required. Multiple approaches show promise, such as the ballistocardiogram (BCG), impedance plethysmography, inductive sensing, RF techniques such as dual-antenna nanosecond pulse near-field sensing (NPNS), and micro-ultrasound sensors [35]. As of this writing, none of these techniques has yielded a wearable technology and been validated across various physiological states against a gold standard (Doppler ultrasound). The combination of ECG, PWV, and flow measures is required in a wearable microsystem to allow for cuff-less, continuous non-invasive blood pressure monitoring.

1.6. Thesis Organization

This thesis is organized into the following chapters:

Chapter 2 reviews the background of fluid dynamics as it relates to pulsatile pressure and flow in a cylindrical tube or artery. One-dimensional (1D) and two-dimensional (2D) stress-strain relationships are considered. The basic stress-force relationships are covered without accounting for deformation. Building upon this information, the 2D linear vessel is reviewed. Special attention is given to define both the axial and longitudinal stress. The focus is then shifted to consider the effects of nonlinearity. Considering the effect of deformation, Cauchy-Euler, Piola-Lagrange, and Kirchoff stresses are defined and related.

Chapter 3 begins with a background of fluid dynamics as it relates to pulsatile pressure and flow in a cylindrical tube or artery. Using that foundation, the effect of nonlinear fluids on a linear elastic thin-walled vessel is derived. This work creates a one-dimensional model for blood pressure wave propagation in compliant arteries that accounts for nonlinear fluids in a linear elastic thin-walled vessel. This model is then validated using an *in-vitro* simulator. The *in-vitro* physiological electromechanical cardiovascular simulator used for the validation is described in detail. There is a complete review of the theoretical and measured results. The chapter concludes with a description of the mechanisms causing the association between PWV and LVET. Specifically, it describes how the model incorporates the classical solitary wave-based solution, connecting speed of propagation to the ejection time, ejection volume, and

peak pressure, accounting for nonlinear wave propagation effects, elastic deformable vessels, and the inertia of the distensible vessel walls.

Chapter 4 presents a novel approach to PWV prediction in compliant arteries. In this chapter, the nonlinear contributions of finite deformation, hyperelasticity, fluid convective phenomena, and longitudinal pre-stress are analyzed and used to extend the 1D model presented in Chapter 3. The model is then validated across available *in-vivo* experimental data. Specifically, it is compared to *Histand-Anliker and Muehlsteff-Schett* using a 4-point calibration technique. The impact of different nonlinearities on a quality of the best fit is analyzed. In addition, the topology of the Least Square as a function of material properties ($c, a_{11}, a_{12}, a_{22}$) is presented. We specifically compare our model results for *Histand-Anliker* to Zhou-Fung's five mongrel dogs. The chapter concludes with an explanation of steps necessary for a per person calibration to generate a predictive PWV versus pressure curve that can be used in non-invasive BP measurement.

Chapter 5 extends the model further to consider the effect of a thick multilayered arterial vessel. The goal of this chapter is to re-examine the accuracy of PWV prediction based on traditional homogeneous structural models for thin-walled arterial segments. In reality, arterial walls are heterogeneous composite structures formed of three clearly defined layers. An essential ingredient is the notable dependence of results on nonlinear aspects of the model: convective fluid phenomena, hyperelastic constitutive relation of each layer, and finite deformation. The contribution of each of the nonlinearities is analyzed.

Chapter 6 uses the model developed in Chapter 5, in which a physics-based mathematical model of PWV that explains flow velocity is additive to the classic pressure wave as estimated by arterial material properties, suggesting that flow velocity correction may be important for cuff-less non-invasive blood pressure measurements. The developed model allows us to understand the impact of systolic flow correction of measured PWV on systolic blood pressure prediction accuracy using data from two published *in vivo* studies. Both studies examined the relationship between PWV and blood pressure under pharmacological manipulation, one in mongrel dogs and the other in healthy adult males. The results support the hypothesis that systolic flow correction is an essential element of non-invasive, cuff-less blood pressure estimation based on PWV measures.

Chapter 7 summarizes the conclusions and describes opportunities for future work.

1.7. References

[1] ONG KL, AW Tso, KS Lam, BM Cheung , "Gender difference in blood pressure control and cardiovascular risk factors in Americans with diagnosed hypertension," *Hypertension*, vol. 51, no. 4, pp. 1142-8, 2008.

[2] Yoon SS, V. Burt, T. Louis, MD. Carroll , "Hypertension among adults in the United States, 2009–2010," *NCHS data brief*, vol. no 107, no. Hyattsville, MD: National Center for Health Statistics.

[3] Keenan NL, KA. Rosendorf , "Prevalence of hypertension and controlled hypertension United States, 2005–2008," *MMWR*, vol. 60(suppl), pp. 94-7, 2011.

[4] CDC, "Racial/ethnic disparities in the awareness, treatment, and control of hypertension United States, 2003–2010," *MMWR*, vol. 62, no. 18, pp. 351-5, 2013.

[5] Farley TA, MA. Dalal, F. Mostashari, TR. Frieden , "Deaths preventable in the U.S. by improvements in use of clinical preventive services," *Am J Prev Med*, vol. 38, no. 6, pp. 600-9, 2010.

[6] Nwankwo T, SS. Yoon,V. Burt, Q. Gu , "Hypertension among adults in the United States: National Health and Nutrition Examination Survey, 2011–2012," *NCHS data brief, no 133*, Hyattsville, MD: National Center for Health Statistics 2013.

[7] J. G. Thomas, "A method for continuously indicating blood pressure.," *J Physiol*, vol. 129, pp. 75-76, 1955.

[8] Heidenreich P.A. et al. , "Forecasting the future of cardiovascular disease in the United States: a policy statement from the american heart association.," *Circulation*, vol. 123, pp. 933-944, 2011.

[9] Lebrun C.E., Y.T. Van Der Schouw,A.A. Bak, et. al. , "Arterial Stiffness in postmenopausal women, determinants of pulse wave velocity," *J. Hypertens.*, vol. 20, no. 11, pp. 2165-2172, 2002.

[10] Sutton-Terrel K., R. H. Mackey, R. Holukbov, et. al. , "Measurement variation of aortic pulse wave velocity in the elderly," *Am. J. Hypertens.*, vol. 14, pp. 463-8, 2001.

[11] Nurnberger J.,A. Saez,S. Dammer,A. Mitchell,R. Wenzel,T. Philipp, R. Schafers , "Left Ventricular ejection time: a potential determinant of pulse wave velocity in young, healthy males," *J. Hypertens.*, vol. 21, no. 11, pp. 2125-2132, 2003.

[12] Blacher J.,R. Asmar,S. Djane,G.M. London,M.E. Safar , "Aortic pulse wave velocity as a marker of cardiovascular risk in hypertensive patients," *Hypertension*, vol. 33, pp. 1111-17, 1999.

[13] Lloyd-Jones D.M. et al. , "Heart disease and stroke statisticsa 2010 update," *Circulation*, vol. 121, no. 7, pp. 46-215, 2010.

[14] Verdecchia P. et al. , "Circadian blood pressure change and left ventricular hypertrophy in essential hypertension," *Circulation*, vol. 81, no. 2, pp. 528-536, 1990.

[15] Ohkubo T. et al. , "Prognosis of masked hypertension and white-coat hypertension detected by 24-h ambulatory blood pressure monitoring, 10-year follow up from the Ohasama study ," *JACC*, vol. 46, no. 3, pp. 508-515, 2005.

[16] V. Hardung, "Propagation of pulse waves in Visco-elastic tubings," *Handbook of Physiology*, vol. 2, no. 1, pp. 107-135, 1962.

[17] Hughes D., F. Babbs, C. Geddes , "Measurement of Young's modulus of elasticity of the canine aorta with ultrasound," *Ultrasound Imaging 1*, vol. 4, pp. 356-367, 1979.

[18] Kobayashi T, Ichikawa S, Takeuchi Y, and Togawa T. Chen W, "Continuous estimation of systolic blood pressure using the pulse arrival time and intermittent calibration," *Med Biol Eng Comput*, vol. 38, pp. 569-574, 2000.

[19] Salvi P., C. Palombo, G. Salvl, C. Labat, G. Parati, A. Benetos , "Left ventricular ejection time, not heart rate, is an independent correlate of aortic pulse wave velocity," *J Appl Physiol*, Sept 2013.

[20] Payne R. A., Symeonides C., Webb D., Maxwell S. , "Pulse transit time measured from the ECG: an unreliable marker of beat-to-beat blood pressure," *J. Appl. Physiol.*, vol. 100, pp. 136-141, 2006.

[21] Kim EJ., CG Park, JD Park, SY Suh, CU Choi, JW Kim, SH Kim, HE Lim, SW Rha, HS Seo, DJ Oh , "Relationship between blood pressure parameters and pulse wave velocity in normotensive and hypertensive subjects: invasive study," *J Hum Hypertens*, vol. 21, pp. 141-148, 2007.

[22] Chen Y., W. Changyun, T. Guocai, B. Min, G. Li , "Continuous and Noninvasive Blood Pressure Measurement: A Novel Modeling Methodology of the Relationship Between Blood Pressure and Pulse Wave Velocity," *Ann. Biomed. Eng*, vol. 37, no. 11, pp. 2222-2233, Nov 2009.

[23] Blacher J., A. P. Guerin, B. Pannier, et al. , "Impact of aortic stiffness on survival in end stage renal disease," *Circulation*, vol. 99, no. 18, pp. 2434-2439, 1999.

[24] Asamar R. , "Arterial stiffness and pulse wave velocity, clinical applications," *Elsevier*, 1999.

[25] Meaume S., A. Benetos, O. F. Henry, et. al. , "Aortic pulse wave velocity predicts cardiovascular mortality in subjects >70 years of age.," *Arteriosclerosis, Thrombosis, and Vascualr Biology*, vol. 21, pp. 2046-50, 2001.

[26] London G.M.,J.N. Cohn, , "Prognostic application of arterial stiffness, task forces," *Am. J. Hypertens.*, vol. 15, no. 8, pp. 754-8, 2002.

[27] Safar M.E., O. Henry,S. Meaume, , "Aortic Pulse Wave Velocity, an independent marker of cardiovascular risk," *American journal of geriatric cardiology*, vol. 11, pp. 295-98, 2002.

[28] Ohnishi H.,S. Saitoh,S. Takagi, et. al. , "Pulse wave velocity as an indicator of atherosclerosis in impaired fasting glucose, the tanno and sobetsu study," *Diabetes Care*, vol. 26, no. 2, pp. 437-40, 2003.

[29] O'Rourke M., *McDonald's Blood Flow in Arteries: Theoretical, Experimental and Clinical Principles*, 5th ed. USA: Oxford University Press, 2005.

[30] Vlachopoulos C.,K. Aznouridis,C. Stefenadis, , "Prediction of cardiovascular events and all-cause mortality with arterial stiffness," *JACC*, vol. 55, no. 13, pp. 1318-27, March 2010.

[31] J. D. Kortweg, "Uber die Fortpflanzungsgeschwindigkeit des Schalles in elastischen Rorren," *Ann. Phys. Und Chem., Neue Folge*, vol. 5, p. 225, 1878.

[32] O'Rourke M., Gallagher D., "(1996). Pulse wave analysis," *J. Hypertens*, vol. 14, pp. 147-157, 1996.

[33] Bramwell JC, Hill AV., "Velocity of transmission of the pulse wave and elasticity of arteries," *Lancet*, vol. 1, pp. 891-2, 1922.

[34] Poon C. C. Y., Y. T. Zhang , "Cuff-less and Noninvasive Measurements of Arterial Blood Pressure by Pulse Transit Time.," in *Proceedings of the 2005 IEEE Engineering in Medicine and Biology 27th Annual Conference*, Shanghai, 2005.

[35] Oralkan O., B.T Khuri-Yakub, "Capacitive micromachined ultrasonic transducers: next-generation arrays for accoustic imaging," IEEE T. of Ultrasonics, V 49, N. 11, 2002

Chapter 2: Elements of Linear and Nonlinear Theory of Elasticity

You must do things you think you cannot do. - Eleanor Roosevelt

2.1. Abstract

This chapter reviews fluid dynamics as it relates to pulsatile pressure and flow in a cylindrical tube or artery. One-dimensional and two-dimensional stress-strain relationships are considered. The basic stress-force relationships are covered without accounting for deformation. Based on this information, the 2D linear vessel wall is reviewed. Special attention is given to define both the axial and longitudinal stress. The focus is then shifted to consider the effects of nonlinearity. Considering the effect of deformation, Cauchy-Euler, Piola-Lagrange, and Kirchoff stresses are defined and related. The background information is then expanded for the three different models described in Chapters 3-5.

2.2. Nomenclature

E	Modulus of elasticity (Pa)
F	Force (N)
G	Green strain (Pa)
h_0, h	Thickness of the wall in zero-stress and deformable conditions, respectively (m)
L	1D length (m)
ΔL	Elongation (m)
p	Transmural pressure (Pa)
r	Radius (m)
S	Kirchoff stress (Pa)
T	Piola-Lagrange stress (Pa)
u	Axial flow velocity (m/s)
W	Potential energy (J)
ε	Strain
ρ	Density of an incompressible fluid (kg/m^3)
η	Circumferential wall strain
σ	Cauchy stress (Pa)
λ	Stretch ratio
ν	Poisson's coefficient

Subscripts

10,20,30	Initial coordinate independent measure; for Cartesian, it would be a measure in the x,y,z directions, respectively
1,2,3	Final coordinate independent measure; for Cartesian, it would be a measure in the x,y,z directions, respectively

2.3. Introduction of Elements of Linear and Nonlinear Theory of Elasticity

When inelasticity, anisotropy, and nonlinearity are coupled, the problem of how to describe the mechanical properties of arteries in a simple and accurate mathematical form becomes quite acute [*1*]. In this chapter, the 1D and 2D stress-strain relationships are defined. This information is extended to understand the stress-force relationship on a simple 3D object. In order to tie the information back to a simple artery, a 2D linear vessel is covered. The effect of axial and circumferential deformation is described as a way to introduce nonlinearity to the system. This information is used as the foundation for the one-dimensional models for blood pressure wave propagation in compliant arteries.

2.3.1. Stress and Strain in 1D Linear Mechanics

A one-dimensional object stretched in the x-direction (shown in Figure 2.1) has an original length L_0, and a final length after force is applied in the x-direction of L.

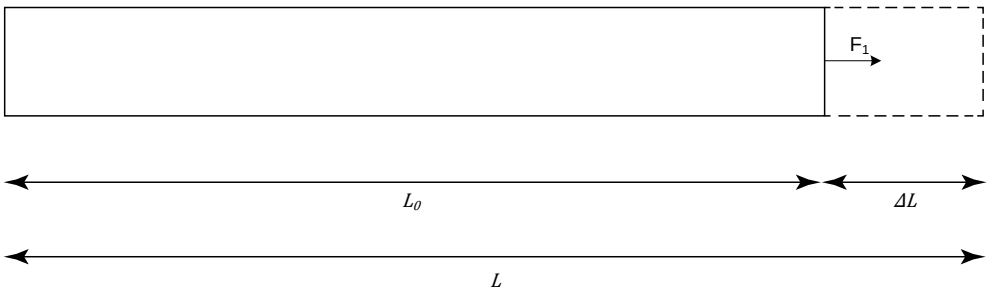

Figure 2.1. 1D object with an initial length L_0 and a final length of L after a forceF_1 is applied.

The stretch ratio and elongation are defined as

$$\lambda = \frac{L}{L_0} \tag{2.1}$$

$$\Delta \mathrm{L} = \mathrm{L} - L_0 \tag{2.2}$$

The ratio of *ΔL* to L_0 defines strain as a function λ according to

$$\varepsilon = \frac{\Delta \mathrm{L}}{L_0} = \frac{L - L_0}{L_0} = \lambda - 1 \tag{2.3}$$

Hooke's Law now relates stress to strain by the modulus of elasticity *E.*

$$\sigma = \mathrm{E}\varepsilon \tag{2.4}$$

Modulus of elasticity is a number that measures an object or substance's resistance to being deformed elastically (non-permanently) when a force is applied to it. The elastic modulus of an object could be interpreted as the slope of its stress-strain curve in the elastic deformation region [*2*].

An alternative form in which to present constituent equations is based on defining potential energy of deformation as

$$W = \frac{1}{2}\sigma\varepsilon = \frac{E\varepsilon^2}{2} \tag{2.5}$$

(Lagrange principle). Taking the partial derivative of strain energy with respect to strain, the constituent equation for stress-strain relationship is formed (Hooke's Law).

$$\sigma = \frac{\partial W}{\partial \varepsilon} = E\varepsilon \tag{2.6}$$

This approach will be used to build the constituent equations in nonlinear mechanics in Chapter 4.

2.3.2. 2D Linear Stress and Strain

A two-dimensional object stretched in x,y directions (shown in Figure 2.2) has an initial length L_{10}, L_{20}, in the x,y directions, respectively, and a final length after force is applied of L_1, L_2.

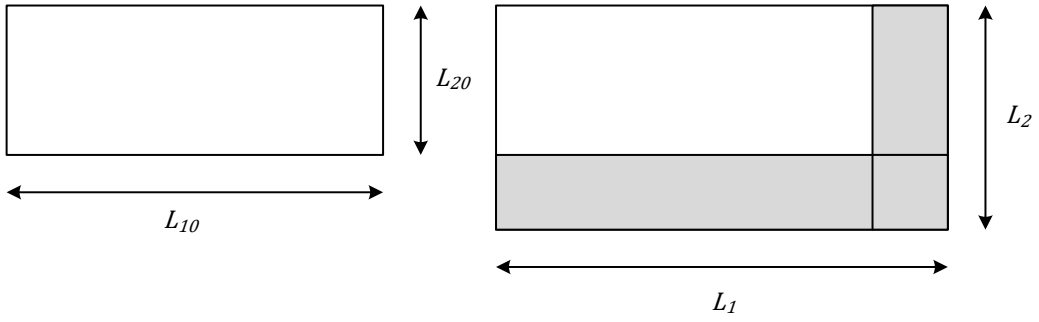

Figure 2.2. 2D object with an initial length of (L_{10},L_{20}) and final length after a force is applied of (L_1, L_2). The subscripts (1,2) are used to represent general notation, valid for Cartesian, cylindrical or spherical coordinates [1].

The stretch ratios are defined as

$$\lambda_1 = \frac{L_1}{L_{10}}, \quad \lambda_2 = \frac{L_2}{L_{20}} \tag{2.7}$$

where subscripts *1, 2* are in the *x,y* direction, respectively. Similar to stretch, the components of strain are defined as the ratio of change in length to original length.

$$\varepsilon_1 = \frac{L_1 - L_{10}}{L_{10}} = \frac{\Delta L_1}{L_{10}} \tag{2.8}$$

$$\varepsilon_2 = \frac{L_2 - L_{20}}{L_{20}} = \frac{\Delta L_2}{L_{20}} \tag{2.9}$$

$$\varepsilon_1 = \lambda_1 - 1, \varepsilon_2 = \lambda_2 - 1 \tag{2.10}$$

Strain is also related to the stretch ratio minus one. Hooke's Law generalized to its 2D counterpart now relates stress by introducing Poisson's coefficient.

$$\varepsilon_1 = \frac{1}{E}(\sigma_1 - \nu\sigma_2) \tag{2.11}$$

$$\varepsilon_2 = \frac{1}{E}(\sigma_2 - \nu\sigma_1) \tag{2.12}$$

$$\sigma_1 = \frac{E}{1-\nu^2}(\varepsilon_1 + \nu\varepsilon_2) \tag{2.13}$$

$$\sigma_2 = \frac{E}{1-\nu^2}(\varepsilon_2 + \nu\varepsilon_1) \tag{2.14}$$

When a 2D material is stretched in one direction, it usually tends to compress in the other direction perpendicular to the direction of extension. This phenomenon is called the Poisson effect. Poisson's coefficient ν is a measure of this effect.

Extending Hooke's law, it is then possible to define strain energy.

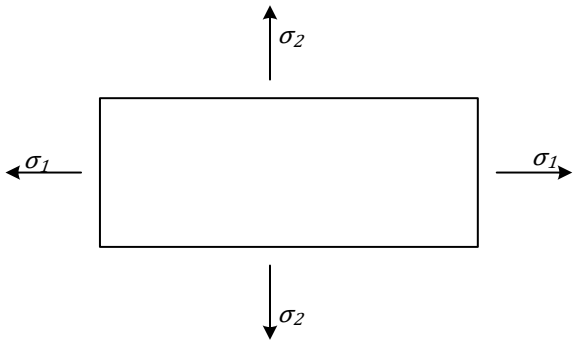

Figure 2.3. 2D strain energy under extension in both directions.

The alternative way to build 2D constituent equations is based on defining potential energy of deformation in the 2D case as

$$W = \frac{1}{2}(\sigma_1\varepsilon_1 + \sigma_2\varepsilon_2) = \frac{E}{2(1-\nu^2)}(\varepsilon_1^2 + 2\nu\varepsilon_1\varepsilon_2 + \varepsilon_2^2) \tag{2.15}$$

(Lagrange approach). By taking the partial derivative of strain energy with respect to strain, the 2D form of Hooke's Law results.

$$\sigma_1 = \frac{\partial W}{\partial \varepsilon_1} = \frac{E}{(1-\nu^2)}(\varepsilon_1 + \nu\varepsilon_2) \tag{2.16}$$

$$\sigma_2 = \frac{\partial W}{\partial \varepsilon_2} = \frac{E}{(1-\nu^2)}(\varepsilon_2 + \nu\varepsilon_1) \tag{2.17}$$

2.3.3. Stress-Force Relationship in Linear Mechanics

To understand the stress-force relationship, consider a simple 3D object as shown in Figure 2.4.

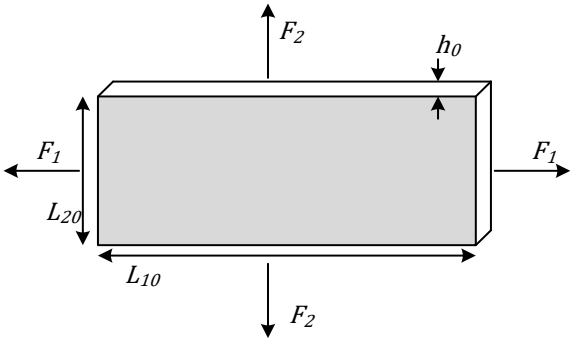

Figure 2.4. Stress-force relationship on a simple 3D object, where F_1,F_2 represent force in the x,y direction, respectively. L_{10},L_{20} represent the initial unstressed length in the x,y direction, and h_0 represents the initial unstressed thickness.

$$\sigma_1 = \frac{F_1}{L_{20}h_0} \tag{2.18}$$

$$\sigma_2 = \frac{F_2}{L_{10}h_0} \tag{2.19}$$

Defining stress components in linear mechanics, the change of geometry during deformation is neglected. In Figure 2.4, a 3D object is shown with a thin third dimension, which is the thickness of the shell. Stresses in the direction of thickness are neglected, but the change in thickness can be predicted from an incompressibility condition.

Stresses in one and two directions are statically determinate (i.e., can be calculated explicitly based on statics). Because σ_3 is neglected, our physical shell model

is two-dimensional, although the third dimension is used to specify the thickness. The information described in this section is used as the foundation to develop the second and third models for pulse wave velocity prediction in nonlinear thin- and thick-walled elastic arterial segments in Chapters 4 and 5.

2.3.4. 2D Linear Vessel

The stress-force relationship is now extended to gain understanding of a simple 2D linear vessel wall [*3*,*4*].

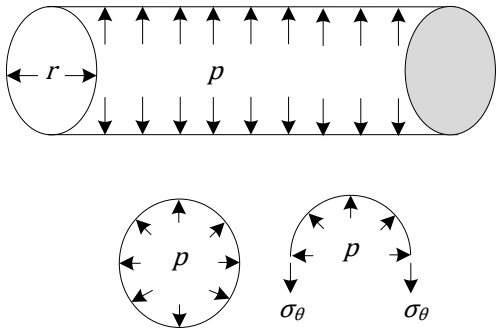

Figure 2.5. 2D linear circumferential stress on a vessel in equilibrium. The lower right image highlights the direction of the circumferential stress with the applied transmural pressure. The thickness (h) is a constant in a linear model in which deformation is not taken into account.

Static equilibrium conditions, as shown in Figure 2.5, result in

$$2\sigma_\theta h = p2r \tag{2.20}$$

$$\sigma_\theta = \frac{pr}{h} \tag{2.21}$$

where σ_θ is circumferential stress. In addition to circumferential stress, a vessel under pressure experiences axial or longitudinal stress (σ_z), calculated from static equilibrium in the axial direction as shown in Figure 2.6.

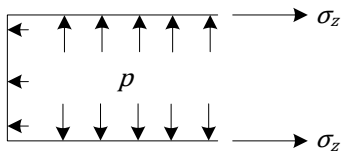

Figure 2.6. 2D linear axial stress on a vessel in equilibrium. The thickness (h) is a constant in a linear model in which deformation is not taken into account.

$$\sigma_z 2\pi r h = \pi r^2 p \tag{2.22}$$

$$\sigma_z = \frac{pr}{2h} = \frac{\sigma_\theta}{2} \tag{2.23}$$

For both circumferential and axial stress, the effect of deformation is not required by the linear model. The information described in this section is used as the foundation to develop the first model for Pulse Wave Velocity Prediction and Compliance Assessment in Linear Elastic Arterial Segments in Chapter 3.

2.3.5. Nonlinear Elasticity, Finite Deformation

In the linear case, deformation was not considered. However, the first step in accounting for nonlinearity is to take the effect of deformation into account. Analyzing uniform stretch for the block along the block sides $\mathrm{L}_{10}, \mathrm{L}_{20}, \mathrm{h}_0$, the stretch ratio is now defined as (L_1, L_2, h - the block sides after deformation)

$$\lambda_1 = \frac{\mathrm{L}_1}{\mathrm{L}_{10}}; \quad \lambda_2 = \frac{\mathrm{L}_2}{\mathrm{L}_{20}}; \lambda_3 = \frac{\mathrm{h}}{\mathrm{h}_0} \tag{2.24}$$

for all three directions [1]. If the material is incompressible, then

$$L_1 L_2 \mathrm{h} = L_{10} L_{20} h_0; \quad \lambda_1 \lambda_2 \lambda_3 = 1 \tag{2.25}$$

which means that the initial volume of the arterial wall must be equal to the final volume. It also sets the product of all stretch ratios equal to one. Figure 2.7 illustrates an infinitesimally small object before and after deformation.

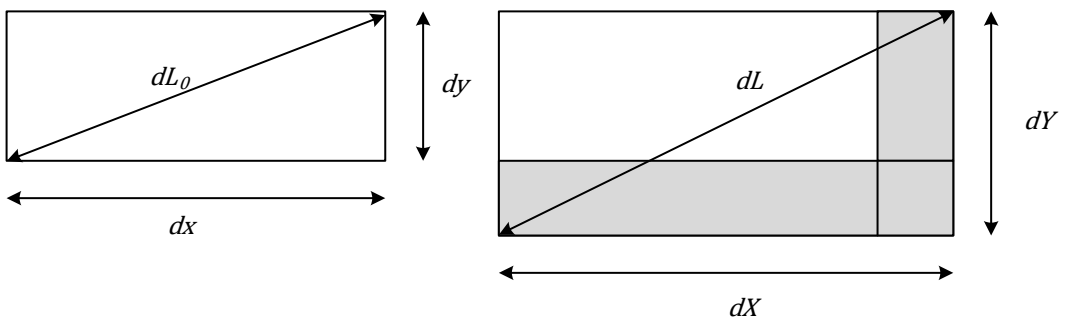

Figure 2.7. Illustration of an infinitesimally small element before (left) and after (right) deformation.

Analyzing deformation for the non-uniform point-dependent stretch, L_{10}, L_{20} are substituted with dx, dy, and L_1, L_2 $with$ dX, dY. As a result,

$$\lambda_x = \frac{dX}{dx}; \quad \lambda_y = \frac{dY}{dy} \tag{2.26}$$

where capital (X,Y) are the Lagrangian coordinates associated with deformed particles, and the lowercase coordinates (x,y) relate to the strain-free case. By using the Pythagorean Theorem

$$dL_0 = \sqrt{dx^2 + dy^2}; \quad dL = \sqrt{dX^2 + dY^2} \tag{2.27}$$

dL_0, dL can be calculated. The Green strain is defined as

$$G = \frac{dL^2 - dL_0^2}{2dL_0^2} \tag{2.28}$$

By combining equations (2.26), (2.27), and (2.28), in terms of *dx,dy*, equation (2.29) results.

$$G = \frac{\lambda_x^2 dx^2 + \lambda_y^2 dy^2 - (dx^2 + dy^2)}{2(dx^2 + dy^2)}; \quad \frac{(\lambda_x^2 - 1)dx^2 + (\lambda_y^2 - 1)dy^2}{2(dx^2 + dy^2)} \tag{2.29}$$

Setting deformation in the y-direction to zero (*dy*=0) results in a one-dimensional x-component of Green strain.

$$G_x = \frac{\lambda_x^2 - 1}{2}; \tag{2.30}$$

Setting deformation in the x-direction to zero (*dx*=0) results in a one-dimensional y-component of Green strain.

$$G_y = \frac{\lambda_y^2 - 1}{2}; \tag{2.31}$$

For small deformation, where $(\Delta L_1 \ll L_{10})$

$$\lambda_x = \frac{L_1}{L_{10}} = \frac{L_{10} + \Delta L_1}{L_{10}};\ (\Delta L_1 \ll L_{10}) \tag{2.32}$$

$$G_x = \frac{1}{2}\left(\left(\frac{L_{10} + \Delta L_1}{L_{10}}\right)^2 - 1\right) = \frac{1}{2}\left(\frac{L_{10}^2 + 2L_{10}\Delta L_1 + \Delta L_1^2 - L_{10}^2}{L_{10}^2}\right) \tag{2.33}$$

$$G_x \cong \frac{\Delta L_1}{L_{10}} = \varepsilon_x; \quad G_y \cong \frac{\Delta L_2}{L_{20}} = \varepsilon_y \tag{2.34}$$

Green strain components are identical to deformation introduced in a linear theory of elasticity.

Cauchy-Euler stress takes into account the change in geometry during deformation, defined as the ratio of force to the real area.

$$\sigma_1 = \frac{F_1}{L_2 h}; \quad \sigma_2 = \frac{F_2}{L_1 h} \tag{2.35}$$

Piola-Lagrange stress uses the initial state of the area.

$$T_1 = \frac{F_1}{L_{20} h_0}; \quad T_2 = \frac{F_2}{L_{10} h_0} \tag{2.36}$$

The two different types of stress (35,36) are related by

$$\frac{\sigma_1}{T_1} = \frac{L_{20}}{L_{20} h_0} = \frac{1}{\lambda_2 \lambda_3} = \lambda_1 \tag{2.37}$$

$$\sigma_1 = T_1 \lambda_1;\ \ \sigma_2 = T_2 \lambda_2 \tag{2.38}$$

the stretch ratio.

Kirchhoff's stress components (S_1, S_2) are related to the corresponding Cauchy and Lagrange components as the following:

$$S_1 = \frac{\sigma_1}{\lambda_1^2} = \frac{T_1}{\lambda_1}; \quad S_2 = \frac{\sigma_2}{\lambda_2^2} = \frac{T_2}{\lambda_2} \tag{2.39}$$

Kirchhoff's stress components can be expressed as a partial derivative of strain energy by relating Green's strain components

$$S_1 = \frac{\partial W}{\partial E_1}; \quad S_2 = \frac{\partial W}{\partial E_2} \tag{2.40}$$

The information described in this section is used as the foundation to develop the second and third models for pulse wave velocity prediction in nonlinear thin- and thick-walled elastic arterial segments in Chapters 4 and 5.

2.4. Conclusion

In this chapter, 1D and 2D stress strain relationships were reviewed. The basic stress-force relationships were covered without accounting for deformation. Incorporating this information, the 2D linear vessel was reviewed. Special attention was given to define both the longitudinal and circumferential stress. The effects of nonlinearity were then considered. Considering the effect of deformation, Cauchy-Euler, Piola-Lagrange, and Kirchoff stresses were defined and related. The foundation of nonlinear mechanics of material presented in this chapter will be used for the models that are described in Chapters 3-5.

2.5. References

[1] Fung Y.C., K. Fronec, P. Patucci , "Pseudo-elasticty of arteries and the choice of mathematical expression," *Am J Physiol-Heart C*, vol. 237, no. 5, pp. H620-31, Nov 1979.

[2] Askeland D.R., W.J. Wright , *The science and engineering of materials*, 5th ed., p. 198. ISBN 978-0-534-55396-8, Ed.: Cengage Learning.

[3] Nichols M., M. O'Rourke , *McDonalds Blood Flow in Arteries*, 50340809418th ed.: Hodder Arnold, 2005.

[4] Pedley T.J., "Mathematical modeling of arterial fluid dynamics," *Journal of Engineering Mathematics*, vol. 47, pp. 419–444, 2003.

Chapter 3: Pulse Wave Velocity Prediction and Compliance Assessment in Linear Elastic Arterial Segments

…when you can measure what you are speaking about, and express it in numbers, you know something about it; but when you cannot measure it, when you cannot express it in numbers, your knowledge is of a meagre and unsatisfactory kind; it may be the beginning of knowledge, but you have scarcely, in your thoughts, advanced to the state of Science whatever the matter may be. - Lord Kelvin

3.1. Abstract

Pressure wave velocity (PWV) is commonly used as a clinical marker of vascular elasticity [1-9]. Recent studies have increased clinical interest in also analyzing the impact of heart rate (HR), blood pressure, and left ventricular ejection time (LVET) on PWV. In this chapter, the focus is on the development of a theoretical one-dimensional model and validation via direct measurement of the impact of ejection time and peak pressure on PWV using an *in vitro* hemodynamic simulator. A simple nonlinear traveling wave model was developed for a compliant thin-walled elastic tube filled with an incompressible fluid. This model accounts for the convective fluid phenomena, elastic vessel deformation, radial motion, and inertia of the wall. An exact analytical solution for PWV is presented that incorporates peak pressure, ejection time, ejection volume, and modulus of elasticity. To assess arterial compliance, the solution is introduced in an alternative form, explicitly determining compliance of the wall as a function of the other variables. The model predicts PWV in good agreement with the measured values, with a maximum difference of 3.0%. The results indicate an inverse quadratic relationship ($R^2 = .99$) between ejection time and PWV, with ejection time dominating the PWV shifts (12%) over those observed with changes in peak pressure (2%). Our modeling and validation results both explain and support the emerging evidence that, in both clinical practice and clinical research, variables related to cardiac systolic function should be regularly taken into account when interpreting arterial function indices, namely PWV.

3.2. Nomenclature

A	Cross-sectional area (m^2)
c	Velocity of a traveling wave (m/s)
c_{MK}	Moens-Korteweg speed of propagation (m/s)
E	Modulus of elasticity (Pa)
F	Force (N)
h_0, h	Thickness of the wall in zero-stress and deformable conditions, respectively (m)
L_0	1D initial length (m)
L	1D final length (m)
ΔL	Elongation (m)
ν	Poisson's coefficient
p	Transmural pressure (Pa)
ρ	Density of an incompressible fluid (kg/m^3)
ρ_w	Density of the cylindrical wall (kg/m^3)
PTT	Pulse transit time (s)
PWV	Pressure wave velocity (m/s)
r	Radius (m)
u	Axial flow velocity (m/s)
η	Circumferential wall strain
Subscripts	
(t,z)	Derivatives by time and axial coordinates
Superscripts	
‘	Derivative

3.3. Introduction

The pulse wave, generated by left ventricular ejection, propagates at a velocity that has been identified as an important marker of atherosclerosis and cardiovascular risk [1-9]. Increased pulse wave velocity indicates an increased risk of stroke and coronary heart disease [1]. This velocity is considered a surrogate marker for arterial compliance [2], is highly reproducible [2], and is widely used to assess the elastic properties of the arterial tree [3]. Research shows that aortic compliance measurement using pulse wave velocity could allow for early identification of patients at risk for cardiovascular disease [1,3,7]. The ability to identify these patients would lead to better risk stratification and earlier, more cost-effective preventative therapy [4]. Several studies have shown the influence of blood pressure [1,11-13] and LVET [3, 5] on pulse wave velocity.

Over the past several decades, there has been ongoing research focused on improving the theoretical prediction of PWV. The clinical relationship between PWV and arterial stiffness is often based on classic linear models [8,15] or on the combination of the linear models and measured results with an incorporated correction factor [16-18]. Whereas linear models predict PWV as a function of only geometric and physical properties of the fluid and the wall, there is strong evidence that PWV is also correlated with pressure [11-13] and ejection time [3, 5]

While both pressure and LVET are shown clinically to affect pulse wave velocity, a predictive model that provides mechanistic insight and incorporates peak pressure, ejection time, ejection volume, and modulus of elasticity has yet to be developed. The

aim of this study is to develop and validate a model to provide this missing insight. The approach used is based on a one-dimensional nonlinear model for pressure wave propagation in a compliant tube with a linear elastic wall filled with an incompressible fluid. The model incorporates the classical solitary wave-based solution, connecting speed of propagation to the ejection time, ejection volume, and peak pressure. It accounts for nonlinear wave propagation effects, elastic deformable vessels, and the inertia of the distensible vessel walls. The model is validated using a physiologically based electromechanical hemodynamic simulator.

To assess the impact of arterial stiffness, the theoretical solution is introduced in an alternative form, to enable explicit determination of the vascular wall's elasticity (or compliance) as a function of PWV, peak pressure, ejection volume, and ejection time. This solution is a natural generalization of Bramwell–Hill theory [6] that directly relates compliance to PWV only, independent of the other factors.

3.4. Theory

3.4.1. Nonlinear Model for Pressure Wave Propagation

A nonlinear one-dimensional model for blood pressure wave propagation in compliant arteries was created. As shown Figure 3.1, this model assumes a compliant tube with a linear elastic wall filled with an incompressible inviscid fluid.

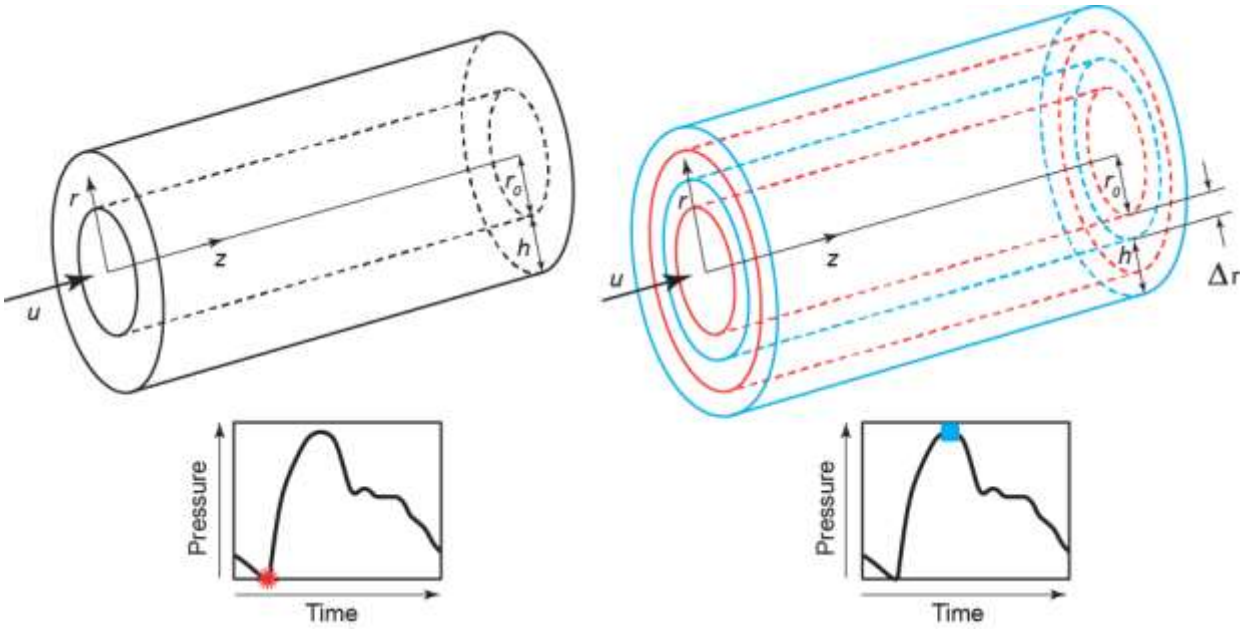

Figure 3.1. Longitudinal cross section of the arterial wall being modelled in the r, z plane, where r, z are the radial and axial coordinates, respectively. The cylinder is represented at two specific times in the cardiac cycle: diastolic pressure (shown at foot red circle, lowest pressure) and systolic pressure (shown by blue square, peak pressure). The wall thickness h, initial inner diameter r_0, and wall displacement Δr are exaggerated for the purpose of illustration.

At each spatial location *z* and at each time *t,* the average cross-sectional axial flow velocity *u=u(z,t)*, static pressure *p=p(z,t)*, cross-sectional area *A=A(z,t)*, and membrane circumferential strain (ratio of the normal displacement to the radius) *η=η(z,t)* are calculated. Application of the laws of conservation of mass and conservation of momentum results in the following set of 1D equations [20,21], correspondingly:

$$A_t + (uA)_z = 0 \tag{3.1}$$

$$u_t + (\frac{u^2}{2} + \frac{p}{\rho})_z = 0 \tag{3.2}$$

where: ρ is the density of the fluid, assumed to be constant. Subscripts indicate partial derivative by the corresponding space and time variables (z, t), respectively. Equilibrium conditions maintain the following relationship between pressure, circumferential stress, and inertia of the moving wall:

$$p = \frac{\bar{E}h}{r_0}\eta + \rho_w h r_0 \eta_{tt} \tag{3.3}$$

where: E is the elastic modulus for the wall, ν is Poisson's coefficient; and $\bar{E} = E/(1-\nu^2)$; h is the constant thickness of the wall, r_0 is the cross-sectional radius of the unstressed cylindrical vessel $(p = 0)$, ρ_w is the density of the cylindrical wall, and η is circumferential wall strain. Noting that $A = \pi r_0^2(1+\eta)^2$, the total system of equations can be presented in the following non-conservative form:

$$\eta_t + u\eta_z + \frac{1+\eta}{2}u_z = 0 \tag{3.4}$$

$$u_t + uu_z + \frac{1}{\rho}p_z = 0 \tag{3.5}$$

$$p = \frac{\bar{E}h}{r_0}\eta + \rho_w h r_0 \eta_{tt} \tag{3.6}$$

Following [22], we are looking for the solitary traveling wave solution in a form $\eta(z,t) = \eta(Z),\ u(z,t) = u(Z)$, where $Z = z - ct$ and c represents the velocity of the traveling wave. The functions $\eta(Z),\ u(Z),\ p(Z)$ are assumed to be smooth, and decaying monotonically as $Z \to \pm\infty$.

Substituting $\eta(Z), u(Z)$ into equations (3.4-3.6), we obtain the following system of ordinary differential equations where prime indicates the derivative with respect to Z:

$$(-c+u)\eta' + \frac{1}{2}(\eta + r_0)u' = 0 \tag{3.7}$$

$$-cu' + uu' + \frac{Eh}{\rho r_0^2}\eta' + \frac{\rho_w h}{\rho}c^2\eta''' = 0 \tag{3.8}$$

By neglecting the nonlinear terms in equations (3.7) and (3.8) and the wall inertia terms in (3.8), the linearized hyperbolic system of equations can be presented as:

$$-c\eta' + \frac{1}{2}u' = 0 \tag{3.9}$$

$$\frac{Eh}{\rho r_0}\eta' - cu' = 0 \tag{3.10}$$

A non-trivial solution exists only if $\begin{Vmatrix} -c & \frac{1}{2} \\ \frac{\bar{E}h}{r_0} & -c \end{Vmatrix}$ is presented in matrix form, where

$$c = c_{MK} = \sqrt{\frac{\overline{E}h}{2r_0\rho}} \tag{3.11}$$

is the Moens-Korteweg speed of propagation, which is a function of the mechanical properties of the system only. For the general case, the total nonlinear dispersive wave model in equations (3.7) and (3.8) must be considered. Separating variables in equation (3.7), $2\eta'/(1+\eta) = u'/(c-u)$, integrating, and noting $u(\eta = 0) = u_0$ which represents the average flow velocity, the following relationship can be obtained:

$$u = c - \frac{c - u_0}{(1+\eta)^2} \tag{3.12}$$

Integrating equation (3.8) results in

$$-c(u-u_0) + \left(\frac{u^2}{2} - \frac{u_0^2}{2}\right) + \frac{Eh}{\rho r_0}\eta + \frac{\rho_w h r_0}{\rho}c^2\eta'' = 0 \tag{3.13}$$

A nonlinear momentum equation is obtained by multiplying equation (3.13) by $d\eta$ and integrating to yield:

$$-c\int_0^{\eta}(u-u_0)d\eta+\frac{1}{2}\int_0^{\eta}(u^2-u_0^2)d\eta+\frac{Eh}{2\rho r_0}\eta^2+\frac{\rho_w h r_0}{2\rho}c^2(\eta')^2=0 \qquad (3.14)$$

Equation (3.14) can be reduced to an algebraic form by analysis of the peak value of the wave profile, $\eta'=0$. Calculating integrals of equation (3.14) based on equation (3.12), and setting equation (3.14) at peak pressure, one can reduce the momentum equation to the following form:

$$PWV=c=u_0\pm c_{MK}\frac{A_\eta}{\sqrt{\Gamma(A_\eta)}} \qquad (3.15)$$

where $\Gamma(\eta)=\frac{\eta}{2}-\frac{1}{6}(1-\frac{1}{(1+\eta)^3})$, and $A_\eta=max\big(\eta(Z)\big)$ is the peak circumferential strain. Equation (3.15) presents PWV of the forward and backward solitary wave propagation. Based on asymptotic expansion $\frac{A_\eta}{\sqrt{\Gamma(A_\eta)}}=1+\frac{5}{6}A_\eta+O(A_\eta^2)$, where *O* is the order of accuracy, equation (3.15) reduces to a simplified form using the second order of accuracy:

$$c=u_0+c_{MK}(1+\frac{5}{6}A_\eta) \qquad (3.16)$$

indicating a correction to the classical Moens-Korteweg model, introduced by the present theory. The peak of flow velocity A_u, volume flow rate A_Q, and pressure A_p are dependent on *c* as follows from equations (3.6), (3.12), (3.13), and (3.15):

$$A_u=c-\frac{c-u_0}{(1+A_\eta)^2} \qquad (3.17)$$

$$A_Q/\pi r_0^2=A_u\times(1+A_\eta)^2 \qquad (3.18)$$

$$A_p/\rho=c(A_u-u_0)-(\frac{A_u^2}{2}-\frac{u_0^2}{2}) \qquad (3.19)$$

According to the traveling wave model, pressure, flow, and wall displacement propagate with the same speed of propagation, *c*. The linear model predicts that all waves travel with the Moens-Korteweg speed (c_{MK}), but accounting for nonlinearities predicts a speed of propagation that exceeds c_{MK}. As expected for soliton nonlinear waves, the higher peak pressure wave travels with a higher speed [7]. This trend is similar to the results derived differently in [7], and it is consistent with the clinical data obtained in [8]. As ejection time decreases, the average flow velocity u_0 increases, thereby increasing PWV as seen in equation (3.16).

3.4.2. Assessment of Arterial Compliance

Quantification of pulse wave velocity is typically considered the ‘‘gold standard’’ method to assess arterial compliance [9]. The nonlinear model can be extended to estimate aortic compliance as a function of PWV, peak pressure, ejection time, and ejection volume. The classic definition of compliance (*C*) is $C = \Delta V/\Delta P$, where (ΔV) is the change in arterial blood volume for the defined arterial segment and (ΔP) is the associated change in arterial blood pressure. Using the pressure/displacement and volume/displacement relationships (A_s is the surface area, and *V* is the internal volume of the arterial segment):

$$\Delta P = \frac{\bar{E}h}{r_0}\eta = 2\rho\eta c_{MK}^2 \tag{3.20}$$

$$\Delta V = A_s r_0 \eta = 2V\eta \tag{3.21}$$

the Bramwell-Hill compliance (C_{BH}) can be determined as:

$$\frac{\Delta V}{\Delta P} = C_{BH} = \frac{V}{\rho c_{MK}^2} \tag{3.22}$$

In practice, the volumetric compliance is calculated based on the measured pressure wave velocity [9]:

$$C = \frac{V}{\rho PWV^2} \tag{3.23}$$

To estimate the error introduced by equation (3.23), we transform it using equation (3.15), and we form the expression that explicitly estimates its proximity to the exact value:

$$C = \frac{V}{\rho c_{MK}^2 (\frac{u_0}{c_{MK}} + \frac{A_\eta}{\sqrt{\Gamma(A_\eta)}})^2} = C_{BH}[1 - \frac{5}{3}A_\eta - 2\frac{u_0}{c_{MK}} + O(A_\eta^2) + O(\frac{u_0}{c_{MK}})^2] \tag{3.24}$$

Neglecting the quadratic terms, we introduce a corrected coefficient for elastance, defined as a ratio of compliance (*C)* to the Bramwell-Hill compliance (C_{BH})

$$C/C_{BH} = (1 - \frac{5}{3}\,A_\eta - 2\frac{u_0}{c_{MK}}) \tag{3.25}$$

This coefficient could be useful to decrease the error associated with equation (3.23).

3.5. Materials and Methods

3.5.1. Hemodynamic Simulator

A physiologically based electromechanical cardiovascular simulator was developed, which is a modified version of that described in [10]. The simulator is capable of producing arterial hemodynamic flows and pressures associated with the circulatory system. As shown in Figure 3.2*,* a linear actuator *(THK linear actuator, VLA-ST-60-12-0250),* driven by a servomotor *(*Yaskawa Sigma-V) is used to produce repeatable fluid flow by displacement of a given fluid volume creating a repeatable pressure in the compression chamber. LabVIEW is used to control the servomotor for accurate control of the fluid ejection time. LabVIEW was also used to record the measurements from the pressure and flow sensors used in the simulator.

The pressure sensors (P1, P2, venous pressure) and flow sensors (F1, F2) are located as shown in Figure 3.2. Sensors are placed at a location representing the proximal aorta (P1, F1) and distal aorta (P2, F2). The venous pressure sensor is located distal to the resistive element. Systemic vascular resistance (SVR) is controlled by the Windkessel resistive elements (E1, E2). Mean aortic flow was determined from measurements obtained using the distal flow sensor (F2). The mean was calculated in MATLAB for each sixty-second dataset. SVR and ejection volume were calculated as described in [11], $SVR = (MAP_a - MAP_v)/F_a$, where MAP_a is mean aortic pressure; MAP_v is mean venous pressure; F_a is mean aortic flow; and the units of SVR, mean aortic flow, and aortic and venous MAP are $mmHg \cdot min/L$, L/min, *and* $mmHg$, respectively. The experimental pulse rate was kept at a constant 60 beats per minute (BPM) with

ejection volume (EV) calculated as $\mathrm{EV} = F_a/\mathrm{PR}$, where *PR* is pulse rate and the units of ejection volume, mean aortic flow, and pulse rate are L, L/min, and $beats/min$.

The simulator contains both an arterial afterload and a venous preload compliance chamber with air volumes of 0.72 *L* and 3.83 *L*, respectively. A sphygmomanometer bulb controls chamber pressures with manual pressure readout via an associated mechanical pressure gauge. Prior to starting an experiment, both chambers were pressurized to ~5 mmHg. This resulted in a dynamic MAP of 85 *mmHg* during experiments.

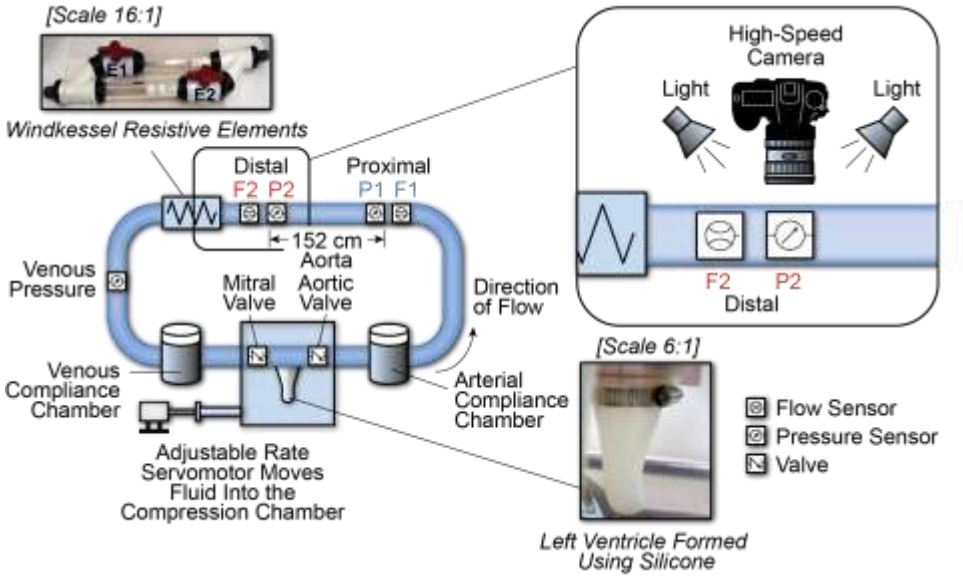

Figure 3.2. Illustration of the cardiovascular hemodynamic simulator with a total volume of 5.75 L. P1, P2 are the proximal and distal aortic pressure sensors. F1, F2 are the proximal and distal aortic flow sensors. The Windkessel resistive elements are used to model SVR as in [12]. An adjustable-rate servomotor was used to control ejection time. In the right part of the figure is an expanded view showing the addition of the high-speed camera setup used to measure wall displacement.

3.5.1.1. Pressure and Flow Sensors

Pressure was measured using factory calibrated ($\pm$1 mmHg), catheter-based, solid-state pressure transducers (Millar Instruments, Mikro-Cath 3.5F pressure catheter, sterile, disposable, 120 *cm*). Flow was measured using precision tubing transit time flow sensors (Transonic Systems Inc., ME-PXL-Series) calibrated to achieve a flow measurement accuracy of $\pm$2%. Transonic Systems, Inc. calibrated the flow sensors with the tubing used for all experiments.

3.5.1.2. Aortic Tubing

Tubing was selected with compliance values to approximate the elasticity of the aorta. Papageorgiou and Jones [13] studied Tygon, Silastic, PVC, and Latex tubing and determined that Latex tubing was most suitable for arterial simulation because the incremental modulus of elasticity was close to that of major arteries. In this study (McMaster-CARR, 5234K631), (ID = 19.05 *mm*, OD = 22.22 *mm*, wall thickness = 1.59 *mm*), Latex rubber was selected. Static pressurization tests were performed on the selected tubing to empirically measure the tubing compliance. The tubing was pressurized in 12 equal steps [0-200 *mmHg*] while monitoring the internal pressure with a catheter pressure transducer (Validyne P855). The outer diameter of the compliant tubing was imaged using a digital camera (IDT Motion Pro X3, 1280x1024 pixels, 500 frames per second). The images were post-processed to determine the outer diameter of the tubing at each pressure level. There was an approximately linear (R^2 = 0.99) relationship between the expansion of the compliant tubing and the increasing static pressures within the tested operating pressure range, with a slope of 0.15 *mm/mmHg* and an intercept of 22.22 *mm*. The linear relationship indicates that the tubing remains within the linear elastic range, which is consistent with the results obtained by [26,27].

Based on the referenced studies and the measured results, this tubing was then used for all experiments.

3.5.1.3. Systemic Vascular Resistance

A physical Windkessel resistance was constructed to serve as a laminar flow control element and was attached 20 *cm* distal from sensors (P2, F2), to provide realistic outflow impedances, as shown in Figure 3.2. The construction methods used in this work were adapted from Taylor and Kung [12]. The resistance modules were connected to PVC tubing at each end. To avoid turbulence and maintain laminar flow, care was taken to minimize abrupt diameter changes at the connection junction.

3.5.2. Hemodynamic Simulation Experiment

Hemodynamic parameters were directly measured and PWV was determined while varying ejection time, at a fixed ejection volume, SVR, mean aortic flow, and HR of 60 BPM for a duration of 60 seconds. All signals were low pass filtered (Butterworth filter, eight pole zero phase) with a corner frequency set at 20 Hz [14]. Automated MATLAB algorithms were used to extract the foot-to-foot delta time for the proximal and distal pressure. The percent height method was implemented to find the diastolic foot [15, 16]. The associated PWV was calculated by dividing the distance between the sensors, shown in Figure 3.2, by the extracted foot-to-foot delta time. Extracted results were averaged, and the standard deviation was calculated across a 60-second interval for each ejection time. *GraphPad Prism* 5 statistical analysis software was used to determine the correlation between PWV and ejection time. Simple Pearson linear regression analysis was applied to detect and describe the strength and sign of correlation of PWV with respect to LVET.

3.6. Results and Discussion

3.6.1. Comparison of the Model to the Hemodynamic Simulator Data

Figure 3.3 compares theoretical simulated prediction of PWV as a function of a average flow velocity and peak pressure to the measured values using the hemodynamic simulator.

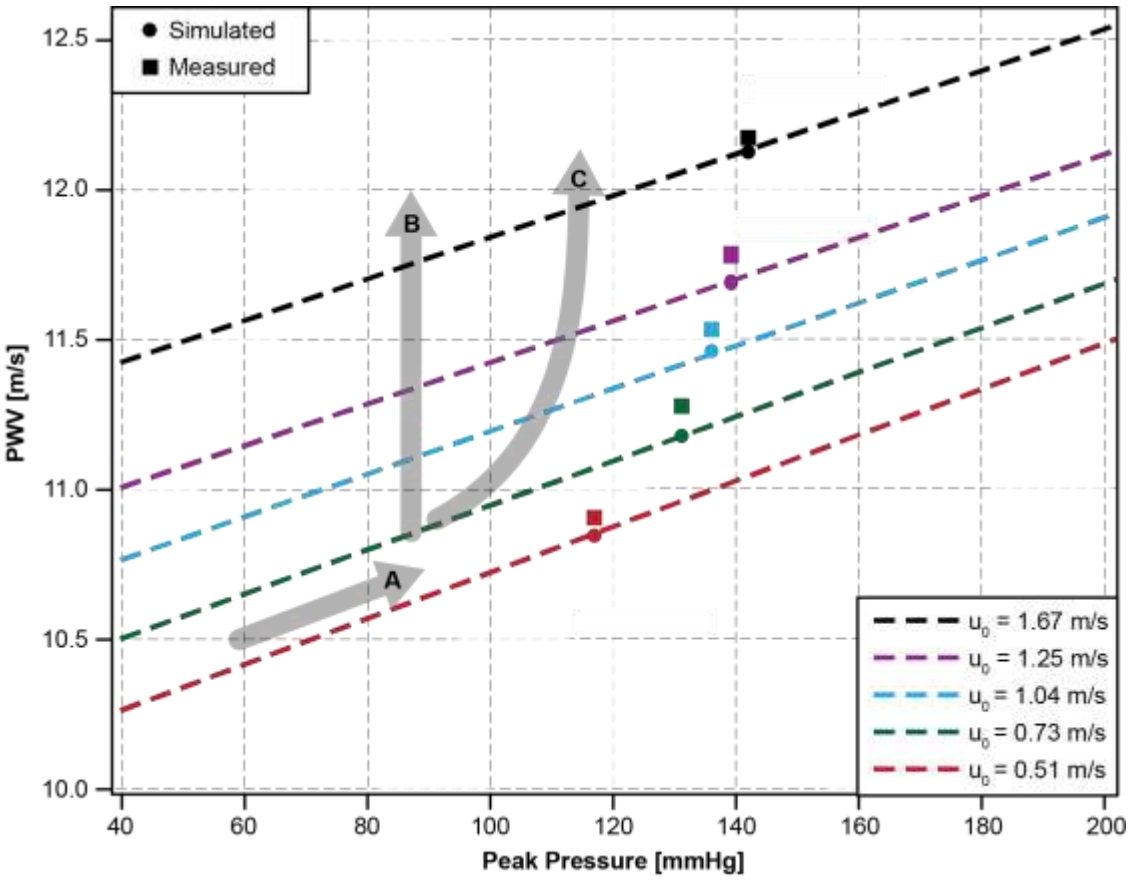

Figure 3.3. Dashed lines present prediction from the theoretical model for five different average flow velocities u_0 and peak pressure controlled by ejection time at a fixed SVR. Data points allow comparison of predicted (circle) and measured (square) PWV. To move left to right along arrow (A), peak pressure increases while average flow velocity remains constant. Movement vertically along arrow (B) occurs if average flow velocity increases while peak pressure remains constant. Finally, to move upward along the quadratic arrow as in the measured data points (C), both peak pressure and average flow velocity increase as demonstrated by data obtained from the set of experiments and those calculated from the 1D nonlinear traveling wave model.

Dashed lines present predictions based on equation (3.16) for the five different average flow velocities u_0 and peak pressure controlled by ejection time at a fixed SVR. The

maximum difference between theoretically simulated and measured results is 3.0%. Flow velocity and peak pressure changes controlled by ejection time result in the quadratic PWV curve observed in Figure 3.3 (arrow C).

The coefficient of determination and p-value were calculated to be $R^2 = 0.99$ and $p = 0.0001$, respectively, demonstrating a strong correlation between PWV and ejection time. PWV is substantially affected by average flow velocity (~10%) and peak pressure (~2%) changes controlled by ejection time (12% over the analyzed range, arrow C), as seen in the measured and simulated results. However, for a fixed ejection time, changes in PWV due to shifts in peak pressure alone are relatively small (2%).

Table 3.1 lists the calculated values of ejection volume and SVR with respect to ejection time. As shown in the table, ejection volume, SVR, MAP, and aortic flow rate do not change with varying ejection time in the hemodynamic simulator. The small changes in calculated ejection volume were caused by small mean aortic flow variations.

Table 3.1. Hemodynamic measured values are maintained within the clinical range.

Ejection Time [*ms*]	**Ejection Volume* [*ml*]**	**SVR* [*mmHg ·min/L*]**	**SBP/DBP/MAP [*mmHg*]**	**Venous MAP [*mmHg*]**	**Mean Aortic Flow [*LPM*]**
434	66.1	15.4	117/60/82	22	3.9
382	67.8	15.7	131/56/86	23	4.0
326	66.1	15.9	136/53/85	23	3.9
297	66.9	15.4	139/51/85	24	3.9
252	66.8	15.5	142/49/85	24	3.9

**Calculated Value*
Values maintained within a clinical range using the cardiovascular hemodynamic simulator. Changes in ejection volume were caused by aortic flow variation. Clinical range for LVET (150-450) [17]; Ejection Volume (55-100 ml) [17]; SVR (9-20 mmHg ·min/L) [18]; SBP (90-180) [17]; DBP (40-110) [17]; Mean Aortic Flow (4-7) [17]. Values are expressed as means over each 60-second interval. For all measures of ejection time, pressure, and flow, the standard deviations were below 1.3 ms, 0.1 mmHg, 0.02 LPM respectively.

For a constant MAP, the associated PWV varied by up to 12% (182 ms) over the range of measured ejection time (252-434 ms). The mean and standard deviation for both MAP and SVR are 84.1, ±1.4 *mmHg* and 15.4, ±0.25 $mmHg \cdot min/L$ respectively, which confirms that both remained nearly constant across the range of ejection times tested. The MAP remained approximately constant. However, the SBP increased by 25 *mmHg,* and the DBP decreased by approximately 11 *mmHg* as a function of LVET decreasing.

As can be seen across the range of ejection times in Table 3.1, the associated DBP changed from approximately 60-49 mmHg, for a nearly constant SVR and MAP. In our experiment, no adjustments were made across the five steps of decreasing ejection time. Since the ejection time decreased while heart rate and ejection volume remained constant, the time spent in diastole increased and thus resulted in a decreasing DBP. The opposite effect is observed for SBP, which increased from 117-142*mmHg* as ejection time decreased. The observed changes for both SBP and DBP are consistent with those observed clinically with changes in ejection time [17], but are on the low side of clinical relevance. Increases in flow rate would have further increased the effect on PWV, as can be seen by equation (3.16).

The contour plot Figure 3.4(a) enables visualization of the effect of ejection time and peak pressure on PWV. Ejection time decreasing at a fixed peak pressure affects PWV to a greater extent than increases to peak pressure at a fixed ejection time, as seen in Figure 3.3 and Figure 3.4. Referencing equation (3.16) and Figure 3.4(b) gives insight into the effects of average flow velocity (~10%) and wall strain (~2%) on PWV.

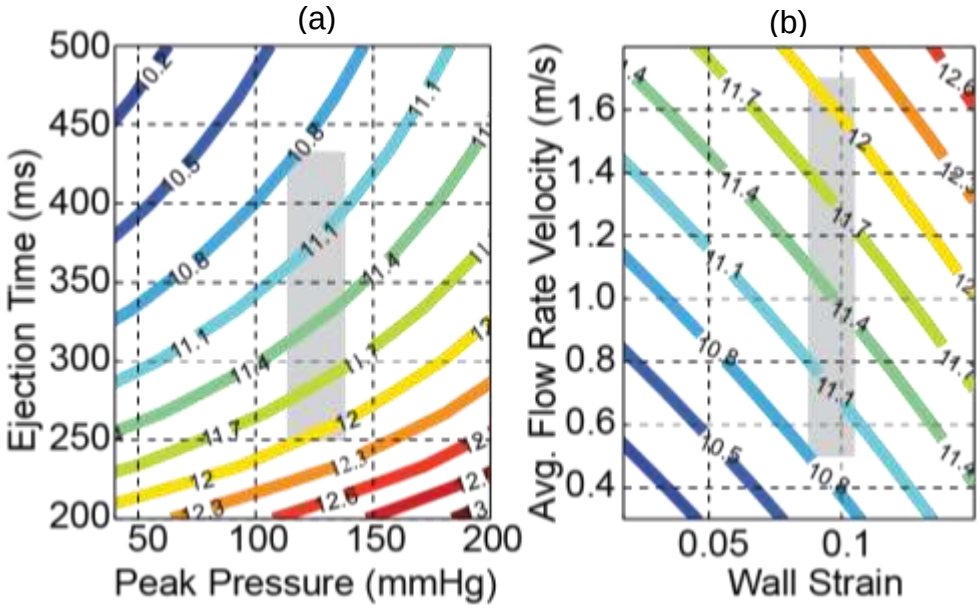

Figure 3.4. (a) PWV (m/s) contour plot that illustrates a greater change in PWV caused by ejection time when compared with a change in peak pressure alone. The simplified linear result (c_{MK} = ~9.8 m/s) occurs as peak pressure approaches zero and ejection time approaches infinity. (b) PWV (m/s) contour plot that illustrates the effect of both average flow velocity and wall strain as seen in equation (3.16). In each plot, the vertical gray rectangle encloses the range of our measured data using the hemodynamic simulator.

3.6.2. Mechanisms Causing the Association between PWV and LVET

The main novel contribution of the present study is the creation and validation of an analytical model that explains the mechanism for the observed inverse association between PWV and LVET. We used the nonlinear traveling wave model to investigate mechanisms underlying the effects of pressure, ejection time, ejection volume, geometric properties, and physical properties on PWV. The model is based on mass and momentum conservation applied to the incompressible fluid propagating in a thin-walled compliant elastic tube. The presented nonlinear traveling wave model accounts for the convective fluid phenomena, elastic vessel deformation, and inertia of the wall. Data analysis results in an analytical expression, generalizing the classical Moens-Korteweg speed of propagation to include the effect of peak pressure and ejection time on PWV, as shown in equation (3.16).

For very small changes in transmural pressure approaching ~0 mmHg, results simplify to those obtained from the linear Moens-Korteweg model (c_{MK}), as shown in equation (3.11). However, for clinically relevant changes in transmural pressure (SBP/DBP), our nonlinear model shows that as ejection time decreases, the average flow velocity (u_0), pressure (p), and wall strain (η) increase. Since PWV is a function of the average flow velocity (u_0) and the Moens-Korteweg velocity c_{MK} scaled by the wall strain as seen in equation (3.16), this results in an increase in PWV with reductions in ejection time. Accounting for these nonlinearities predicts a speed of propagation that exceeds c_{MK} by 12% across the physiological range of transmural pressures and ejection times examined in this work.

Physiologic states involve a complex interaction of multiple variables. The three arrows in Figure 3.3 provide insight into these complex relationships. It is possible to suggest clinical scenarios for the changes in PWV as shown in Figure 3.3. In moving left to right along arrow (A), SVR changes while ejection time and stroke volume remain constant, which can occur in hypertension [19]. During digestion, SVR decreases while ejection volume increases [20], which will approximately follow arrow (B). Finally, in moving along the quadratic arrow, as in our measured data points (C), ejection time changes while stroke volume and SVR remain constant (this work), which can occur during sleep [21].

The presented model and validation results both show an inverse quadratic relationship between LVET and PWV that has been previously observed. Nurnberger et al. [11] used myocardial stimulation to modulate ejection time and measure the associated change in PWV that was found to correlate only with LVET ($R^2 = 0.52$,

p = 0.0325). In their study, a change in ejection time of ~40 ms caused a change in PWV of ~1 m/s. Salvi et al. [14] performed a large population study to explore the link between PWV and LVET. An inverse association was found between PWV and LVET at all ages ($<R^2 = 0.43$; $p < 0.001$). In both studies, it was not possible *in vivo* to control LVET, SVR, and ejection volume, which likely decreased their observed correlation. We recognize that our PWV was higher than those measured by Nurnberger. This was likely caused by the higher modulus of elasticity of our tube when compared with that of the healthy human aorta. However, our PWV was within the range of that measured in an older-age population (>45 years of age) [5]. A lower modulus of elasticity would have shifted c_{MK} as shown in equation (3.11) and resulted in a lower PWV range, as shown by equation (3.16).

An analytical solution was obtained in equation (3.16) that presents PWV in an explicit form as a nonlinear function of the average flow velocity and the peak pressure of the wave. Measured and theoretical values agreed to within 3%. Our model showed the impact of the nonlinear effects of ejection time on PWV, which varied by up to 12% over a clinical range of ejection time. PWV is substantially affected by average flow velocity (~10%) and peak pressure (~2%) changes controlled within the physiological range of LVET, and it is affected to a lesser extent by peak pressure changes alone (~2%). These results are consistent with the conclusions supported by clinical studies of Nurenberg et al. [3] and Salvi et al. [5], regarding LVET as an important predictor of PWV.

We recognize that further work is necessary to incorporate the viscoelastic model of an arterial wall and to solve for PWV at both SBP and DBP. In addition, we recognize

that a set of clinical studies is required to validate this model. To investigate whether our model could be extended for use *in vivo*, we extracted the intra-arterial data from Chen et al. [22] and compared it against our model. Since our model was derived for a linear elastic tube, we use the nonlinear elastic modulus approximation presented by Hughes et al. [23] ($E = E_0 e^{aP}$, where *E* is the elastic modulus adjusted for pressure, E_0 is the elastic modulus at zero pressure, '*a*' is the per-patient constant, and *P* is pressure) to calculate a pressure-dependent c_{MK} for equation (3.16).

To compare the model to the extracted clinical data (19-year-old female, Figure 3.5 (a); and 58-year-old female, Figure 3.5 (b)), c_{MK} was estimated from the zero crossing of an extension of the fitting curve presented in [34]; c_{MK} was ~4.8 m/s and ~5.2 m/s for Figure 3.5 (a) and (b), respectively.

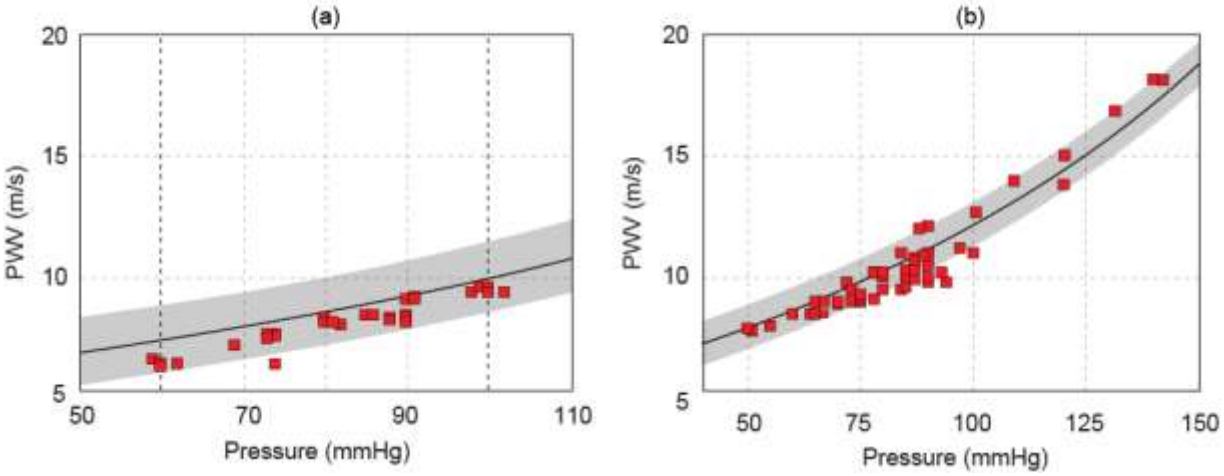

Figure 3.5. Extracted clinical data (squares) [34] of PWV vs intra-arterial blood pressure for a 19-year-old female (a) and a 58-year-old female (b) obtained during surgery. Sweeping the model across the range of possible ejection times and volumes (Table 3.1 footnote) results in the gray region. The solid line represents the best-fit pressure PWV curve for each patient.

The radii for the 19-year-old and 58-year-old patient were selected based on age as 12.2 mm and 15 mm, respectively [8]. The wall thickness and blood density were kept constant at 2.0 mm and 1025 kg/m^3, respectively [8]. Using these values, we calculated

the resulting E_0 using equation (3.11). The per-patient constant '*a'* (left to right a=0.01, 0.009 respectively) was adjusted to closely fit the individual's PWV versus pressure response, which is likely dominated by the dynamic elasticity of the aorta. In both cases, the altered variables were maintained within the clinical range [17,18]. Since ejection volume and time were not measured in the referenced study, the PWV versus pressure relationship was estimated based on the ranges identified in the footnote of Table 3.1. Differences in flow velocity (as determined from ejection time and volume) potentially account for the measured scatter in the PWV versus pressure data points. The model demonstrates the correct curvature, and the expected range (shown in gray) based on flow velocity encompasses most of the measured data points. Data points outside of the expected range could be due to surgically induced changes in ejection time and volume beyond the range assumed for healthy individuals.

By adjusting the per-patient constant '*a*', the model compares closely with the extracted intra-arterial data, as seen in Figure 3.5. Using the best-fit line to the measured data over the range of ejection times and volumes, we calculated an R^2 value between our model and the extracted data Figure 3.5 (a) and (b) of 0.87 and 0.85, respectively. In addition, we generated a histogram and Gaussian fit to the residuals. For both datasets, the residuals fit a Gaussian distribution. This indicates that the delta from the model is likely due to random error, with calculated variance in Figure 3.5 (a) and (b) of +/-1.04 and +/-0.90, respectively.

The finding of a relationship between LVET and PWV may be of clinical importance [3]. Results from Nurenberg et al. [3], Salvi et al. [5], and this study indicate that LVET affects PWV. Large studies of PWV have shown an intra-individual variability

of approximately 10% [1]. Correcting for LVET may allow for a decrease in the measured intra-individual variability and more accurate comparisons between studies. To correct for ejection time, both average flow velocity and wall strain need to be measured and applied to equation (3.16). Average flow velocity can be measured using Doppler ultrasound, and circumferential aortic wall strain can be measured using two-dimensional ultrasound. We recognize that the circumferential wall strain measurement gives a localized measure of arterial stiffness, while the goal of the PWV measurement is a global measure. This global measure typically incorporates multiple bifurcations which are more prone to atheroscerosis. We also recognize that the circumferential wall strain measure is ideally repeated before the start of each PWV measurement. Wall strain is affected by vascular state, which is known to change due to various physiological states and can be influenced by medications.

3.6.3. Non-Invasive Measurements of Elastance

To assess arterial stiffness, the theoretical solution was introduced in an alternative form, explicitly determining arterial compliance as a function of PWV, peak pressure, ejection volume, and ejection time. To determine elastic modulus using the contour plot generated by the theoretical model equation (3.25), shown in supplemental material Figure 3.6, we simply need to know the previously stated measured inputs of the corresponding waveform.

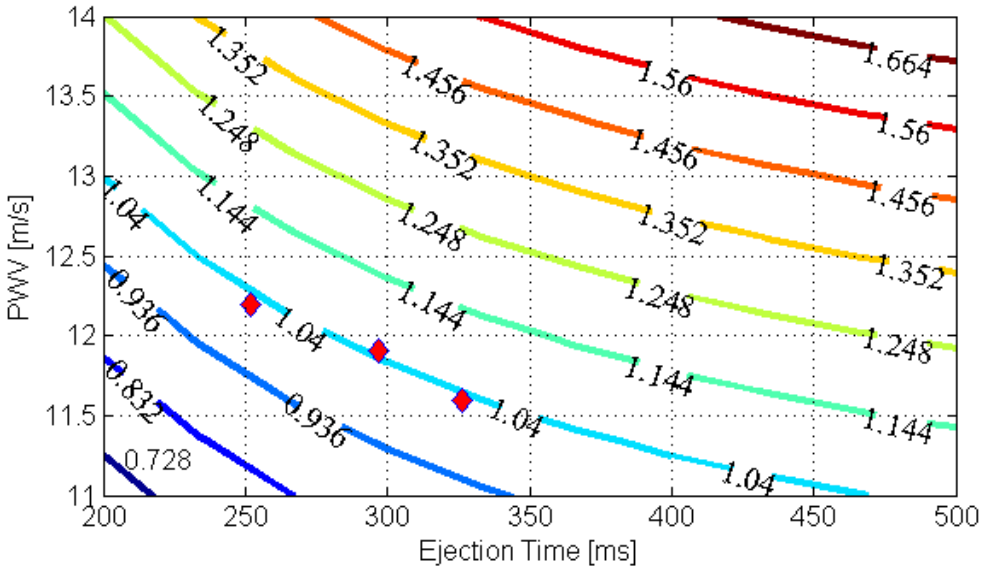

Figure 3.6. Elastance contour plot for fixed ejection volume (66 ml) and peak pressure (140 mmHg). The model calculated a 1.04 MPa elastic modulus based on the measured peak pressure, ejection time, and PWV. The three annotated red diamonds are the model results using measurements taken at ejection times (252, 297, 326). Each of these ejection times had a measured peak pressure of ~140 mmHg.

We used the hemodynamic simulators measured data for ejection times (252, 297, 326 ms) from Table 3.1. The output of the theoretical model was then compared against the measured static elastance for the latex tube. The model calculated an elastance of ~1.04 MPa, with a worst-case percent difference of 2% when compared against the static elastance for the three selected points. The result highlights the point that global compliance was found with a PWV measure using our model.

Figure 3.7 presents contour lines for the correction coefficient C/C_{BH} equation (3.25) for compliance. Setting for instance typical values, $A_\eta = 0.05, \frac{u_0}{c_{MK}} = 0.1$, one can quantify an asymptotic error in the compliance calculation based on equation (3.23) as $(C - C_{BH})/C_{BH} = 0.25$. This means that equation (3.23) overestimates compliance at

this point by ~25%. These new results suggest that Bramwell-Hill theory can overestimate compliance by ~25% within the realistic range of physiological parameters.

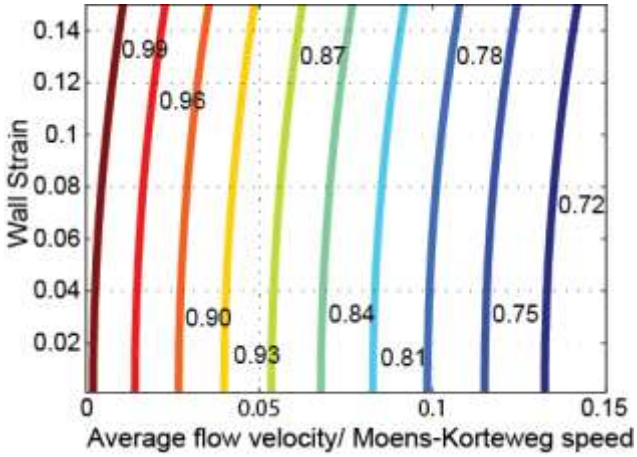

Figure 3.7. Contour plot for the compliance correction coefficients C/C_{BH} , calculated using the ratio of the average flow velocity to the Moens-Korteweg speed ($\boldsymbol{u_0/c_{MK}}$) equation (3.25). The lower lefthand corner of the plot represents $\boldsymbol{C_{BH}}$ ($C/C_{BH}=1$).

.

Knowledge of these properties is clinically important for diagnosis and medical treatment. A decrease in compliance is associated with increased central blood pressure, cardiac afterload, cardiac energy requirements, and decreased coronary perfusion (lower diastolic pressure) [6]. The inverse solution offers the possibility of improving the accuracy of compliance measurement by incorporating the effects of peak pressure and ejection time into the classical Bramwell-Hill compliance equation. The transit time, required for the determination of PWV, can be measured between two flow pulses simultaneously recorded by continuous Doppler probes or sequentially with ECG gating. Measurements are usually made at the root of the left subclavian artery (i.e., suprasternal notch on the skin) and near the bifurcation of the abdominal aorta (i.e., umbilicus level on the skin) [24]. Transit time can be automatically calculated following automatic recognition of the foot of the pulse. To correct for ejection time, both average flow velocity and wall strain must be measured and applied to equation (3.16). Average

flow velocity (u_0) can be measured using Doppler ultrasound and peak circumferential aortic wall strain (A_η); associated volume (V) can be measured using two-dimensional ultrasound. These values can be used with the measured PWV in equation (3.16) to determine $c_{MK,}$ which can then be used in equations (3.22) and (3.25) to determine the aortic compliance.

While initial results are compelling, a complete *in-vitro* analysis using a range of pressures and compliance is needed to validate this model. This work should also include analysis using a more complex viscoelastic model of an arterial wall that accounts for stress relaxation and possibly nonlinear behavior of the arterial wall.

3.7. Conclusion

A traveling wave-based mathematical approach was applied to predict the dependence of PWV on the peak pressure wave and LVET. The presented model incorporates nonlinear convection effects and the inertia of the vibrating wall. The model showed that 12% of the observed change in PWV was caused by ejection time and that 2% of the observed change was caused by peak pressure alone. This insight is important and explains why Nurenberg et al. [3] and Salvi et al. [5] observed that LVET was a predictor of PWV. Our modeling and validation results contribute to the emerging evidence that, both in clinical practice and in clinical research, cardiac systolic function-related variables should be regularly taken into account when interpreting arterial function indices, namely PWV. A predictive model that provides mechanistic insight into the nonlinear effects on PWV (average flow velocity and peak pressure) can be used for future research both *in vivo* and *in vitro*. This work is expanded on in Chapter 4, in which nonlinear, thin-walled elastic arterial segments are modelled. This work is also applied in Chapter 6 to improve blood pressure prediction using systolic flow correction of PWV.

3.8. References

[1] Lebrun C.E., Y.T. Van Der Schouw,A.A. Bak, et. al. , "Arterial Stiffness in postmenopausal women, determinants of pulse wave velocity," *J. Hypertens.*, vol. 20, no. 11, pp. 2165-2172, 2002.

[2] Sutton-Terrel K.,R. H. Mackey,R. Holukbov, et. al. , "Measurement variation of aortic pulse wave velocity in the elderly," *Am. J. Hypertens.*, vol. 14, pp. 463-8, 2001.

[3] Nurnberger J.,A. Saez,S. Dammer,A. Mitchell,R. Wenzel,T. Philipp, R. Schafers , "Left Ventricular ejection time: a potential determinant of pulse wave velocity in young, healthy males," *J. Hypertens.*, vol. 21, no. 11, pp. 2125-2132, 2003.

[4] Blacher J.,R. Asmar,S. Djane,G.M. London,M.E. Safar , "Aortic pulse wave velocity as a marker of cardiovascular risk in hypertensive patients," *Hypertension*, vol. 33, pp. 1111-17, 1999.

[5] Salvi P., C. Palombo, G. Salvl, C. Labat, G. Parati, A. Benetos , "Left ventricular ejection time, not heart rate, is an independent correlate of aortic pulse wave velocity," *J Appl Physiol*, Sept 2013.

[6] Vardoulis O., T. G. Papaioannou, N. Stergiopoulas , "On the Estimation of Total Arterial Compliance from Aortic Pulse Wave Velocity," *Ann. Biomed. Eng.*, vol. 40, no. 12, pp. 2619-2626, Dec. 2012.

[7] Cascaval C.R., "A Boussinesq model for prerssure and flow velocity waves in arterial segments," *Math Comput Simul*, vol. 82, 2012.

[8] Kim E.J., CG Park, JD Park, SY Suh, CU Choi, JW Kim, SH Kim, HE Lim, SW Rha, HS Seo, DJ Oh , "Relationship between blood pressure parameters and pulse wave velocity in normotensive and hypertensive subjects: invasive study," *J Hum Hypertens*, vol. 21, pp. 141-148, 2007.

[9] Laurent S., H. S. Boulder, et al. , "Expert consensus document on arterial stiffness: methodolgical issues and clinical applications," *Eur. Heart J*, vol. 27, pp. 2588-2605, 2006.

[10] Varble N., (2011, June) A Hemodynamic Investigation of a Complete Arteriovenous Model of the Arm, Arteriovenous Fistula, and Distal Revascularization and Interval Ligation. Masters Thesis, https://ritdml.rit.edu/handle/1850/14265.

[11] O'Rourke M., *McDonald's Blood Flow in Arteries: Theoretical, Experimental and Clinical Principles*, 5th ed. USA: Oxford University Press, 2005.

[12] Kung E., C. Taylor , "Development of a Physical Windkessel Module to Re-Create In Vivo Vascular Flow Impedance for In Vitro Experiments," *Cardiovasc. Eng. Tech.*, vol. 2, no. 1, pp. 2-14, March 2011.

[13] Papageogiou G., N. Jones , "Physical modeling of the arterial wall. Part 1: Testing of tubes of various materials," *J. Biomed. Eng.*, vol. 9, no. 2, pp. 153-56, 1987.

[14] Allen J., A. Murray , "Age-related changes in the characteristics of the photoplethysmographic pulse shape at various body sites," *Pysiol. Meas.*, vol. 24, pp. 297-307, 2003.

[15] Chiu Y. C., W. P. Arand, G. S. Shroff , "Determination of pulse wave velocities with computerized algorithms," *American Heart Journal*, vol. 5, no. 121, pp. 1460-1469, May 1991.

[16] Karr A., S. George , "Theoretical and experimental determination of arterial pulse propogation speed," Northwestern University, Illinois, 8225949, 1982.

[17] Klabunde R., *Cardiovascular Physiology Concepts*, 2nd ed. Philadelphia, USA: Lippincott Williams & Wilkins, 2011.

[18] Klingensmith M., L. Chen, S. Glasgow, , *The Washington Manual of Surgery*, S. Melby, Ed. Philadelphia, USA: Wolters Kluwer Health/Lippincott Williams & Wilkins, 2008.

[19] Freis E. D., "Hemodynamics of Hypertension," *Physiol*, vol. 40, no. 27, 1960.

[20] Fullwood F., M. Hawkins, A.J. Cowley Mueller A. F., "The integrated response of the cardiovascular system to food," *Digestion*, vol. 52, pp. 184-193, 1992.

[21] Freis E.D., I. M. Khatri, "Hemodynamic changes during sleep in hypertensive patients," *J Appl Physiol*, vol. 22, no. 867, 1967.

[22] Chen Y., W. Changyun, T. Guocai, B. Min, G. Li , "Continuous and Noninvasive Blood Pressure Measurement: A Novel Modeling Methodology of the Relationship Between Blood Pressure and Pulse Wave Velocity," *Ann. Biomed. Eng*, vol. 37, no. 11, pp. 2222-2233, Nov 2009.

[23] Hughes D., F. Babbs, C. Geddes, "Measurement of Young's modulus of elasticity of the canine aorta with ultrasound," *Ultrasound Imaging 1*, vol. 4, pp. 356-367, 1979.

Chapter 4: Pulse Wave Velocity Prediction in Nonlinear Thin-Wall Elastic Arterial Segments

Science like life feeds on its own decay. New facts burn old rules; then newly developed concepts bind old and new together into a reconciling law. - William James

4.1. Abstract

A new theoretical model for pulse wave propagation in a compliant arterial segment is presented within the framework of pseudoelastic deformation of biological tissue undergoing finite deformation. An essential ingredient is the dependence of results on nonlinear aspects of the model: convective fluid phenomena, hyperelastic constitutive relation, large deformation, and a longitudinal pre-stress load. An exact analytical solution for PWV is presented as a function of pressure, flow, and pseudoelastic orthotropic parameters. Results from the model are compared with published *in-vivo* PWV measurements under diverse physiological conditions. Contributions of each of the nonlinearities are analyzed. It was found that the completely nonlinear model achieves the best match with the experimental data. To retrieve individual vascular information of a patient, the inverse problem of hemodynamics is presented, calculating local, orthotropic, hyperelastic properties of the arterial wall. The proposed technique can be used for non-invasive assessment of arterial elastance, and of blood pressure using direct measurement of PWV.

4.2. Nomenclature

E	Modulus of elasticity (Pa)
PWV	Pulse wave velocity (m/s)
FSI	Fluid structure interaction
BP	Blood pressure
A	Cross-sectional area (m^2)
u	Axial flow velocity (m/s)
p	Transmural pressure (Pa)
ρ	Density of incompressible fluid (kg/m^3)
R,r	Internal wall radii at zero-stress and loaded conditions, respectively (m)
η	Ratio of the wall deflection to R
c_{MK}	Moens-Korteweg speed of propagation (m/s)
H, h	Thickness of the wall at zero-stress and loaded conditions, respectively (m)
F	Axial pretension force (N)
σ_θ, σ_z	Circumferential and axial Cauchy stress components (Pa)
G_θ, G_z	Circumferential and axial Green-Lagrange strain components
$\mathbf{A}$	$\begin{bmatrix} a_{11} & a_{12} \\ a_{12} & a_{22} \end{bmatrix}$ symmetric tensor of material constants (Pa)
Subscripts	
(r,θ,z)	Radial, circumferential, and axial components of a corresponding 3D vector

4.3. Introduction

Historically, PWV has conceptually been based on the Moens-Korteweg equation, which predicts PWV based on an acoustical approach applied to a fluid structure interaction (FSI) of blood flow with a linear elastic cylindrical artery [1]. A nonlinear traveling wave model was developed for a compliant thin-walled linear elastic tube filled with an incompressible fluid [2,3]. This model accounts for the convective ideal fluid flow interacting with a linearly elastic aortic vessel. However, assumptions regarding linear deformation of an arterial vessel are not precisely applicable to living blood vessels, as is proven in numerous related publications [1,4-14]. Nonlinearities in blood vessel elasticity and finite deformation are vitally important to match static testing results for an internal pressure load and an axial tension of a cylindrical artery under physiological conditions [4-7].

The link between PWV or pulse transit time (PTT), and blood pressure (BP) has previously been investigated based on statistical regression models, or empirical representation of an incremental isotropic elastic modulus as a function of a transmural pressure [15-18]. The model proposed here is a physics-based mathematical model that predicts the general relationship between PWV and BP with a rigorous account of nonlinearities in the fluid dynamics model, blood vessel elasticity, finite deformation of a thin anisotropic wall, and a longitudinal pre-stress. The combined effect of BP and blood flow on PWV is derived and agrees with clinical evidence presented in [4,5]. Contributions of the nonlinearity effect, between the published experimental data and theoretical prediction, are analyzed. In order to retrieve the individual vascular

information of a patient, a PWV-based solution for the inverse problem of hemodynamics is used that calibrates the individual orthotropic hyperelastic arterial properties, based on typical diagnostic measurements and an optimization technique. For many materials, linear elastic models do not accurately describe the observed material behavior. The most common example of this kind of material is rubber, whose stress-strain relationship can be defined as nonlinearly elastic, isotropic, incompressible, and generally independent of strain rate. Hyperelasticity provides a means of modeling the stress-strain behavior of such materials. This study is a continuation of the previous work [2,3] in the context of *in-vivo* validation and application of the proposed methodology to continuous, noninvasive blood pressure measurements. The proposed technique can be used for non-invasive assessment of arterial elastance, directly related to the direct measurement of PWV, accounting for hyperelastic orthotropic properties of a biological vessel.

4.4. Theory

4.4.1. *Dynamics of Incompressible Flow in a Compliant Vessel*

One-dimensional models simulating blood flow in arteries effectively describe pulsatile flow in terms of averages across the section flow parameters (systolic flow velocity, diastolic flow velocity). The details of flow separation, recirculation, or shear stress analysis are not calculated in one-dimensional models, but should accurately represent the overall and average pulsatile flow characteristics (particularly PWV). Derivations of one-dimensional models can be found in a number of papers, for example [2,3,21], and are not repeated here.

Conservation of mass and momentum results in the following system of one-dimensional equations:

$$\frac{\partial A}{\partial t} + \frac{\partial}{\partial z}(uA) = 0 \tag{4.1}$$

$$\frac{\partial u}{\partial t} + \frac{\partial}{\partial z}\left(\frac{u^2}{2} + \frac{p}{\rho}\right) = 0 \tag{4.2}$$

The model described by equations (4.1) and (4.2) is applied exclusively to the large arteries, where viscosity is important only in the regions of a boundary layer and has no practical impact on PWV [22,23]. As it follows from monographs of Caro et al. [22] and Li et al. [24], the introduction of viscoelastic, rather than elastic, vessel wall properties results in a slight increase in wave speed, but noticeably affects the attenuation of a waveform. For an impermeable thin-walled membrane, neglecting inertia forces, the vessel pressure-strain relationship is maintained by equilibrium conditions as a function $p=p(\eta)$, based on relevant constitutive relations. Noting that $A = \pi R^2(1+\eta)$, and assuming that transmural pressure is a smooth function of a wall normal deflection

(derivative $p_\eta = \partial p/\partial \eta$ exists at any point), the total system of equations can be presented in the following non-conservative form:

$$\frac{\partial U}{\partial t} + H(U)\frac{\partial U}{\partial z} = 0 \tag{4.3}$$

where

$$U = \begin{bmatrix} \eta \\ u \end{bmatrix}; H = \begin{bmatrix} u & \frac{1+\eta}{2} \\ \frac{p_\eta}{\rho} & u \end{bmatrix} \tag{4.4}$$

The eigenvalues of $H(U)$ are real and distinct. PWV is associated with the forward-running wave velocity (i.e., the largest eigenvalue [26]); hence, it is identified as

$$PWV = u + \sqrt{\frac{1+\eta}{2\rho}p_\eta} \tag{4.5}$$

The partial derivative P_η indicates sensitivity of pressure with respect to the wall normal deflection *η*, and it has a clear interpretation as tangent (incremental) moduli in finite strain inelasticity. The system described by equations (4.1) and (4.2) is typically closed by defining an explicit algebraic relationship between pressure and normal deflection. For example, in case of small deformation and linear elastic response, where *E* is the Young's modulus, v is Poisson's coefficient, and pressure relates to the circumferential strain *η* via

$$p = \frac{\bar{E}H}{R}\eta, \qquad \bar{E} = \frac{E}{1-\nu^2} \tag{4.6}$$

so that equations (4.4) and (4.5) can be transformed to the simplified form derived differently in [2,3,21]

$$PWV = u + c_{MK}\sqrt{1+\eta}, c_{MK} = \sqrt{\frac{\bar{E}h}{2\rho R}} \tag{4.7}$$

Under the assumption $u \ll c_{MK}, \eta \ll 1$ (linearized approach), equation (4.7) converts into the Moens-Korteweg equation for the forward- and backward-travelling waves. In the general case, equation (4.5) should be supplemented by appropriate constituent equations for a hyperelastic anisotropic arterial wall, accounting for finite deformation.

4.4.2. *Hyperelasticity of the Vessel Wall*

It is assumed that arterial wall is hyperelastic, incompressible, anisotropic, and undergoing finite deformation. After a few original loading cycles (preconditioning), the arterial behavior follows some repeatable, hysteresis-free pattern with a typical exponential stiffening effect regarded as pseudoelastic [6,8]. Numerous formulations of constitutive models for arteries have been proposed based on polynomials [9], exponential functions [6,7,10,11], log functions [12], or their mixtures [14], applied to the pseudoelastic strain-energy density formulation. In a comparison paper [13], it is concluded that the exponential descriptor of the passive behavior of arteries, due to Zhou-Fung, is “the best available”. According to Fung et al. [6,7,10], the strain energy density function W for the pseudoelastic constitutive relation may be presented in the form

$$W = \frac{1}{2}c(e^{Q} - 1) \tag{4.8}$$

where *c* is a material coefficient, and *Q* is the quadratic function of the Green-Lagrange strain components. For the finite inflation and extension of a thin-walled cylindrical artery, the following strain energy function is used:

$$Q = a_{11}G_\theta^2 + 2a_{12}G_\theta G_z + a_{22}G_z^2 \tag{4.9}$$

where $c, a_{11}, a_{12}, a_{22}$ are material constants. The Cauchy stress components in circumferential and axial directions are:

$$\begin{aligned} \sigma_\theta &= \lambda_\theta^2 \frac{\partial W}{\partial G_\theta} = c\lambda_\theta^2 e^Q S_\theta, \quad s_\theta = a_{11}G_\theta + a_{12}G_z \\ \sigma_z &= \lambda_z^2 \frac{\partial W}{\partial G_z} = c\lambda_z^2 e^Q S_z, \quad s_z = a_{12}G_\theta + a_{22}G_z \end{aligned} \tag{4.10}$$

With the geometry of the reference state determined, we define R, Z, and H as an internal radius, axial coordinate, and a wall thickness in a stress-free configuration. We define *r, z, h* as an internal radius, axial coordinate, and a wall thickness in a physiologically loaded configuration. The corresponding principal stretch ratios are

$$\lambda_\theta = r/R\,, \lambda_z = dz/dZ\,, \lambda_r = h/H \tag{4.11}$$

Assuming isochoric deformation, incorporate the incompressibility condition as

$$\lambda_z \lambda_\theta \lambda_r = 1 \tag{4.12}$$

The Green-Lagrangian strain components relate to the principal stretch ratios of equation (4.12) by

$$G_i = \frac{1}{2}(\lambda_i^2 - 1), (i = \theta, z, r) \tag{4.13}$$

For the membrane thin-walled cylindrical artery undergoing finite inflation and axial deformation, the load-stress relations follow from the static conditions

$$\sigma_\theta = \frac{pr}{h} = \frac{pR\lambda_\theta}{H\lambda_r} = \frac{pR}{H}\lambda_\theta^2\lambda_z \tag{4.14}$$

$$\sigma_z = \frac{F}{2\pi RH}\lambda_z = f\lambda_z$$

A substitution back into equation (4.10) yields the desired relations:

$$\lambda_z^{-1} c e^{Q} s_\theta = \frac{pR}{h}$$

$$\lambda_z = c e^{Q} s_z = f \tag{4.15}$$

The solution of equations (4.9), (4.13), and (4.15) results in a load-strain relation, which with account of the identity $\lambda_\theta = \frac{r}{R} = \frac{r-R}{R} + 1 = \eta + 1$ converts into $p = p(\eta)$, required by equation (4.5) to predict a wave front speed of propagation (i.e., PWV).

4.4.3. *Numerical Computation of a Tangent Moduli in a Finite Strain Hyperelasticity*

To solve the nonlinear deformation problem from equations (4.9), (4.13), and (4.15), the theory of continuation method is applied [27]. It enables the transformation of algebraic, functional, or differential equations into initial value problems by introducing a parameter and embedding the particular problem into a family of relating parametric problems. When the load parameter $0 \leq \tau \leq 1$ is introduced, and $p \to \tau p$ is substituted, $f \to \tau f$ describes a continuous successive loading on the vessel by internal pressure τp and axial load τf from zero to nominal values. Assume the solution to equation (4.15) depends continuously on load-strain and is differentiable with respect to the parameter τ. Starting from the known answer for a certain value of the parameter ($\tau = 0$ at a stress-free case), the solution to the equation for other values of the parameter may be obtained by integrating the rate of change of the solution with respect

to the parameter. To find the rate of strain components with respect to τ, take the natural log of equation (4.15).

$$\begin{aligned} -\ln\lambda_z + Q + \ln s_\theta &= \ln\tau + ln\frac{pR}{cH} \\ \ln\lambda_z + Q + \ln s_z &= \ln\tau + \ln f \end{aligned} \tag{4.16}$$

and differentiate both sides (the dot above the variable means partial derivative by τ), which yields

$$M(G)\dot{G} = b \tag{4.17}$$

where

$$M(G) = \begin{bmatrix} 2s_\theta^2 + a_{11} & -\dfrac{s_\theta}{1+2G_z} + 2s_\theta s_z \\ 2s_\theta s_z + a_{12} & \dfrac{s_z}{1+2G_z} + 2s_z^2 + a_{22} \end{bmatrix}, \tag{4.18}$$

$$G = \begin{pmatrix} G_\theta \\ G_z \end{pmatrix}, b = \begin{pmatrix} \dfrac{s_\theta}{\tau} \\ \dfrac{s_z}{\tau} \end{pmatrix}$$

As it follows from equation (4.18), when τ =0, a singular point results. To find the strain rates at infinitesimally small τ , the following asymptotic relations deduced from the Taylor expansions in the proximity of a stress-free state ($O(\ldots)$ stands for the asymptotic approximation)

$$G_\theta = \dot{G_\theta}\tau + O(\tau^2), \qquad G_z = \dot{G_z}\tau + (\tau^2) \tag{4.19}$$

$$s_\theta = \left(a_{11}\dot{G_\theta} + a_{12}\dot{G_z}\right)\tau + O(\tau^2), \qquad s_{z=}\left(a_{12}\dot{G_\theta} + a_{22}\dot{G_z}\right)\tau + O(\tau^2)$$

$$\lambda_z = 1 + O(\tau),\ Q = O(\tau^2),\ e^Q = 1 + O(\tau^2)$$

should be substituted into equation (4.15). As a result, the linear equation for the strain rates at τ =0, are $M_0\dot{E}(0) = b_0$, where

$$M_0 = \begin{bmatrix} a_{11} & a_{12} \\ a_{12} & a_{22} \end{bmatrix},\ b_0 = \begin{pmatrix} \frac{pR}{cH} \\ \frac{f}{c} \end{pmatrix} \tag{4.20}$$

Once G is known at $\tau = 0$, equation (4.18) can be integrated to result in

$$G(\tau + \Delta\tau) = G(\tau) + M^{-1}(\tau)b(\tau)\Delta\tau \tag{4.21}$$

The process continues to provide solutions for $\tau = 1$. Once strain components are known, the Cauchy stress components can be calculated from equation (4.14), and stretch ratios and load-deflection relations can be calculated from equations (4.11) and (4.13).

Alternative approaches to solving hyperelastic anisotropic finite strain problems can be found in [28,29] using finite element approximations, and in [30,31], based on finite difference methods.

4.5. Methods

To validate the algorithm, the theoretical prediction of the relationship between circumferential Lagrangian stress component $T_\theta = \lambda_\theta \frac{\partial W}{\partial G_\theta}$ and circumferential stretch ratio λ_θ is compared with experimental results in [7]. Zhou-Fung's work was selected because in a comparison paper [13] it is concluded that the exponential descriptor of the passive behavior of arteries is "the best available". Each loading curve corresponds to the constant value of an axial Lagrange stress component $T_z = \lambda_z \frac{\partial W}{\partial G_z}$ recorded in protocol 2, where the force in the longitudinal direction was held at 4 or 5 constant levels. At each level, the force in the circumferential direction was cycled from the preload to the maximum load and back to the preload in the triangular waveform at 0.05 Hz [7].

Four different models are compared for PWV prediction: the finite deformation hyperelastic (FDH), small deformation hyperelastic (SDH), small deformation linear elastic (SDE), and the Moens-Korteweg (MK) model. The first two models, FDH and SDH, have the same set of variables specifying hyperelastic constants (*c,a11,a12,a22*) within the frame of Fung's model. SDE is obtained from Fung's exponential model accounting for the linear terms only in a Taylor series expansion of Fung's exponential function, presenting potential energy of deformation. The latter results in a quadratic expression for the potential energy, typical for classical linear orthotropic theory of elasticity. In this case, the number of varying parameters was reduced to three, where coefficient *c* appears as the amplification factor for orthotropic constants *a11, a12,* and *a22*. The Moens-Korteweg model is a classical model using a single elastic constant, which is *a priori* independent of pressure.

The FDH model is utilized to determine the material constants noninvasively using PWV versus transmural pressure. Experimental data of Histand and Anliker [33,34], who introduced short trains of artificial, high-frequency waves to measure their propagation speed in canine aorta at different static pressures, was selected. This experiment was selected because it recorded PWV over a wide range of pressures in the aorta. The noninvasive extracted material constants for mongrel dogs are then compared to an invasive method obtained from a biaxial static load of a canine aorta for five mongrel dogs performed by Zhou-Fung [7].

4.6. Results and Discussion

4.6.1. *Algorithm Validation*

The mechanical properties (c=124.5 kPa, a_{11}=0.264, a_{12}=0.379, a_{22}=0.0461) are identified in [7] from experimental data on mongrel dogs' canine aorta, subjected to inflation and longitudinal stretch within the physiological range. The theoretical curves, calculated based on the algorithm described above, are shown in Figure 4.1 as continuous lines. The stress-strain relationship recorded by protocol 2 in [7] is presented by markers for different values of axial stress. The circumferential stress becomes typically nonlinear around $\lambda_\theta = 1.3$, increasing its slope monotonically as shown in Figure 4.1(a). The theoretical prediction is in good correspondence with experimental data within the entire strain range, with the correlation coefficient R^2 exceeding 0.99 for all cases.

Contour lines of an overall residual $\sqrt{R_1^2 + R_2^2}$, where R_1 and R_2 are the individual relative residuals of each of the equations (4.15), are presented in Figure 4.1(b). The accuracy of numerical computation within physiological range of transmural pressure and axial extension force is better than 1%, which justifies application of a numerical scheme as in equation (4.21). An accurate quantification of arterial stiffness is a key factor affecting precision of a PWV prediction.

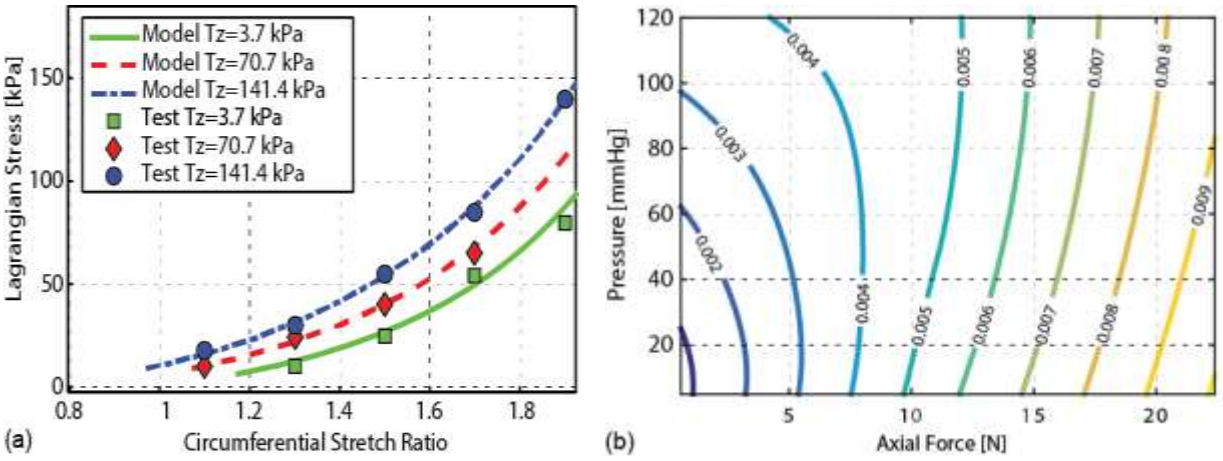

Figure 4.1. The model predictions of stiffness match experimental in-vivo data, which is essential for accurate PWV determination. (a) Dependence of circumferential stress on circumferential stretch ratio during inflation and extension. The comparison of the Zhou-Fung test to our model shows close correlation, with R^2=0.99. (b) Contour lines representing an overall residual of solved equations for different combinations of transmural pressure and extension force.

4.6.2. *Material Properties Identification*

In order to find the relationship between PWV and BP, it is essential to identify the associated material properties of the vessel. Typically, to identify material properties, the fitting process is used, minimizing the least square difference between the measured and predicted stress-strain (or load-displacement curves) [6,7,10]. A PWV-based methodology, evaluating arterial stiffness by minimizing the difference between measured and model-based predicted wave velocities, is presented in [32]. The theoretical model used in [32] is the Moens-Korteweg model, which is based on a linear elastic behavior of the wall undergoing acoustic interaction with internal flow. As a conclusion, the authors affirm “acceptable performance except the region of a soft wall.” Due to the strong evidence of essential hyperelastic nonlinearities coupled with finite deformations [3,25-37], no limitations are applied to the physical and geometric aspects of an arterial wall deformation in the present work. The current chapter investigates a

possibility for the arterial wall properties using a noninvasive PWV-based approach. There is a noticeable formal similarity between material parameters identification problems that are based on measurements of a static pressure versus stretch ratio, and those that are based on a static pressure versus PWV. In both cases, the tangent (incremental) modulus is a key factor affecting modeling. In both cases, the components of Cauchy stress (σ_θ and σ_z) contribute to the solution.

Histand and Anliker results are presented in [1,33,34], and they are reproduced in Figure 4 by square markers as PWV plotted against a single independent variable - transmural pressure. The theoretical model, recast in the form ($\lambda_\theta = \eta + 1$),

$$PWV^{mod} = u + \sqrt{\frac{\lambda_\theta}{2\rho} p_\eta} \tag{4.22}$$

is calibrated based on a subset of four experimental points (shown in Figure 4.2 by solid squares) and verified across the total set of eight experimental points (shown by square markers). The mean flow velocity *u* was estimated using the ratio of $u/PWV = 0.2$ recommended by T.J. Pedley [34]. The fitting process was based on minimization of the sum of squares $\sum_i (PWV_i^{exp} - PWV_i^{mod})^2$, where PWV_i^{exp} and PWV_i^{mod} are the measured and modeled pulse wave velocities corresponding with the i-th experimental data point. The Nelder-Mead algorithm available from the MATLAB Optimization Toolbox was utilized as an optimization tool. The Fung's model material properties [*c, a11, a12, a22*] serve as control variables.

The dashed line in Figure 4.2 indicates theoretical prediction based on the totally nonlinear model (i.e., hyperelastic characterization accounting for the finite deformation). Using properties identified based on the totally nonlinear characterization,

the partially nonlinear model, combining hyperelasticity with a small deformation, was used to create a PWV distribution (shown by the solid line in Figure 4.2). Given the material properties of an arterial wall, the chart indicates proximity of two models in terms of PWV distribution.

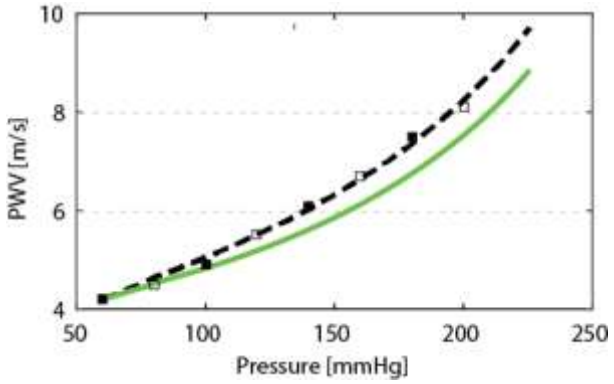

Figure 4.2. The nonlinear model produced the best fit of the PWV vs. transmural pressure function. The dashed line indicates the theoretical prediction. Square markers illustrate the total set of experimental points [31,32]. Solid square markers correspond with the subset of experimental points used for calibration. Using the properties extracted from the nonlinear model, the lower (solid) line shows the effect on PWV using the partially nonlinear model, combining hyperelasticity with small deformation.

The quality of a fitting process accounting for different nonlinearities is presented in Table 4.1, quantified in terms of the error function (sum of squares). Four different models have been compared: the finite deformation hyperelastic (FDH), small deformation hyperelastic (SDH), small deformation linear elastic (SDE), and the Moens-Korteweg (MK) model. Material parameters have been identified for each model independently, based on a best fit procedure. The SDE model is obtained from Fung's model, accounting for the linear terms only in a Taylor series expansion of Fung's exponential function (4.8) of a potential energy of deformation. The latter results in a quadratic expression for the potential energy, typical for a classical linear orthotropic theory of elasticity. In this case, the number of varying parameters was reduced to three: *c*a11, c*a12*, and *c*a22*, since coefficient c appears only as the amplification

factor for orthotropic constants *a11, a12* and *a22*. The Moens-Korteweg model is a classical model using a single elastic constant, which serves as a control variable. The finite deformation hyperelasticity (FDH) model and small deformation hyperelasticity (SDH) model have the highest quality of fitting, creating practically the same model-based regression in Figure 4.2 within the physiological range of BP. The small deformation with linear elasticity (SDL) model and Moens-Korteweg (MK) model cannot be used to predict dependence of PWV on BP. Recall that the SDL model accounts only for the convective flow type nonlinearity [3], whereas the MK model is a totally linear model in which prediction of PWV is independent of pressure.

Table 4.1. Contribution of nonlinearities to the quality of the best fit

Model	FDH	SDH	SDE	MK
Error Function	0.0147	0.0242	1.08	5.16

It is interesting to compare mechanical properties predicted using the PWV-based methodology applied to the FDH model, to those identified *in vivo* by traditional static load. In [7] the thoracic aortas of five mongrel dogs were subjects of a mechanical test in which each specimen was stretched biaxially. From the test measurements, material constants from the Zhou-Fung hyperelastic model were obtained in [7] for canine aortas of mongrel dogs using the least square minimization procedure. The extraction of the corresponding five datasets from [7] fills the columns S1-S5 in Table 4.2. The last column represents the material properties of a canine aorta of a mongrel dog, identified based on an experimentally measured PWV versus BP, obtained by Histand and Anliker [33,34] and the current methodology.

Table 4.2. Material constants, obtained from a biaxial static load of a canine aorta for five mongrel dogs (cases S1-S5), performed by Zhou-Fung [7], and from the present results based on data collected with PWV versus transmural pressure in mongrel dogs in [33,34].

Constants	S1	S2	S3	S4	S5	Present Result
c [mmHg]	901	945	372	1152	1297	1595
a_{11}	0.320	0.289	0.338	0.175	0.200	0.1205
a_{22}	0.451	0.397	0.441	0.314	0.292	0.8080
a_{12}	0.068	0.073	0.010	0.041	0.039	0.001

It can be seen that the proximity of material properties predicted by the described methodology and traditional static test in terms of PWV versus BP distributions are similar. Figure 4.3 illustrates distributions of PWV for Zhou-Fung's five static test cases (S1-S5 columns in Table 4.2) and its counterpart relating to the properties extracted by the present method (the last column of Table 4.2). Except for case S3, which is characterized by an anomalously low material coefficient *c*, the relative variation in PWV prediction does not exceed 4% of all other cases within the range of transmural pressure presented in the figure.

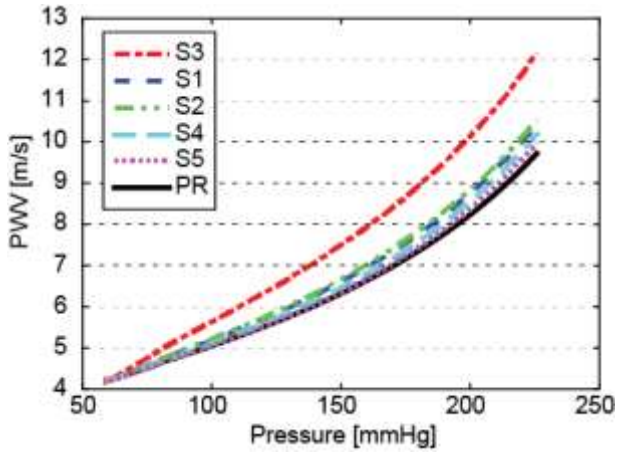

Figure 4.3. The material properties of a canine aorta of mongrel dogs extracted from static measures [7] predict PWV vs. BP distributions in close proximity to those extracted from direct PWV vs. BP experiments [33,34]. S1-S5 and Present Result (PR)-associated material constants are shown in Table 4.2.

According to [35], longitudinal pre-stress may well play a dominant role in wall stress distribution and effective arterial stiffness. To illustrate the effect of a longitudinal

force on PWV, as a result of a numerical simulation, the variation of PWV due to the variability of a longitudinal pre-stress force is presented in Figure 4.4. According to simulation, within the realistic physiological range of a longitudinal stress [36], the relative deviation in PWV does not exceed 3%.

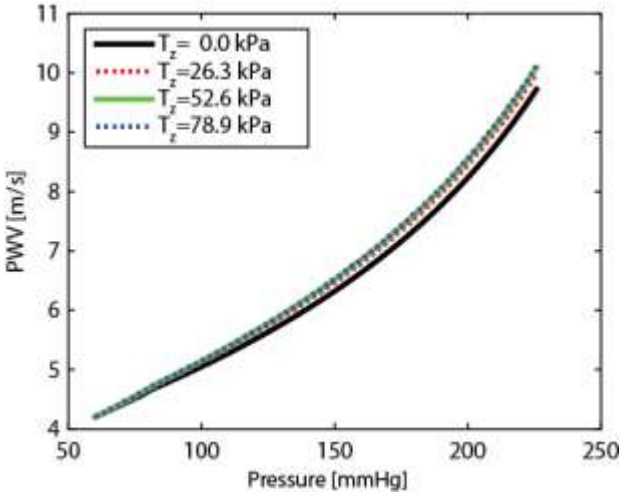

Figure 4.4. Simulation results show that within a physiological range [36], longitudinal pre-stress load affects PWV by ~3%. T_z denotes the axial physiological Lagrangian stress.

4.6.3. *Stability of the Model Convergence*

Theoretically, a least square procedure can lead to a non-unique set of material parameters in the case of a non-convex objective function, when there are a large number of control variables. In general, the problem depends on a convexity of an objective function, and possibly on a particular least square numerical algorithm and starting point of optimization. Stable convergence has been achieved using the Nelder-Mead algorithm available from the MATLAB Optimization Toolbox. Different initial points (corresponding with the five cases presented in Table 4.2) for numerical minimization were used. In each case, all varying material constants, except a_{22}, converged to the same values, which are presented in the last column of Table 4.2. The quality of the fit is characterized by the least square value 0.011 in each case. The coefficient a_{22} varied

from 0.299 to 0.505, which did not affect the distribution of the PWV vs. transmural blood pressure (i.e., the quality of the fit).

4.6.4. *Prediction of Compliance and Distensibility of a Hyperelastic Segment*

Arterial stiffness or its reciprocals (arterial compliance and distensibility) provide an indication of vascular changes that predispose an individual to the development of major vascular disease. In an isolated arterial segment filled with a moving fluid, compliance is defined as a change in a volume *V* for a given change in pressure, and distensibilty as compliance divided by initial volume [1]. As functions of pressure, the local (tangent) compliance *C* and distensibility *D* are defined as [37]

$$C = \frac{dV}{dP}, D = \frac{C}{V} = \frac{dV}{VdP} \tag{4.23}$$

Equations (4.23) determine arterial wall properties as local functions of transmural pressure, contrary to the assessment using the diastolic-systolic pulse pressure.
It is possible to write equations (4.23) in the following equivalent form:

$$C = \frac{dV/d\eta}{dP/d\eta} = \frac{2V}{P_\eta}, D = \frac{C}{V} = \frac{2}{P_\eta} \tag{4.24}$$

For the linear elastic response and small deformation, as it follows from equations (4.6), (4.7),

$$P_\eta = \frac{EH}{R} = 2\rho c_{MK}^2 \tag{4.25}$$

which in turn transforms Equation (4.24) to the classical Bramwell-Hill relations [1]

$$C = \frac{V}{\rho c_{MK}^2}, D = \frac{V}{\rho c_{MK}^2} \tag{4.26}$$

Generalization of a Bramwell-Hill equation, based on an empirical exponential relationship between transmural pressure and a cross-sectional area, was presented in

[34]. Classical results are generalized and discussed for the case of a hyperelastic arterial wall, accounting for finite deformation and flow velocity.

It is possible to determine p_η from equation (4.5) and then substitute it into equation (4.23), arriving at the following relations:

$$D = \frac{1+\eta}{\rho(PWV-u)^2}, C = VD \tag{4.27}$$

Figure 4.5 illustrates the dependency of distensibility on pressure and flow velocity. Because PWV is monotonically increasing with pressure, distensibility is a decreasing function. In the classical Bramwell-Hill model (which is linked to the Moens-Korteweg model), wave speed predicts arterial distensibility as a constant, irrespective of the pressure level. By contrast, the present model predicts distensibility as a function of PWV, pressure, and blood flow.

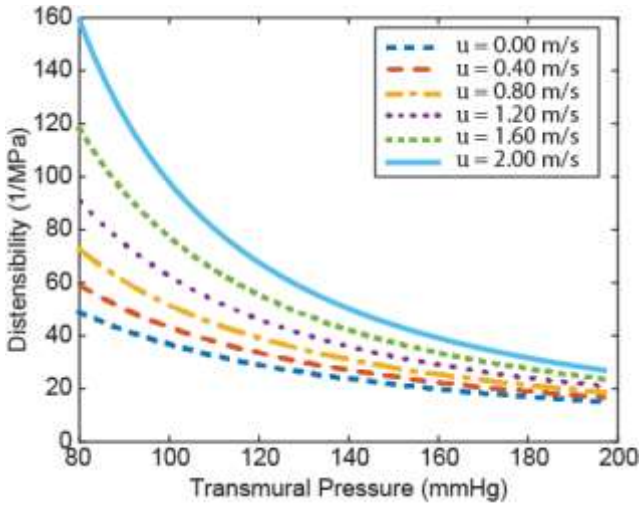

Figure 4.5. Dependence of distensibilty on transmural pressure and a flow velocity.

4.7. Conclusion

A physics-based model predicting PWV in compliant arterial segment is presented within the framework of pseudoelastic deformation of biological tissue undergoing finite deformation. The model is a natural generalization of a Moens-Korteweg-Hughes family of equations [1], which accounts for the constant Young's modulus, or exponentially increasing elasticity as a function of BP. The model was analyzed and validated across the available *in-vivo* experimental data. The method shows potential to be used for non-invasive continuous long-term blood pressure monitoring. This work is expanded upon in Chapter 5, in which nonlinear thick-wall elastic arterial segments are modelled.

4.8. References

[1] O'Rourke M., *McDonald's Blood Flow in Arteries: Theoretical, Experimental and Clinical Principles*, 5th ed. USA: Oxford University Press, 2005.

[2] Liberson A., J. S. Lillie, D.A. Borkholder, "Numerical Solution for the Boussinesq Type Models with Application to Arterial Flow," *JFFHMT*, vol. 1, pp. 9-15, 2014.

[3] Lillie J.S., A.S. Liberson, D. Mix, K. Schwarz, A. Chandra, D.B. Phillips, S.W. Day, D.A. Borkholder, "Pulse wave velocity prediction and compliance assessment in elastic arterial segments," *Cardiovasc Eng Tech*, vol. 6, no. 1, pp. 49-58, Dec 2014.

[4] Cox R. H., "Anisotropic properties of the canine carotid artery in vitro," *J Biomech*, vol. 8, pp. 293-300, 1975.

[5] Demiray H., HW Weizsäcker, K Pascale, HA Erbay , "A stress-strain relation for a rat abdominal aorta," *J Biomech*, vol. 21, no. 5, pp. 369-74, 1988.

[6] Fung Y.C., K. Fronec, P. Patucci , "Pseudo-elasticty of arteries and the choice of mathematical expression," *Am J Physiol-Heart C*, vol. 237, no. 5, pp. H620-31, Nov 1979.

[7] Zhou J., Y.C. Fung , "The degree of nonlinearity and anisotropy of blood vessel elasticity," *Proc Natl Acad Sci*, vol. 94, pp. 14255-14260, 1997.

[8] Holzaphel G.A., T.C. Gasse, R.W. Ogden, , "A new constitutive framework fro arterial wall mechanics and a comparative study of material models," *J Elast*, vol. 61, pp. 1-48, 2000.

[9] Vaishnav R.N., J.T. Young, D.J. Patel, , "Nonlinear anisotropic elastic properties of the canine aorta," *J Biophys*, vol. 12, pp. 1008-1027, 1972.

[10] Chuong C.J., Y.C. Fung, , "Three-dimensional stress distribution in artries," *J Biomech Eng*, vol. 105, pp. 268-274, 1983.

[11] Holzaphel G.A., *Nonlinear solid mechanics. A continuum approach for engineeing*, Chichestre, Ed.: Wiley, 2000.

[12] Takamizawa K., K. Hayashi, , "Strain energy density function and uniform strain hypothesis for arterial mechnaics," *J Biomech*, vol. 20, pp. 7-17, 1987.

[13] Humphrey J.D., "An evaluation of pseudoelastic descriptors used in arterial mechnaics," *J Biomech Eng*, vol. 121, pp. 259-262, 1999.

[14] Humphrey J.D., "Mechanics of arterial wall: review and directions," *Biomed Eng*, vol. 121, pp. 1-162, 1995.

[15] Chen W., T. Kobayashi,S. Ichikawa,Y. Takeuchi,T. Togawa , "Continuous estimation of systolic blood pressure using the pulse arrival time and intermittent calibration," *Med Biol Eng Comput*, vol. 38, pp. 569-574, 2000.

[16] Chen Y., W. Changyun, T. Guocai, B. Min, G. Li , "Continuous and Noninvasive Blood Pressure Measurement: A Novel Modeling Methodology of the Relationship Between Blood Pressure and Pulse Wave Velocity," *Ann. Biomed. Eng*, vol. 37, no. 11, pp. 2222-2233, Nov 2009.

[17] Muehlsteff J., M. Schuett , "Cuffless estimation of systolic blood pressure for short effort bicycle tests: The prominant role of the Pre-ejection period," *IEEE, EMBS*, pp. 5088-5092, Aug 2006.

[18] Zhang Q., Y. Shi, et al. , "Pulse transit time based blood pressure estimation using Hilbert-Huang transform," in *IEEE EMBS*, Minn, Sept 2009, pp. 1785-88.

[19] Nurnberger J., A. Saez,S. Dammer,A. Mitchell,R. Wenzel,T. Philipp, R. Schafers , "Left Ventricular ejection time: a potential determinant of pulse wave velocity in young, healthy males," *J. Hypertens.*, vol. 21, no. 11, pp. 2125-2132, 2003.

[20] Salvi P., C. Palombo, G. Salvl, C. Labat, G. Parati, A. Benetos , "Left ventricular ejection time, not heart rate, is an independent correlate of aortic pulse wave velocity," *J Appl Physiol*, Sept 2013.

[21] Cascaval C. R., "A Boussinesq model for prerssure and flow velocity waves in arterial segments," *Math Comput Simul*, vol. 82, 2012.

[22] Caro C.G., T.J. Pedley, R.C. Schroter, W.A. Seed, The Mechanics of the Circulation, 2nd ed. USA: Cambridge University, 2012

[23] Parkhusrt K. et al “Contribution of blood viscosity in the assessment of flow

mediated dilation and arterial stiffness”, Vascular Medicine, 17 (4), p. 231-234, 2012

[24] Li J., J. Melbin, R. Riffle, A. Noordercraaf “Pulse wave propagation”. Cir.res.,49, 442-452

[25] Sherwin S.J., Franke V., Peiro J., Parker K , "One-dimensional modeling of a vascular network in space-time variables," *Journal of Engineering Mathematics*, vol. 47, pp. 217–250, 2003.

[26] Hirsch C., *Numerical Computation of Internal and External Flows: The Fundamentals of Computational Fluid Dynamics*, 2nd ed.: John Wiley & Sons, 2006.

[27] Grigolyuk E. I., V.I. Shalashilin , *Problems of nonlinear deformation: The continuation method applied to nonlinear problems in solid mechanics*.: Springer, 2012.

[28] Holzaphel G. A., R. Eberlein, P. Wriggeres, H.W. Weizsaker , "A new axisymmetric membrane element for anisotropic, finite strain analysis of arteries," *Comm Num Meth Eng*, vol. 12, pp. 507-517, 1996.

[29] Humphrey J.D., "Cardiovascular Solid Mechanics. Cells, Tissues, adn Organs," *Journal of Biomechanics*, vol. 36, no. 6, 2003.

[30] Wineman A.S., Waldron W. K. , "Normal stress effects induced during circular shear of a compressible nonlinear elastic cylinder," *Int J. Non-Lin Mech*, vol. 30, pp. 323-329, 1995.

[31] Zidi M., M. Cheref, "Finite deformation of a hyperelastic compressible and fiber reinforced tube.," *Eur J Mech Solids*, vol. 21, pp. 971-980, 2002.

[32] Shahmirzadi D., R.X. Li, E.E. Konofagou , "Pulse wave propogation in straight geometry vessels for stiffness estimation: theory, simulations, phantoms and in-vitro findings," *J. Biomech Eng*, vol. 134, no. 11, 2012.

[33] Histand M., M. Anliker, "Influence of flow and pressure on wave propagation in the canine aorta," *Circ Res*, vol. 32, pp. 524-29, 1973.

[34] Pedley T.J., The fluid mechanics of large blood vessels., 2008.

Chapter 5: Pulse Wave Velocity Prediction in Nonlinear Thick-Wall Elastic Arterial Segments

'Principles' and 'Reasons' underlie all good practice. 'Evidence' follows. - William W. Nichols, Michael F. O'Rourke

5.1. Abstract

Pulse wave velocity (PWV) is an important index of arterial hemodynamics, which lays the foundation for continuous, noninvasive blood pressure automated monitoring. Chapter 4 described a nonlinear thin-walled arterial segment with predictions of PWV. The goal of this chapter is to examine the accuracy of PWV prediction based on a homogeneous structural model for thin-walled arterial segments and compare it to the thick wall model. In reality, arteries are described as composite heterogeneous hyperelastic structures, in which the thickness dimension cannot be considered small compared to the cross section size. In this chapter, a hemodynamic fluid-structure interaction model accounting for the variation of geometry and material properties in a radial direction is presented. The model is suitable to account for the highly nonlinear orthotropic material undergoing finite deformation for each layer. Numerical analysis of one- and two-layer arterial segments shows that a single layer thick model provides sufficient accuracy to predict PWV. The dependence of PWV on pressure for three vessels of different thicknesses is compared against our thin wall model of a membrane shell interacting with an incompressible fluid described in Chapter 4. The presented thick wall model provides greater accuracy in the prediction of PWV, and it will be important for blood pressure estimation based on PWV measurements.

5.2. Nomenclature

$\boldsymbol{A}$	$\begin{bmatrix} a_{\theta\theta} & a_{\theta r} \\ a_{\theta r} & a_{rr} \end{bmatrix}$ Symmetric tensor of material constants
A	Cross-sectional area (m^2)
G_θ, G_z	Circumferential and radial Green-Lagrange strain components, respectively
H	Arterial wall thickness (m)
p	Transmural pressure (Pa)
Q	Quadratic function of the Green-Lagrange strains
R_i, R_e	Internal and external wall radii in a zero-stress condition, respectively (m)
u	Axial flow velocity (m/s)
W	Strain energy density function
$\delta_{\alpha\beta}$	Kronecker delta: is 1 if the variables are equal, and 0 otherwise
η	Ratio of the wall internal surface normal displacement to the related radial coordinate (r)
$\lambda_r, \lambda_\theta, \lambda_z$	Stretch ratios in radial, circumferential, and axial directions, respectively
ρ	Density of incompressible fluid (kg/m^3)
σ_θ, σ_r	Circumferential and radial Cauchy stress components (Pa), respectively

5.3. Introduction

The potential of estimating arterial blood pressure based on PWV has been investigated in a number of publications considering a linearized acoustical approach (Moens-Korteweg equation), or its empirical generalization, introducing exponential presentation of the Young's modulus as a function of a blood pressure (BP) [1-3]. A physics-based characterization built by modeling arteries as fluid-filled compliant thin-walled cylindrical membrane shells is presented in Chapters 3 and 4 [4,5]. The present chapter describes a mathematical model predicting PWV propagation with rigorous account of nonlinearities in the fluid dynamics model, blood vessel elasticity, and finite dynamic deformation of multi-layer thick-wall arterial segments. This model is validated within the context of published vessel characteristics and finite element simulations, with extension to PWV and application to continuous, noninvasive blood pressure measurements.

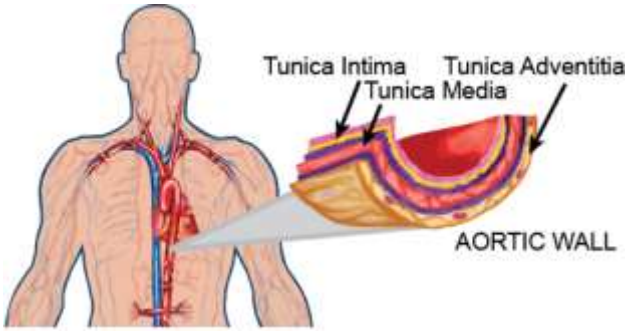

Figure 5.1. The anatomy of the aortic wall.

In the present work, the arterial wall is considered as a heterogeneous composite, hyperelastic structure. Healthy arteries are composed of three distinct layers: the tunica intima (the innermost layer), the tunica media (the middle layer), and

the tunica adventitia (the outer layer), as shown in Figure 5.1. A material description for each layer without thin-wall assumptions is presented, based on a material description of an artery in a passive state originally proposed by Zhou and Fung [6]. A novel mathematical model predicting PWV is proposed, accounting for nonlinear aspects of a convective fluid phenomena, hyperelastic constitutive relations, and finite deformation of a thick arterial wall. The errors introduced by the “thin-” walled assumptions have been explored by Bergel [7] based on a linear elastic model for the vessel walls undergoing small deformations. The present work extends this analysis by accounting more accurately for material properties in arterial hydro-elastodynamics and by comparing the proposed model against our thin wall model described in Chapter 4.

5.4. Theory

5.4.1. Fluid-Structure Interaction Model

One-dimensional models simulating blood flow in arteries effectively describe pulsatile flow in terms of averages across the section flow parameters. Although they are unable to provide the details of flow separation, recirculation, or shear stress analysis, they should accurately represent the overall and averaged pulsatile flow characteristics, particular PWV. Building on the derivation of dynamics of incompressible flow in a compliant thin wall vessel detailed in Chapter 4, section 4.4.1 and references [4,5], the mechanical framework for the thick wall is now considered. For the membrane thin-walled cylindrical artery undergoing finite inflation and axial deformation, the load-stress relations follow from the static conditions. Finite deformation of a thick arterial wall is now considered, and the physical relationships for Cauchy stresses and Green strains are derived.

5.5. Mechanical framework

Consider an axisymmetric case with polar coordinate R describing material point in a load-free state (Lagrangian frame of reference), and a polar coordinate $r = r(R)$ associated with a moving particle (Eulerian description) – in a deformed state. Axial tethering is not considered here, and axial strain component is neglected. The corresponding principal stretch ratios $\lambda_r, \lambda_\theta$ and the Green strains G_r, G_θ, are considered [8].

$$\lambda_r = \frac{dr}{dR}, \lambda_\theta = \frac{r}{R}, G_\alpha = \frac{1}{2}(\lambda_\alpha^2 - 1), (\alpha = r, \theta) \tag{5.1}$$

Numerous formulations of constitutive models for arteries have been proposed in the literature. In a comparison paper [10], it is concluded that the exponential descriptor of the passive behavior of arteries, due to Zhou-Fung, is “the best available”. According to Zhou-Fung [6], the strain energy density function for the pseudoelastic constitutive relation may be presented in the form

$$W = \frac{1}{2}c(e^Q - 1) \tag{5.2}$$

where *c* is the material coefficient, *Q* is the quadratic function of the Green-Lagrange strains G_r, G_θ, and material parameters tensor $\boldsymbol{A}$ [6]. The thick wall model uses tensor $\boldsymbol{A}$ material parameters described by $a_{\theta\theta}, a_{\theta r}, a_{rr}$. For the finite inflation and extension of a thin-walled cylindrical artery in Chapter 4, equation (4.9) material constants $c, a_{11}, a_{12}, a_{22}$ were used. The quadratic function of Green-Lagrange strains is described as

$$Q = a_{\theta\theta}G_\theta^2 + 2a_{\theta r}G_\theta G_z + a_{rr}G_z^2 \tag{5.3}$$

For infinitesimally small strains, the exponential form of energy function is reduced to the following quadratic form that relates to the plane theory of linear anisotropic elasticity.

$$W = \frac{1}{2}c(e^{Q} - 1) = \frac{c}{2}(Q + \frac{Q^2}{2!} + \cdots) \cong \frac{c}{2}(a_{\theta\theta}G_{\theta}^2 + 2a_{\theta r}G_{\theta}G_z + a_{rr}G_z^2) \tag{5.4}$$

The Cauchy-Green stress components are defined as the following [6]:

$$\begin{aligned} \sigma_{\theta} &= \lambda_{\theta}^2 \frac{\partial W}{\partial G_{\theta}} = c\lambda_{\theta}^2 e^{Q} S_{\theta}, \quad S_{\theta} = a_{\theta\theta}G_{\theta} + a_{\theta r}G_r \\ \sigma_r &= \lambda_r^2 \frac{\partial W}{\partial G_r} = c\lambda_r^2 e^{Q} S_r, \quad S_r = a_{\theta r}G_{\theta} + a_{rr}G_r \end{aligned} \tag{5.5}$$

Neglecting inertia forces, the problem of an artery subjected by transmural pressure is described by solving the equation of equilibrium in an Eulerian frame [8]

$$\frac{\partial \sigma_r}{\partial r} + \frac{\sigma_r - \sigma_{\theta}}{r} = 0 \tag{5.6}$$

that could be transformed to the Lagrangian coordinates using equation (5.1)

$$\frac{\partial \sigma_r}{\partial R} + \frac{\lambda_r(\sigma_r - \sigma_{\theta})}{\lambda_{\theta}R} = 0 \tag{5.7}$$

Note that an additional equation for the strains, known as the compatibility equation, follows from equation (5.1)

$$\frac{\partial \lambda_{\theta}}{\partial R} = \frac{\lambda_r - \lambda_{\theta}}{R} \tag{5.8}$$

or, in terms of the circumferential Green strain component

$$\frac{\partial G_{\theta}}{\partial R} = \lambda_{\theta}\frac{\lambda_r - \lambda_{\theta}}{R} = 0. \tag{5.9}$$

The boundary conditions for the internal and external radii of the artery are

$$\sigma_r(R_i) = -p, \sigma_r(R_e) = 0. \tag{5.10}$$

Equations (5.1), (5.5), (5.7), and (5.9) and the boundary conditions defined in equation (5.10) allow components of stress, strain, and stretch ratios as functions of a transmural pressure, as well as incremental moduli of hyperelastic finite deformation (required by equation 4.5) to predict a wave front speed of propagation (i.e., *PWV*).

In view of numerical analysis, we have to derive the tangent moduli (D) by differentiation of a stress-strain relationship (12) ($\delta_{\alpha\beta}$- Kronecker delta: is 1 if the variables are equal and 0 otherwise)

$$\mathrm{D}_{\alpha\beta} = \frac{\partial \sigma_\theta}{\partial \mathrm{G}_\beta} = \mathrm{c}\lambda_\alpha^2 \mathrm{e}^{\mathrm{Q}} \left(\mathrm{a}_{\alpha\beta} + 2S_\alpha S_\beta + \frac{2S_\alpha}{\lambda_\alpha^2} \delta_{\alpha\beta} \right), \qquad \alpha, \beta = \mathrm{r}, \theta \tag{5.11}$$

5.5.1. Continuation Method for the Nonlinear Boundary Value Problem

The theory of the continuation method enables the transformation of a boundary value problem into an initial value problem, by introducing a parameter and changing it into a family of parametric problems [9]. Assuming a load parameter $0 \leq \tau \leq 1$ and substituting $\rightarrow \tau p$, it is possible to model the continuous successive load on a vessel with an internal pressure ranging from 0 to a nominal value. Assume that the solution of equations (5.1) through (5.10) depends continuously on this parameter and is differentiable with respect to this parameter. Starting from the known answer for a certain value of the parameter ($\tau = 0$ in the present case), the solution of the equation for other values of the parameter may be obtained by integrating the rate of change of the solution with respect to the parameter.

Differentiating constituent equations (5.5) by the continuation parameter (the dot above means partial derivative with respect to τ), yields

$$\dot{\sigma_\alpha} = \sum_\beta D_{\alpha\beta}\dot{G}_\beta,\ \alpha,\beta = r,\theta \tag{5.12}$$

To solve the problem numerically, select the vector variable $\boldsymbol{Z} = (\sigma_r, G_\theta)^T$ as the primary variable in the model, because it preserves continuity for the multilayered structure with discontinuous mechanical properties. The rate of "discontinuous" variables $Y = (\sigma_\theta, G_r)^T$ follows from equation (5.12) accordingly

$$\dot{\boldsymbol{Y}} = \boldsymbol{B}\dot{\boldsymbol{Z}},\ \boldsymbol{B} = D_{\theta\theta}^{-1}\begin{pmatrix}\det(\boldsymbol{D}) & D_{r\theta}\\ -D_{\theta r} & 1\end{pmatrix} \tag{5.13}$$

To differentiate equation (5.7) by τ, expand the logarithm of the right part $F = \lambda_r\lambda_\theta^{-1}(\sigma_\theta - \sigma_r)/R$

$$\ln F = \ln\lambda_r - \ln\lambda_\theta + \ln(\sigma_\theta - \sigma_r) - \ln R \tag{5.14}$$

and take derivatives of both sides

$$\frac{d\dot{\sigma}_r}{dR} = \dot{F} = F\left(\frac{\dot{G}_r}{\lambda_r^2} - \frac{\dot{G}_\theta}{\lambda_\theta^2} + \frac{\dot{\sigma}_\theta - \dot{\sigma}_r}{\sigma_\theta - \sigma_r}\right) \tag{5.15}$$

Using a similar procedure, applied to the compatibility equation, yields equation (5.16)

$$\frac{d\dot{G}_\theta}{dR} = \frac{\lambda_\theta}{R\lambda_r}\dot{G}_r + (\frac{\lambda_r}{R\lambda_\theta} - \frac{2}{R})\dot{G}_\theta \tag{5.16}$$

Now equations (5.15) and (5.16) could be presented in a matrix form

$$\frac{d\dot{\boldsymbol{Z}}}{dR} = \boldsymbol{C}_1\dot{\boldsymbol{Z}} + \boldsymbol{C}_2\dot{\boldsymbol{Y}} \tag{5.17}$$

in which

$$C_1 = \begin{pmatrix} \dfrac{-F}{\sigma_\theta - \sigma_r} & \dfrac{-F}{\lambda_\theta^2} \\ 0 & \dfrac{\lambda_r}{R\lambda_\theta} - \dfrac{2}{R} \end{pmatrix};\ C_2 = \begin{pmatrix} \dfrac{-F}{\sigma_\theta - \sigma_r} & \dfrac{-F}{\lambda_r^2} \\ 0 & \dfrac{\lambda_\theta}{R\lambda_r} \end{pmatrix} \tag{5.18}$$

substituting equation (5.13) into equation (5.17) arrives at the final differential equation

$$\frac{d\dot{Z}}{dR} = \boldsymbol{C}\dot{\boldsymbol{Z}}, \boldsymbol{C} = \boldsymbol{C}_1 + \boldsymbol{C}_2\boldsymbol{B} \tag{5.19}$$

with the boundary conditions, obtained by differentiation of the boundary conditions in equation (5.10). (Note that pressure in equation (5.10) is being multiplied by τ, and $\boldsymbol{I} = [1 \quad 0]$.)

$$\boldsymbol{I} \cdot \boldsymbol{Z}(R_i) = -p;\ \boldsymbol{I} \cdot \boldsymbol{Z}(R_e) = 0 \tag{5.20}$$

The initial parameter method presumes the solution of the linear boundary value problem described in equation (5.19) to be represented in the form

$$\dot{\boldsymbol{Z}} = \dot{\boldsymbol{Z}}_1 + \mu\dot{\boldsymbol{Z}}_2 \tag{5.21}$$

Here the vector functions $\dot{\boldsymbol{Z}}_1, \dot{\boldsymbol{Z}}_2$ are independent solutions of equation (5.19) with the following initial conditions

$$\dot{\boldsymbol{Z}}_1(0) = (-p \ \ 0)^T,\ \dot{\boldsymbol{Z}}_{\boldsymbol{2}}(0) = (0 \ \ 1)^T \tag{5.22}$$

and μ is an unknown constant determined from the second boundary condition in equation (5.20).

$$\mu = -\frac{\boldsymbol{I} \cdot \boldsymbol{Z}_1(R_\mathrm{e})}{\boldsymbol{I} \cdot \boldsymbol{Z}_2(R_\mathrm{e})} \tag{5.23}$$

Once $\dot{\boldsymbol{Z}}$ is known at $\tau = 0$, then vector $\boldsymbol{Z}$ of continuous variables and vector $\boldsymbol{Y}$ of discontinuous functions could be calculated by integrating the relating rate of change

$$\boldsymbol{Z}(\tau + \Delta\tau) = \boldsymbol{Z}(\tau) + \dot{\boldsymbol{Z}}(\tau)\Delta\tau$$

$$\boldsymbol{Y}(\tau + \Delta\tau) = \boldsymbol{Y}(\tau) + \boldsymbol{B}\dot{\boldsymbol{Z}}(\tau)\Delta\tau \tag{5.24}$$

The above process continues to obtain solutions for $\tau = 1$. The pressure versus normal displacement $p = p(\eta)$ is tracked at $R = R_i$ for each level of successively increasing load to create an incremental moduli $p(\eta)$ function, required by equation (4.5) to predict a wave front speed of propagation (i.e., PWV).

5.6. Results and Discussion

To validate the algorithm, the numerical investigation of an inflated rabbit carotid arterial segment is presented and compared with the results based on a finite element analysis, obtained by Holzaphel et al. [10]. The rabbit arterial data presented by Chuong and Fung [11]: c=26.95kPa; $a_{\theta\theta} = 0.9925$, $a_{\theta r} = 0.0193$, $a_{rr} = 0.0089$, R_i=0.71 mm, R_e = 1.1 mm (from experiment number 71) is used. Figure 5.2 (a) shows the predicted mechanical response of the considered artery. Squares relate to the finite element analysis [10] and are in good agreement with the results based on our present single layer thick wall model. The derivative p_η of pressure by radial displacement of an internal surface (i.e., hyperelastic incremental moduli), presented in Figure 5.2 (b), is a primary factor affecting PWV in a cylinder filled with a moving fluid according to equation (4.5). At diastolic pressure when flow is close to zero, PWV is dominated by the physical anisotropic properties of the aorta. At systolic pressure, the pulse wave velocity is also affected by flow velocity, which may be approximated as 20-25% of PWV according to Pedley [15].

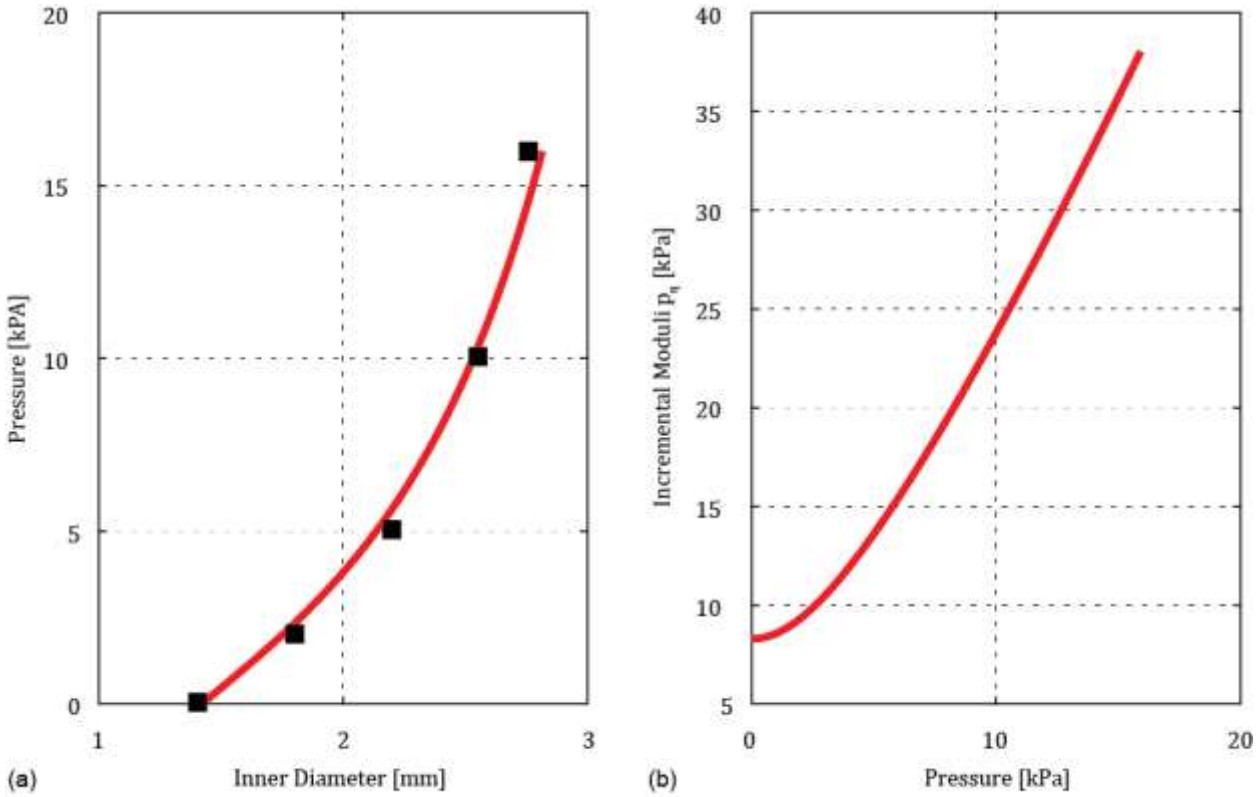

Figure 5.2. Mechanical response of a carotid artery from a rabbit during inflation. a) depicts the dependence of the inner diameter on internal pressure. The solid line is a prediction based on our single-layer thick wall model that is in good correlation with the results (squares) from [10]. b) depicts incremental moduli p_η of the hyperelastic artery (i.e., derivative of a pressure by the radial displacement η).

A single layer thick wall model with homogeneous mechanical properties does not account for the distinct mechanical response of the separate layers (intima, media, and adventitia). Since the intima contributes negligible mechanical strength [10], a two-layer model, incorporating media and adventitia only, is analyzed. Following [10,12], assume that media occupies approximately 0.6 of the arterial wall thickness. Experimental tests indicate that media is about ten times stiffer that adventitia [12,13], which allows to scale accordingly material properties tensor ***A***. Figure 5.3 depicts predicted mechanical response of the considered artery, calculated based on a single layer thick wall model (dashed lines) and a two-layer-thick wall model (solid lines). The

circumferential Cauchy stress is plotted in Figure 5.3 (a), normal displacement in Figure 5.3 (b), and radial component of Green strain in Figure 5.3 (c), all against the radial coordinate. The abrupt change in mechanical properties at the boundary between media and adventitia results in a sharp discontinuity of circumferential stress and radial strain components. Radial displacement is a continuous function, deviating slightly from the single-layer counterpart as shown in Figure 5.3 (b). In the proximity of the internal cylindrical surface, distributions of all parameters calculated by both models (1 layer, 2 layers) are identical as seen in Figure 5.3. Since PWV is determined by the local wall stiffness, relating to the internal cylindrical surface, the latter justifies application of the single layer thick model to the PWV-related problems.

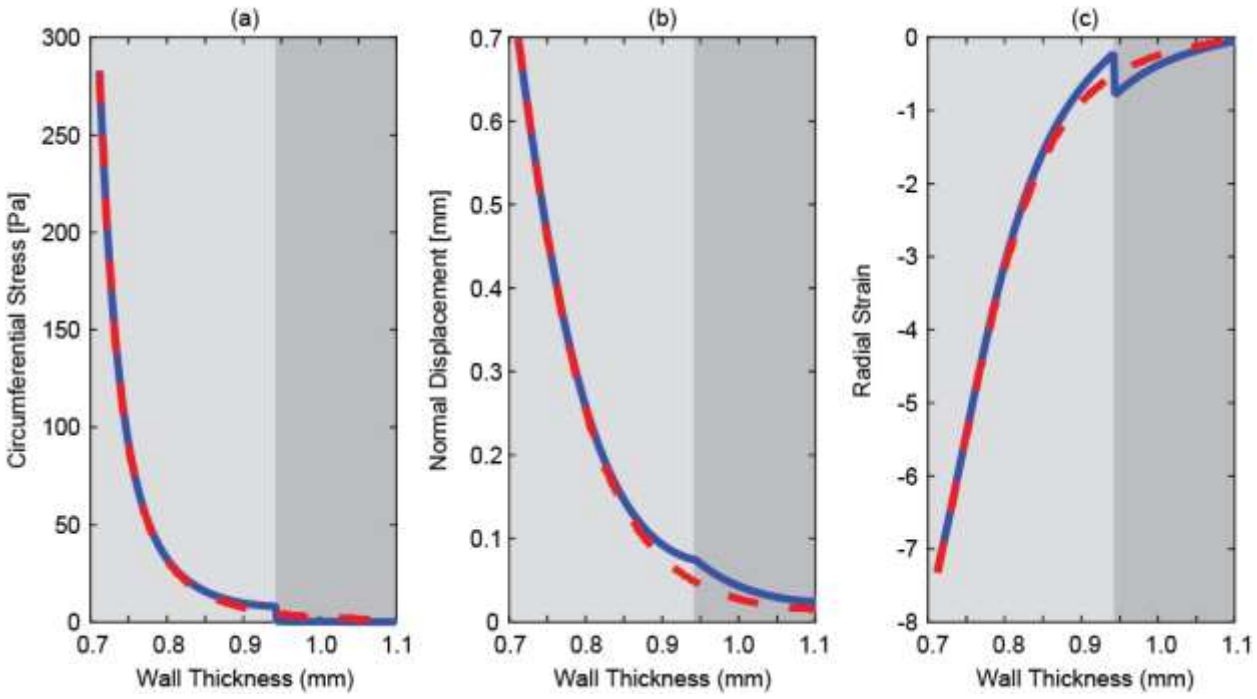

Figure 5.3. Single layer thick wall model (dashed line) is as accurate for PWV prediction as the two-layer thick wall model (solid line) and avoids associated discontinuities. Plots of circumferential Cauchy stress (a), normal displacement (b), and radial component of a Green strain (c) through the wall thickness. For the two-layer model, the light gray represents the media and the dark gray represents the adventitia layer.

Figure 5.4 depicts the dependence of PWV on pressure for the systole phase (marked as “SBP”) and a diastole phase (marked as “DBP”) for three vessels of different thicknesses of a human aorta. The anisotropic material constants for a human aorta with an outer radius of 14.5 mm are taken from Fung et al. [14]. The inner radius is then set based on the three wall thicknesses considered in Figure 5.4. Following [15], assume here that the flow velocity $u = 0$ for the diastole phase and that it is equal to 20% of PWV for the systole phase. All results have been compared with the simplified thin-walled model of a membrane shell interacting with an incompressible fluid [5].

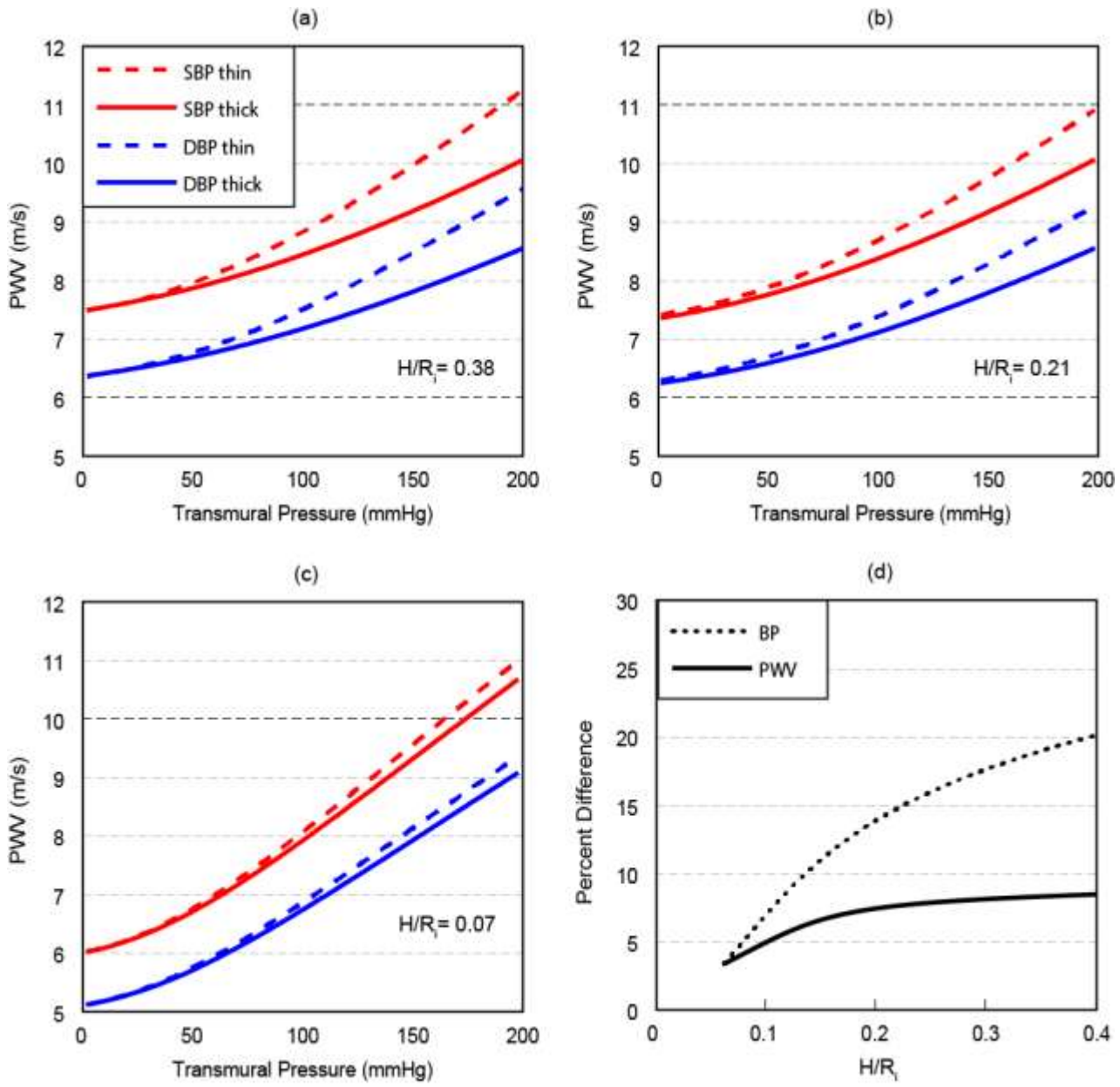

Figure 5.4. PWV curves for systolic blood pressure (SBP) and diastolic blood pressure (DBP) for the nonlinear single layer thin and thick aortic wall. Figure 5.4 (a) corresponds to the vessel thickness of H = 4 mm, $H/R_i = 0.38$; Figure 5.4 (b) to H = 2.5 mm, $H/R_i = 0.21$; Figure 5.4 (c) to H = 1 mm, $H/R_i = 0.07$; Figure 5.4 (d) to the percent difference between the thin and thick wall model predictions at SBP/DBP = 150/95 mmHg for PWV (solid line) and blood pressure (dotted line).

The analysis presented in Figure 5.4 considers normal wall thicknesses of less than 4 mm [16] across a range of transmural blood pressures. To explore inaccuracies induced by use of the less complex thin wall model, errors in both PWV and blood pressure were calculated for a blood pressure of SBP/DBP = 150/95 mmHg, representing the median of stage 1 hypertension [17]. The single layer thick wall model improves PWV accuracy by 4.0-8.4% across a range of normal wall thickness. One of the goals for the model is PWV-based blood pressure prediction, where the thick wall model offers an improvement of 3.3-19.4%. Accuracy improvements are highly dependent on the relative dimensions of wall thickness to arterial radius**.** As the ratio of H/R_i approaches zero, the error of PWV prediction approaches zero, showing an asymptotic accuracy as an order of wall thickness to internal radius ratio.

5.7. Conclusion

A novel mathematical model predicting PWV propagation with rigorous account of nonlinearities in the fluid dynamics model, blood vessel elasticity, and finite deformation of multi-layer thick-wall arterial segments was studied. It was found that the account for the multilayer model affects distribution of local parameters in the proximity of the external layer (adventitia) and does not affect stiffness related to the internal layer. The latter means that the single layer thick model is sufficient to predict PWV of an arterial segment. For a hypertensive subject, the three-dimensional thick- wall model provides improved accuracy up to 8.4% in PWV prediction over its thin-wall counterpart. This translates to nearly 20% improvement in blood pressure prediction based on a PWV measure.

5.8. References

[1] Nichols W., M. O'Rourke. McDonald's blood flow in arteries. Theoretical, experimental and clinical principles. 6 ed., 2011, Hodder-Arnold, 755p

[2] Chen W., T. Kobayashi, S. Ichikawa, Y. Takeuchi, T. Togawa , "Continuous estimation of systolic blood pressure using the pulse arrival time and intermittent calibration," *Med Biol Eng Comput*, vol. 38, pp. 569-574, 2000.

[3] Chen Y., W. Changyun, T. Guocai, B. Min, G. Li , "Continuous and Noninvasive Blood Pressure Measurement: A Novel Modeling Methodology of the Relationship Between Blood Pressure and Pulse Wave Velocity," *Ann. Biomed. Eng*, vol. 37, no. 11, pp. 2222-2233, Nov 2009.

[4] Liberson A. S., J. S. Lillie, D.A. Borkholder , "Numerical Solution for the Boussinesq Type Models with Application to Arterial Flow," *JFFHMT*, vol. 1, pp. 9-15, 2014.

[5] Lillie J.S., A.S. Liberson, D. Mix, K. Schwarz, A. Chandra, D.B. Phillips, S.W. Day, D.A. Borkholder, "Pulse wave velocity prediction and compliance assessment in elastic arterial segments". *Cardiovasc Eng Tech,* vol. 6*,* pp. 49-58*, Dec 2014*.

[6] Zhou J., Y.C. Fung , "The degree of nonlinearity and anisotropy of blood vessel elasticity," *Proc Natl Acad Sci*, vol. 94, pp. 14255-14260, 1997

[7] Bergel D.H., The dynamic elastic properties of the arterial wall. Journal of Physiology 156, 458-69, 1961

[8] Humphrey J.D., "Cardiovascular solid mechanics. Cells, tissues, and organs.", P.757,Springer, 2002

[9] Grigolyuk E. I., V.I. Shalashilin , Problems of nonlinear deformation: The continuation method applied to nonlinear problems in solid mechanics.: Springer, 2011.

[10] Holzapfel G.A., T. Gasser, R.W. Ogden , "Comparison of Multi-Layer Structural Model for Arterial Walls With a Fung-Type Model, and Issues of Material Stability," *Trans of ASME*, vol. 126, April 2004.

[11] Chuong C.J., Fung Y.C., 1983, “Three dimensional stress distribution in arteries”, J.Biomech. Eng, 105, pp.268-274

[12] Schulze-Bauer C.A., G.A. Holzaphel, 2003, “determination of constitutive Equations for human arteries from clinical data”, J.Biomech., 36, pp.185-189

[13] Yu Q., Zhou J., Y.C.Fung., 1993. ,”Neutral axis location in bending and Young’s modulus of different layers of arterial wall”, AM Jo. Physiol., 265,pp.301-312

[14] Zhou J., Y.C. Fung , "The degree of nonlinearity and anisotropy of blood vessel elasticity," *Proc Natl Acad Sci*, vol. 94, pp. 14255-14260, 1997

[15] Pedley T.J., The fluid mechanics of large blood vessels, 2008. 439 P.

[16] Raimund E., H. Eggebrecht , "Aortic Dimensions and the Risk od Disection," *Heart*, vol. 92, pp. 137-142, 2006

[17] Giuseppe M., R. Fagard, "2013 ESH/ESC Guidelines for the management of arterial hypertension," J Hypertens 2013, 31:1281–1357

Chapter 6: Improved Blood Pressure Prediction Using Systolic Flow Correction of Pulse Wave Velocity

Hence, the more rapidly moving elements of a wave will tend to catch up to those which are moving more slowly; in other words the wave will tend to become more vertical, and, under suitable conditions, parts of it may actually tend to topple over and form "breakers." - J. Crighton Bramwell and A. V. Hill; July 7, 1923

6.1 Abstract

Hypertension is a significant worldwide health issue. Continuous blood pressure monitoring is important for early detection of hypertension and for the improvement of treatment efficacy and compliance. Pulse wave velocity (*PWV*) has the potential to allow for a continuous blood pressure monitoring device; however, published studies demonstrate significant variability in relating PWV to blood pressure. In Chapters 3, 4, and 5, the presented physics-based mathematical models of *PWV* describe how flow velocity is additive to the classic pressure wave as estimated by arterial material properties. This suggests flow velocity correction may be important for cuff-less non-invasive blood pressure measures. The present study examined the impact of systolic flow correction of a measured *PWV* on blood pressure prediction accuracy using data from two published *in vivo* studies. Both studies examined the relationship between *PWV* and blood pressure under pharmacological manipulation, one in mongrel dogs and the other in healthy adult males. Systolic flow correction of the measured *PWV* improves the R^2 correlation with blood pressure from 0.51 to 0.75 for the mongrel dog study, and from 0.05 to 0.70 for the human subjects study. The results support the hypothesis that systolic flow correction is an essential element of non-invasive, cuff-less blood pressure estimation based on *PWV* measures.

6.2 Introduction

Pulse wave velocity (*PWV*) is a non-invasive measure that offers the promise to continuously monitor blood pressure and has been studied extensively [4-7]. The *PWV* is calculated based on a measured true transit time (TT) and an arterial distance between measurement points, as shown in Figure 6.1. Measurements may be at two locations on the same artery, or often the electrocardiogram (ECG) R-wave is used as a starting reference combined with a distal measurement point with or without correction for pre-ejection period (PEP). While many studies consider only TT, it may be considered an equivalent corollary to *PWV* because these measures are linked through a distance that is constant within each study.

Intra-arterial PWV	
Gold-standard Invasive Method	Simultaneous pressure recorded invasively with pressure sensors just before the aortic root [a] and above the aortic bifurcation [b]
Alternative Method	Sequential ECG-gated recordings, just before the aortic root [a] and above the aortic bifurcation [b]
Distance	Length measured by radiographic images or catheter lengths
Non-invasive PWV	
Gold-standard Method	Simultaneous carotid [c] and femoral artery tonometry [d]
Alternative Method	ECG R-wave, impedance plethysmography for PEP, and distal pulse wave at the index finger [e]
Distance	Length measured from the sternal notch to the femoral artery at the groin or index finger

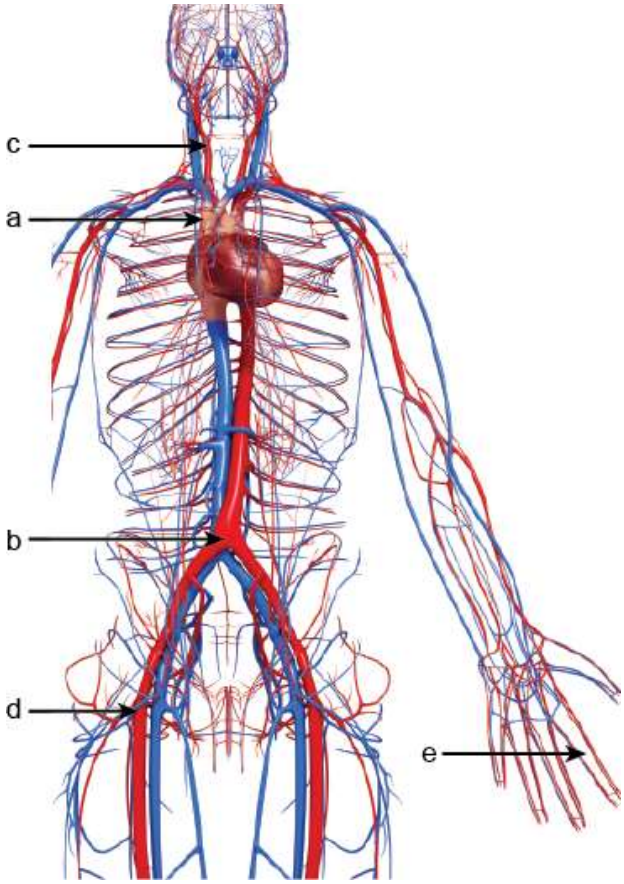

Figure 6.1. Illustration of measurement methods used for PWV and the associated anatomical locations.

Bramwell and Hill recognized that an increase in pressure increases the pulse wave velocity. They concluded that the foot-to-foot wave velocity increased proportional to diastolic pressure [11,12*]*. In their innovative experiment, they replaced blood with mercury to reduce wave velocity. This enabled accurate measurement of *PWV* in an excised human carotid artery. Varying pressure from 20 mmHg to over 200 mmHg, they found an exponential relationship between *PWV* and pressure. Continuing experiments, where the velocity of different points on the pressure wave were measured optically and with a sphygmograph, suggests that the systolic peak of the pressure pulse travels at higher velocity than the diastolic foot *[*12*]*. Histand and Anliker superimposed a low-amplitude pulse train directly on the aorta to enable *PWV* calculations at different

locations on the pulse wave (SBP, DBP) [13]. They found a wave speed change of ~30% between diastole and systole. The interesting implication is that pressure pulse foot-based *PWV* estimations are likely correlated with diastolic pressure, an implication supported by *in vivo* studies. Researchers have used this knowledge and empirically modified the c_{MK} equation (1.1) to use the dynamic Young's modulus equation (1.2) to incorporate blood pressure into the Moens-Korteweg equation [10,14].

Payne et al. conducted an *in vivo* study to determine the correlation between blood pressure and transit time in twelve healthy men [15]. Four vasoactive drugs (glycerol trinitrate, angiotensin II, norepinephrine, and salbutamol) were administered intravenously to modulate physiological state. Two types of transit time were considered: ECG R-wave to the foot of the distal pulse wave (rPTT), and ECG R-wave to the foot of the distal pulse wave minus PEP to provide an estimate of TT. In both cases, the distal pulse wave was measured using photoplethysmography at the dominant index finger. They found TT was most closely correlated with diastolic blood pressure (DBP) R^2=0.85, while rPTT was most closely correlated with systolic blood pressure (SBP) R^2=0.39.

Ochiai et al. conducted a similar *in vivo* study with ten mongrel dogs that determined the correlation between blood pressure and *PWV* [16]. Hypertension was induced by continuous infusion of dobutamine and phenylephrine; hypotension was induced by deepening isoflurane anesthesia, acute blood loss, and nitroglycerine infusion. Two types of transit time were considered: rPTT measured by the ECG R-wave to the foot of the pressure wave measured at the bifurcation of the abdominal aorta, and TT measured by the pressure wave at the ascending aorta to the pressure

wave measured at the bifurcation of the abdominal aorta. Two intra-arterial catheter tip pressure transducers were placed distal to the aortic root and abdominal aorta bifurcation as shown in Figure 6.1, locations a and b, respectively. They found that TT was most closely correlated with both DBP (R^2=0.92) and SBP (R^2=0.81) across all conditions. The correlation of TT with both DBP and SBP, and rPTT with SBP (R^2=0.59) were higher for Ochiai et al. than the correlations found by Payne et al., likely due to the internal aortic measurement locations. It is known that some of the drugs used in the studies affect the elastic arteries differently than the muscular arteries [17]. Nitroglycerin, for example, produces a peripheral vascular effect by relaxing the smooth muscle. The mid-sized peripheral arteries are muscular in nature and thereby susceptible to nitroglycerin action.

Other studies have considered the effect of left ventricular ejection time (LVET) and its relationship to pressure and *PWV* [6,18,19]. Nurnberger et al. conducted a study of young, healthy males to determine if LVET was a determinant of *PWV* [*6*]. He studied 102 subjects under resting conditions and then six subjects under stimulation of β- or α-adrenoreceptors. They found that LVET may be an important determinant of *PWV* under resting conditions and adrenergic conditions in healthy young males. A similar study over a large population of 3020 untreated subjects was conducted by Salvi et al. [19]. They found an inverse linear association between *PWV* and LVET across all five age groups (<25yrs, 25-44yrs, 45-64yrs, 65-84yrs, and >85 yrs.; $p < 0.0001$, R^2=0.35).

In Chapters 3-5, a nonlinear traveling wave-based mathematical approach to predict the dependence of *PWV* on transmural pressure and LVET was developed. This first principles model reduces to the Moens-Korteweg speed of propagation under

conditions of linear elasticity and zero pressure. An *in-vitro* cardiovascular hemodynamic simulator was used to validate the theoretical predictions confirming an inverse quadratic relationship between LVET and PWV [20]. However, the fundamental equations suggest that it is flow velocity and the properties of the aortic wall, and not LVET explicitly, that influence *PWV* in arterial segments. In this study, we found analytically and empirically that flow velocity is additive to the *PWV* predicted based on pressure and material properties alone.

Although published results establish correlation between SBP or DBP and measures of pulse wave velocity (*PWV*, TT, rPTT), no measure has emerged as a robust predictor of blood pressure across the full physiologic range. The aim of this study is to test the theory that accounting for the flow contribution to *PWV* based on fundamental physics of wave propagation in nonlinear elastic arteries will improve overall blood pressure prediction. The approach used is based on a novel mathematical model predicting *PWV*, accounting for nonlinear aspects of a convective fluid phenomena, hyperelastic constitutive relations, and finite deformation of the arterial wall [20]. In this work, the use of peak flow to correct *PWV* for determination of systolic blood pressure is proposed. To test the theory, the mean data presented in Payne et al. and Ochiai et al. [15,16] is used. Using linear regression and the coefficient of determination, the correlation between pressure and measured *PWV*, flow-corrected *PWV* (PWV_f), and rPTT is compared.

6.2.1 Fluid-Structure Interaction Model

The potential for estimating arterial blood pressure based on PWV has been investigated based on statistical regression models, or empirical representation of an

incremental isotropic elastic modulus as a function of a transmural pressure [21,22]. Models treating arteries as fluid-filled compliant thin-walled cylindrical membrane shells have been validated using data from *in vitro* and *in vivo* studies [23,24]. Recent work accounting for nonlinear aspects of a convective fluid phenomena, hyperelastic constitutive relations, and finite deformation of the arterial wall-determined PWV is associated with the forward-running wave velocity [20] as shown in equation (6.1). PWV accounting for flow (PWV_f) is a function of axial flow velocity (u), wall normal displacement nondimensionalized by vessel radius (η), blood density (ρ), and transmural pressure (p).

$$PWV_f = u + \sqrt{\frac{1+\eta}{2\rho} p_\eta} = u + PWV_p \tag{6.1}$$

The partial derivative p_η indicates sensitivity of pressure with respect to the wall normal deflection, and it has a clear interpretation as tangent (incremental) moduli in finite strain inelasticity. The right term of equation (6.1) presents PWV_f as a superposition of a peak flow velocity (u) and a pressure-dependent PWV_p.

6.2.2 Flow-Corrected PWV

PWV is classically measured at the foot of the forward-moving distal pressure wave, since estimation from the peaks, or peak-to-peak velocity, can give considerable errors due to contamination with reflected waves [25,26]. During the diastolic cardiac phase, the axial flow velocity is close to zero, allowing equation (6.1) to simplify to $PWV_f = PWV_p$. In both Payne et al. and Ochiai et al., the diastolic *PWV* is used; there was no determination of a systolic *PWV* associated with peak flow and the peak of the distal wave.

A systolic PWV can be estimated from a foot-based *PWV* measure accounting for flow velocity as in equation (6.1) and a calibration based on arterial pressure and radius. Equation (6.1) reformulated to explicitly indicate a classical *PWV* measurement location for systolic and diastolic is shown in equations (6.2) and (6.3), respectively.

$$PWV_f = u + \sqrt{\frac{[(1+\eta)p_\eta]_{pk}}{2\rho}} \tag{6.2}$$

$$PWV = \sqrt{\frac{[(1+\eta)p_\eta]_{ft}}{2\rho}} \tag{6.3}$$

This leads to a systolic *PWV* based on a diastolic *PWV* measure.

$$PWV_f = u + PWV\sqrt{\frac{[(1+\eta)p_\eta]_{pk}}{[(1+\eta)p_\eta]_{ft}}} \tag{6.4}$$

The subscripts *pk* and *ft* relate to the properties measured at the peak and foot respectively, and *PWV* is measured at the foot of the forward-moving distal pressure

wave. For linear elasticity $p_\eta = constant, \eta = \frac{pR}{Eh}$, in which *E*- linear elastic modulus, *R*- internal radius of the vessel, *h*- wall thickness, equation (6.4) can be written in a simplified form

$$PWV_f = u + PWV\sqrt{\frac{1+\frac{p_{pk}R_{pk}}{Eh}}{1+\frac{p_{ft}R_{ft}}{Eh}}} \tag{6.5}$$

The numerical result under the square root is a correction coefficient that accounts for shifts in *PWV* due to transmural pressure. In this work, the correction coefficient was set to unity since the required measurements were not recorded in the referenced papers [4,5]. *PWV* is calculated by dividing the constant arterial distance by the foot-to-foot transit time of the pressure wave with referenced lengths provided in the supplemental section for Ochiai et al. and Payne et al.

6.3 Methods

Although flow was not directly measured in the referenced papers, the peak flow velocity can be estimated using measured values of ejection volume, LVET, and aortic radius. Peak flow velocity (m/s) was calculated using the diastolic systolic aorta cross-sectional area (CSA) assuming a circular cross-section, LVET, cardiac output (CO), and heart rate (HR) [27].

$$u = \frac{CO/HR}{CSA}/LVET \tag{6.6}$$

Left ventricular ejection time (LVET) was calculated from PEP using a conservative fixed ratio of *PEP/LVET* = 1/3 [27,28], and an average aortic radius was used for each species, human and dog [25,28]. Systolic *PWV* was corrected for flow, using equation (6.5). Statistical analysis was completed to calculate the coefficient of determination (R^2) and analysis of variance (ANOVA).

6.3.1 Aortic Flow and Systolic Flow Velocity

A simple modification of (6.6) accounting for a typical profile of a time-dependent aortic flow is presented in [29]. All distributions are topologically equivalent to a triangle, as shown in Figure 6.32.

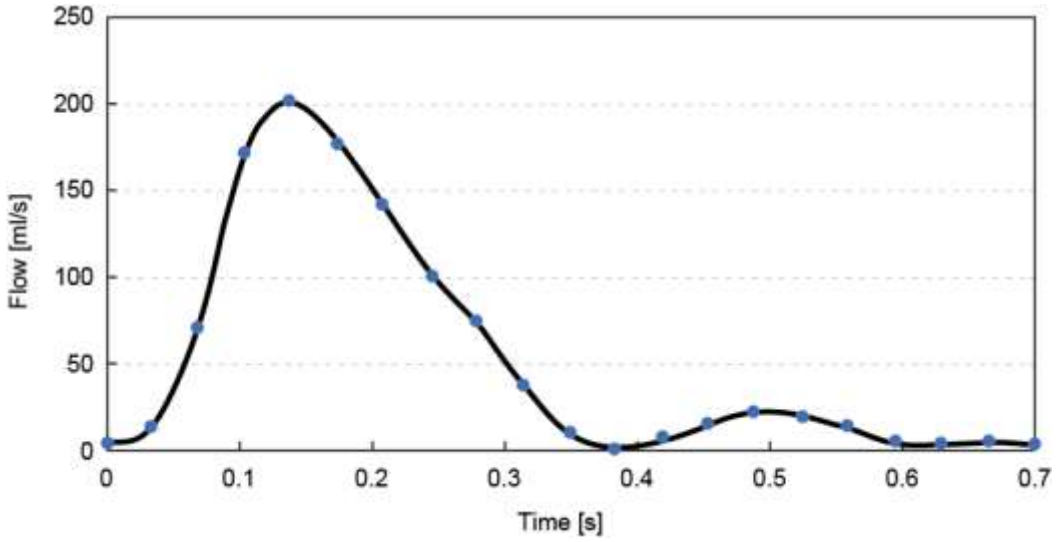

Figure 6.2. Ascending Aortic Flow profile for a heart coupled to a vascular system.

The total stroke volume (SV), consisting of the amount of blood ejected by the left ventricle in one contraction, is calculated as the following integral of flow rate Q by time

$$\text{SV}=\int Q(t)dt \qquad (6.7)$$

Approximating Q(t) as a triangle with a height $Q_{peak} = 560ml/s$ and a base Δt=0.225s, arrives approximately to $\text{SV}=\frac{1}{2}Q_{peak}$ Δt=63 ml/s, instead of the exact value of 64 ml/s presented in [31]. As it follows from (6.7), an average value of a ventricular outflow is equal to approximately half of its peak value.

$$Q_{avg} = \frac{\int Q(t)dt}{\Delta t} = \approx \frac{\frac{1}{2}Q_{pk}\,\Delta t}{\Delta t} \approx \frac{1}{2}Q_{pk} \qquad (6.8)$$

Now we can present systolic velocity u_s using systolic aortic flow Q_{peak} and a systolic cross section area A_s

$$u_s = \frac{Q_{pk}}{CSA_s} = k_s \frac{Q_{avg}}{CSA_s} = k_s \frac{CV}{CSA_s \, \Delta t}, \quad k_s = \frac{Q_{pk}}{Q_{avg}} \approx 2 \tag{6.9}$$

where k_s represents the scale factor to convert from Q_{avg} to Q_{pk}.

6.3.2 Aortic and Peripheral Studies

Payne et al. modulated cardiac output in healthy male subjects (mean age: 22 years) using four drugs. Angiotensin II is a peptide hormone that causes vasoconstriction and a decrease in CO [30]. Glyceryl trinitrate, commonly used to treat angina, is known to decrease both CO and ejection volume. Norepinephrine released by the sympathetic nervous system increases the force with which ventricular muscle fibers contract and affects both cardiac output and ejection volume [31]. Salbutamol is a vasodilator that causes a significant increase in heart rate and associated CO [*32*,*33*]. Blood pressure and *PWV* averages across all subjects for baseline and each pharmaceutical manipulation were used in this analysis. Although the Payne et al. data lacks a direct cardiac output measure, literature provides averages for baseline and each of the pharmaceuticals as shown in Table 6.1.

Table 6.1. Angiotensin II (ARB), Glyceryl Trinitrate (GTN), Norepinephrine (NE), Salbutamol (SAL)

	CO [lpm]	Note
Baseline	5.00	Healthy person at rest [28]
ARB	4.25	Decrease by 15% [30]
GTN	4.60	Decrease by 8% [34]
NE	5.60	Increase by 12% [31]
SAL	6.50	Increase by 30% [33,32]

Table 6.2. Mean physiological measurements from Ochiai et al. [16].

	SBP [mmHg]	DBP* [mmHg]	HR [bpm]	PEP [ms]	LVET* [ms]	CO [lpm]	TT [ms]	PWV* [ms]	Flow* [m/s]	PWV_f** [m/s]
Baseline	127	77	126	72	215	1.79	74	8.1	0.7	8.8
ISO	90	47	118	67	200	1.2	88	6.8	0.6	7.4
Baseline	154	103	128	87	260	1.65	59	10.1	0.5	10.7
NTG	127	78	140	69	207	1.95	71	8.5	0.7	9.2
Baseline	129	105	126	86	260	1.62	65	9.2	0.5	9.7
HVM	79	58	127	86	260	0.75	76	7.9	0.2	8.2
Baseline	168	107	123	69	207	1.75	64	9.4	0.7	10.2
DBT	226	119	139	43	128	3.33	53	11.4	2.0	13.4
Baseline	159	104	127	80	241	1.78	62	9.7	0.6	10.2
PHE	190	132	112	98	294	1.22	50	12.0	0.4	12.4

Isoflurane (ISO), Nitroglycerine (NTG), Hypovolemia (HVM), Dobutamine (DBT), Phenylephrine (PHE), and Baseline represent the measurement before a drug was administered. *Calculated value. **Flow-corrected PWV. DBP was calculated using the measured MAP data [16].

Table 6.3. Mean physiological measurements from Payne et al. [15].

	SBP [mmHg]	DBP [mmHg]	HR [bpm]	PEP [ms]	LVET* [ms]	CO# [lpm]	TT [ms]	PWV* [ms]	Flow* [m/s]	PWV_f** [m/s]
Baseline	139	67	62	100	300	5.00	166	6.0	0.6	6.7
ARB	156	82	60	105	315	4.25	150	6.7	0.5	7.2
Baseline	134	66	63	95	285	5.00	164	6.1	0.7	6.8
GTN	122	61	77	92	276	4.60	184	5.4	0.5	6.0
Baseline	141	68	61	95	285	5.00	165	6.1	0.7	6.7
NE	164	81	57	87	261	5.60	151	6.6	0.9	7.5
Baseline	151	71	66	91	273	5.00	158	6.3	0.7	7.0
SAL	153	39	125	30	81	6.50	188	5.3	1.5	6.9

Angiotensin II (ARB), Glyceryl Trinitrate (GTN), Norepinephrine (NE), Salbutamol (SAL), and Baseline represent the measurement before a drug was administered.
*Calculated value. #Referenced values used. **Flow-corrected PWV.

For Ochiai et al., a reference inner aortic radius at diastolic and systolic of R_i*=4.5, 5.4 mm* respectively and length *d* = 0.6m for the canine aorta [35] was used for all calculations. DBP was calculated from the measured SBP and mean arterial pressure (MAP) using the equation:

$$DBP = 1.5MAP - 0.5SBP \tag{6.6}$$

For the Payne et al. study, a human inner aortic radius at diastolic and systolic of R_i = 10.5, 12.6 mm respectively was used for all calculations [25,36]. The referenced distance from the aortic root to the index finger of d=1.0 m was used to calculate PWV [*28*].

While the PWV versus pressure curve is nonlinear [10,20,23,25], both Payne et al. and Ochiai et al. fit a linear model using regression analysis. We have used the same R-squared statistics to run comparisons with their published results.

6.4 Results

To test the theory that a PWV_f -based estimate of SBP is more accurate than *PWV* uncorrected for flow and rPTT, we used data from both Ochiai et al. and Payne et al. [15,16]. This data allowed comparison of the coefficient of determination across the different physiological changes induced in the two studies and assessment of the statistical significance.

6.4.1 Flow correction improves aortic PWV correlation with blood pressure

Measured and flow-corrected *PWV* and associated blood pressures for the mongrel dog aorta study of Ochiai et al. are provided in Table 6.2. A linear regression was performed, and the associated coefficient of determination was calculated and compared as shown in Figure 6.3a and Figure 6.3b for *PWV* and PWV_f respectively for SBP. The same comparison was made for SBP and DBP (Figure 6.3c and Figure 6.3d). For both comparisons, PWV_f (equation (6.5)) significantly improves the linear fit of the data. ANOVA showed a significant positive relationship between pressure and PWV_f, $R^2 = 0.75$ and $P < 0.0001$. Multivariable ANOVA also shows a significant positive relationship for both systolic pressure and flow to *PWV*, $P < 0.0001$. Analysis of diastolic pressure versus *PWV* resulted in a significant positive relationship with $R^2 = 0.92$ and $P < 0.01$, consistent with prior studies [7,14-16,27].

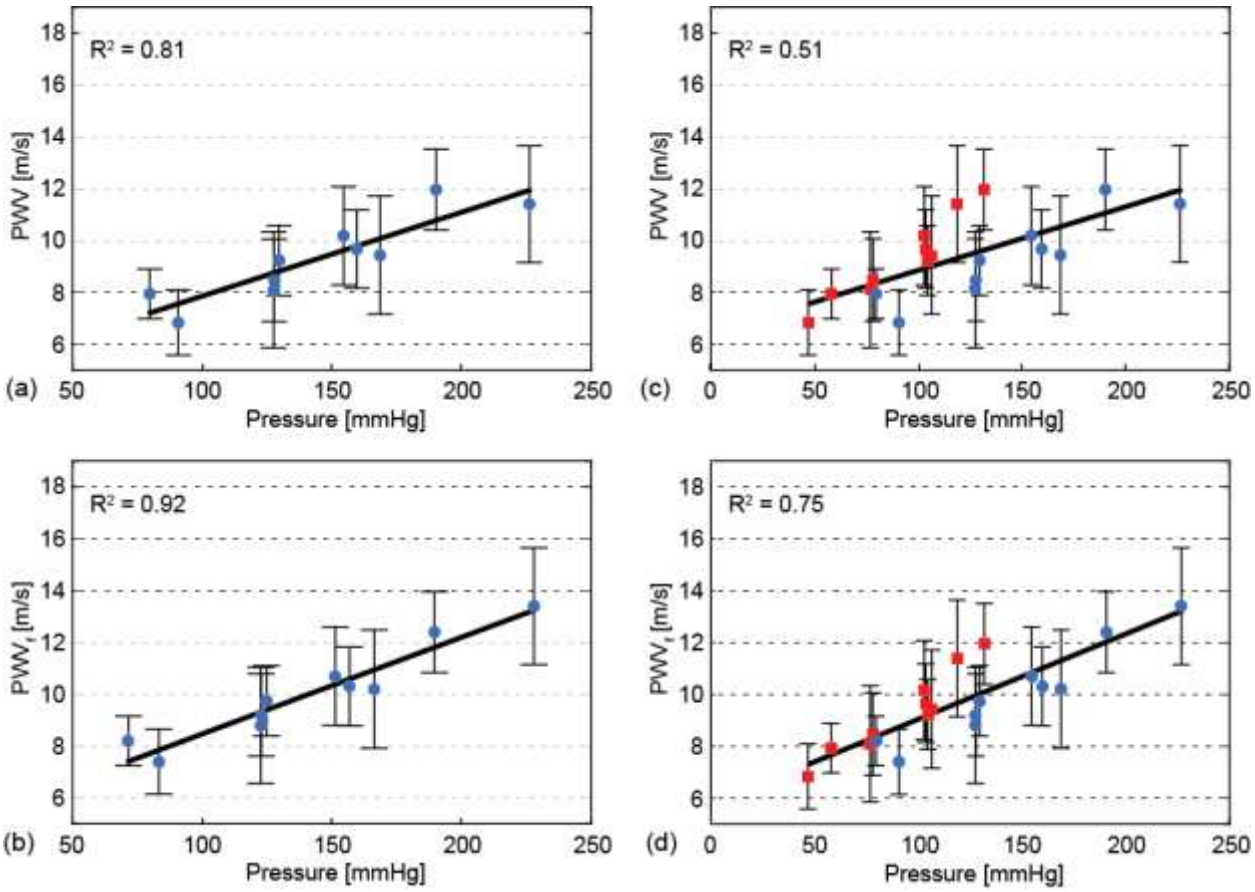

Figure 6.3. PWV_f measured in the aorta improves blood pressure prediction. Error bars represent the standard deviation of PWV calculated from the referenced TT measurements from [16] and uncertainty in measures required for calculation of flow velocity. For all figures, the systolic pressure is represented by a circle, and diastolic pressure is represented by a square. The left side includes SBP only, while the right side includes both pressures (SBP and DBP). a) PWV uncorrected for flow across measured SBP. b) PWV corrected for flow velocity improves the correlation with SBP alone. c) The lowest correlation was observed with PWV uncorrected for flow across measured pressures. d) PWV corrected for flow velocity improves the overall correlation across all pressures. Analysis of diastolic pressure versus PWV (data not shown) produced an $R^2 = 0.92$.

6.4.2 Flow correction improves peripheral PWV correlation with blood pressure

Measured and flow-corrected PWV and associated blood pressures for the human subject study of Payne et al., with the distal *PWV* measurement point at the index finger, are provided in Table 6.3. A linear regression was performed, and the associated coefficient of determination was calculated and compared, as shown in Figure 6.3a and Figure 6.3b, respectively for SBP. The same comparison was made for SBP and DBP (Figure 6.3c and Figure 6.3d). For both comparisons, the PWV_f equation (6.5) significantly improves the linear fit of the data. ANOVA showed there is a significant positive relationship between pressure and PWV_f, R^2=0.70 and P<0.0001. Analysis of diastolic pressure versus *PWV* showed a significant positive relationship with $R^2 = 0.85$ and $P < 0.01$, consistent with prior studies [7,14-16,27]. Multivariable ANOVA also shows there is a significant positive relationship for both systolic pressure and flow to *PWV*, $p < 0.01$.

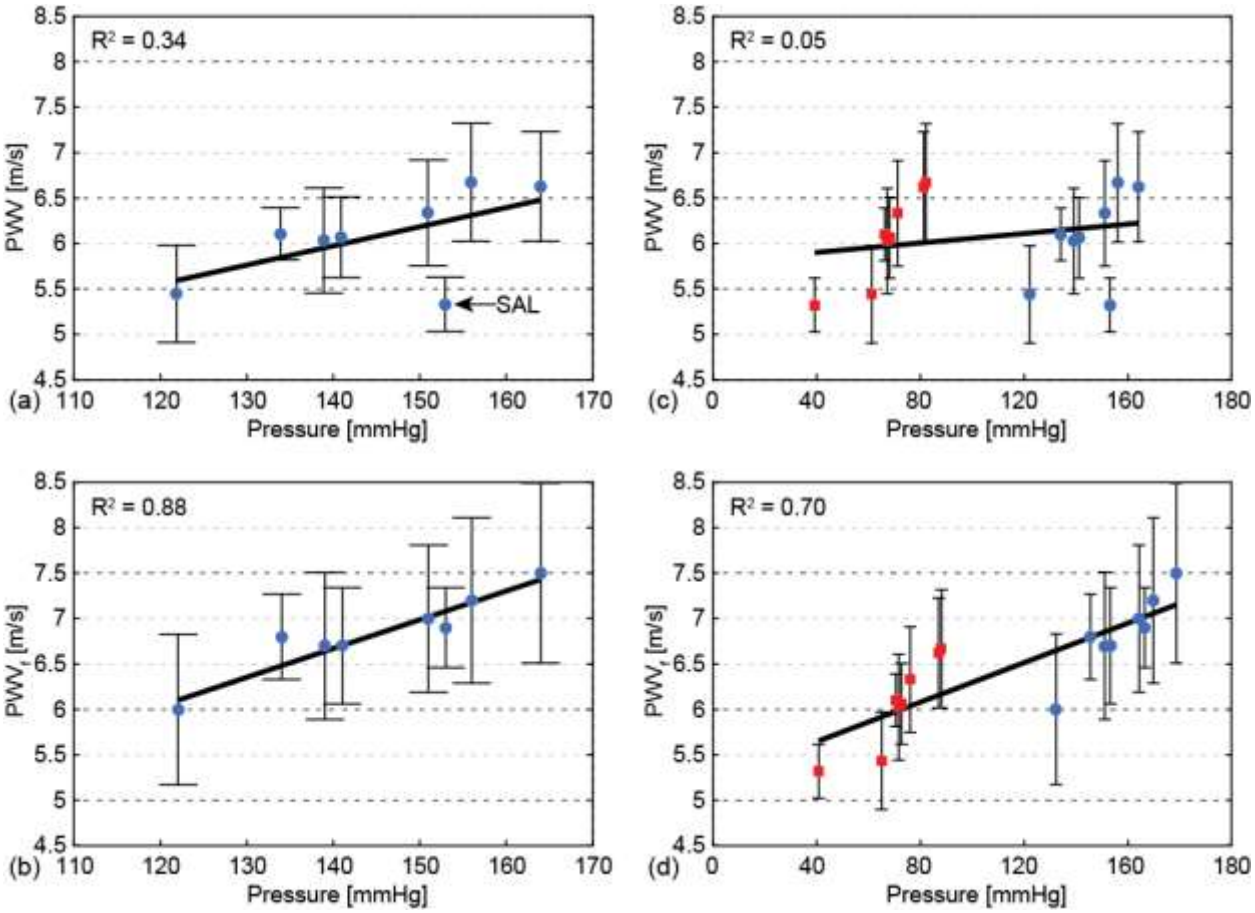

Figure 6.4. PWV_f measured at the finger improves blood pressure prediction. Error bars represent the standard deviation for PWV calculated from the referenced TT measurement [15] and uncertainty in measures required for calculation of flow velocity. For all figures, the systolic pressure is represented by a circle, and the diastolic pressure is represented by a square. The left side includes SBP only; the right side includes both pressures (SBP and DBP). a) PWV uncorrected for flow across measured SBP. Salbutamol (SAL) was the farthest of any other measure from the trend line. b) PWV corrected for flow velocity improves the correlation with SBP alone. c) The lowest correlation was observed with PWV uncorrected for flow across measured pressures. d) PWV corrected for flow velocity improves the overall correlation across all pressures. Analysis of diastolic pressure versus PWV (data not shown) produced $R^2 = 0.85$.

6.4.3 Flow-corrected PWV provides the most robust correlation with blood pressure

It has been previously reported that the rPTT provides a stronger correlation with SBP [*15*], while PWV provides a stronger correlation with DBP [15,16].

Table 6.4. Linear correlation for rPTT, PWV, PWV_f with pressure (SBP, DBP).

	Payne R^2	Ochiai R^2	Note
rPTT to SBP	0.39	0.59	NA
PWV to DBP	0.85	0.92	NA
PWV to SBP	0.34	0.81	No flow correction
PWV_f to SBP	0.88	0.92	Flow correction
PWV to Pressure	0.05	0.51	No flow correction
PWV_f to Pressure	0.70	0.75	Flow correction

As shown in Table 6.4, there was a good correlation between *PWV* and DBP for both Payne et al. and Ochiai et al. (R^2 = 0.92, 0.85 respectively). However, using our PWV_f produced the highest coefficient of determination when compared with both *PWV* uncorrected for flow and rPTT. It is interesting to note that Payne et al.'s peripherally measured *PWV* to SBP data had the lowest R^2, which may be due to the influence of peripheral muscular arteries versus the elastic nature of the aorta.

6.5 Discussion

The main novel contribution of the present study is the introduction of a PWV_f that improves correlation with blood pressure over both uncorrected *PWV* and rPTT. For diastolic pressure prediction, *PWV* measured at the foot, near the diastolic point, should be used. PWV_f calculated using equation (6.5) allows correlation of *PWV* with SBP, with time point measurement at the diastolic foot of the waveform, a robust measurement point.

It has been observed in some papers that rPTT has a stronger correlation with systolic pressure than *PWV* [15,16]. We believe this correlation occurs because of the PEP component of rPTT. PEP accounts for a substantial and variable portion of rPTT, ranging from 12 to 35% [15] and has been shown to inversely correlate with contractility [27]. It is likely that the observed relationship between SBP and rPTT is due to this embedded measure of contractility. For example, exercise results in increased SBP, increased contractility, and decrease in PEP, driving an associated increase in flow velocity that in turn increases *PWV*. The result is a two-fold influence on rPTT: a decrease due to reduced PEP and shorter transit time. It was found that rPTT had an inverse linear correlation with SBP (combined average across all subjects and drugs) for Payne et al. and Ochiai et al. as $R^2 = 0.39$, and $R^2 = 0.59$, respectively. We found that based on equation (6.5), using flow-corrected *PWV* produces an $R^2 = 0.88$ and $R^2 = 0.92$, respectively (Payne et al., Ochiai et al.). This approach offers the strongest fit of all the permutations considered, as seen in Table 6.4.

In this work, equation (6.6) is used as an estimate of peak flow velocity. In other work, aortic peak flow has been found to be ~2 times average aortic flow [29]. Using this alternate estimate of peak flow, our R^2 results improved from 0.7 to 0.87 and 0.75 to 0.85 for the Payne et al. and Ochiai et al. data, respectively. These results are consistent with historic literature in which peak volumetric flow in relation to the aortic pressure is most closely associated with the forward-moving systolic peak pressure wave [25-27]. For a continuous estimation of SBP, a flow-based measure is required. An estimate is possible using a head ballistocardiogram [35] or by using a percentage of PWV [37].

Prior studies have recognized that compensating measured *PWV* with LVET may be important [6,19]. Salvi et al. and Nurnberger et al. found that a change in ejection time of ~40 ms (~12%) caused a change in *PWV* of ~1 m/s (~17%) [6,19]. Salvi et al. [*19*] performed a large population study to explore the link between *PWV* and LVET. An inverse linear association was found between *PWV* and LVET at all ages (R^2=0.35, $p < 0.0001$) [19]. Nurenberger considered all hemodynamic parameters (except flow velocity) and found that at rest, only DBP and LVET correlated with PWV. In our previous work [18], we showed that increased flow velocity was responsible for the increase in *PWV* under conditions of decreasing LVET and fixed ejection volume. *PWV* was substantially affected by flow velocity (~10%) and peak pressure (~2%) changes controlled by ejection time. As represented in equation (6.5), PWV_f is affected by both flow and the physical properties of the aorta as represented by the correction coefficient. At diastolic pressure when flow is close to zero, *PWV* is dominated by the physical anisotropic properties of the aorta. At systolic pressure, the pulse wave velocity

is also affected by flow velocity. To estimate the impact of uncertainty of the input data upon PWV_f, we performed a sensitivity analysis using a variation of +/-10% for each of the following datasets: *C0, LVET,* and *CSA*. We have found that the R^2 varied from 0.73-0.76 for the Ochiai et al. dataset and from 0.64-0.73 for the Payne et al. dataset.

Building on this work, we have developed per patient calibration to allow for the prediction of blood pressure. For this analysis, all data is based on measures taken on a middle-aged, healthy male, in our laboratory. The measured aortic length of ~ 0.6 m was used to calculate PWV from the transit time measures. The first step extracts material characteristics for an artery, using a calibration step that provides at least three values each for blood pressure, internal radius, and wall thickness of an arterial segment. It is assumed that wall thickness is a constant, with minimal change between systolic and diastolic pressure. Ultrasound is used to measure the aortic diameter with an observed variance of ($\pm 0.8mm$). This results in a per patient blood pressure, transit time calibration curve as shown in Figure 6.5 with an observed variance in the measure leading to a maximum uncertainty of ~1.8%.

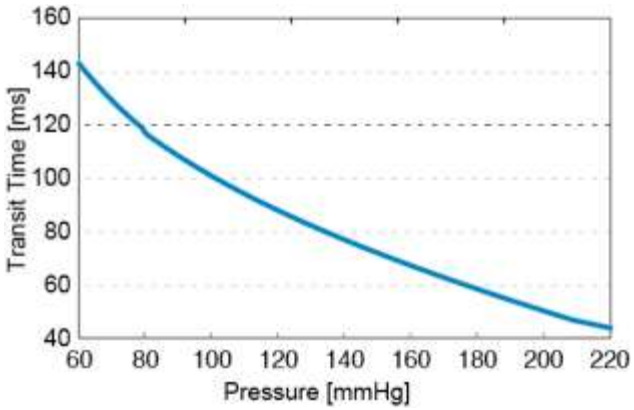

Figure 6.5. The patient's transit time calibration curve created by the fully nonlinear thick wall model described in Chapter 5, using the noninvasive extraction of the aortic material characteristics from the ultrasound aortic radial measures and the cuff-based blood pressure measures.

Using the calibration curve, the accuracy required to meet the Association for the Advancement of Medical Instrumentation (AAMI) standard is analyzed. AAMI stipulates that the mean difference between the test device and the standard shall be less than or equal to $5\ mmHg$ with a standard deviation of less than or equal to $8\ mmHg$ [40]. The transit time accuracy required to achieve the AAMI standard of $\pm 5\ mmHg$ is shown in Figure 6.6. In the range of normal diastolic pressure ($80\ mmHg \pm 5\ mmHg$), an

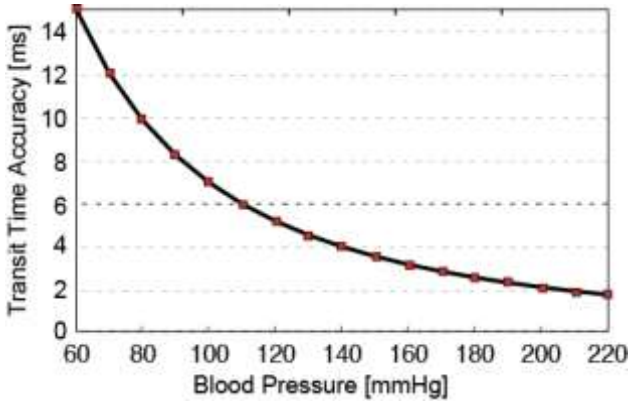

Figure 6.6. The transit time accuracy required to achieve the AAMI blood pressure standard $\pm 5\ mmHg$. An accuracy of 9.8 ms is required for a diastolic pressure of 80 mmHg. For a systolic pressure of 120 mmHg, an accuracy of ~5.1 ms is required. In conditions of hypertension, for a systolic pressure of 200 mmHg, an accuracy ~2.0 ms is required.

associated transit time measure of $117\ ms\ (PWV\ of\ 5.1\ m/s)$ with an accuracy of $\sim 9.8\ ms$ is required, as summarized in Table 6.5. For systolic pressure ($120\ mmHg \pm 5 mmHg$), where the slope of the calibration curve is more gradual, an associated transit time measure of $88.6\ \mathrm{ms}$ $(PWV\ of\ 6.7\ m/s)$ with an accuracy of $\sim 5.1\ ms$ is required.

Table 6.5. The transit time accuracy required to meet the AAMI standard.

Pressure [mmHg]	TT [ms]	PWV [m/s]	Accuracy [ms]
80	117	5.1	9.8
120	88	6.7	5.1

A measured PWV includes both the pressure-dependent PWV term, represented by the calibrated model, and an additive flow velocity component. This flow velocity can be estimated as a percentage (~20%) of PWV [37]. Using the calibrated model, at $120\ mmHg$ the associated PWV is $\sim 6.7\ m/s$. This results in an estimated flow velocity of $1.3\ m/s$. The slope of the calibration curve at a systolic pressure point is $0.04\ (m/s)/mmHg$. Thus, in this example, ignoring flow velocity leads to an underestimate of systolic blood pressure by $\sim 32\ mmHg$ for both normal and hypertensive conditions.

Data for LVET was not presented in either the Ochiai et al. or Payne et al. studies. We recognize that under varying physiological conditions, this ratio is not always fixed. However, a conservative fixed ratio of $PEP/LVET = 0.33$ was used for all drugs and baseline [27,28]. To analyze the effect of a true measure of this ratio, salbutamol was considered, since it produced one of the largest changes in PEP (~ -65 ms from the average baseline, Table 6.3). Burgess et al. found a maximal decrease in $PEP/LVET$ of 0.070 that lasted for ~30 mins for salbutamol via a nebulizer (2.35 mg) [32]. When we decreased the *PEP/LVET* ratio by this amount down to 0.27 (a 20% reduction) for the salbutamol data, the SBP to PWV_f R^2 value improved to 0.92 from the previously reported 0.88. It can be seen that salbutamol has the biggest impact on the uncorrected R^2 value in Figure 6.4a (SAL). Since salbutamol increases cardiac output

and decreases the PEP/LVET ratio, it causes the largest flow increase from the baseline.

The aortic *PWV* measure offered higher correlation than *PWV* measures at the periphery. Prior studies have found a ~20% increase in *PWV* when measured in the periphery (femoral-ankle) versus central measures (carotid-femoral) caused by changes in arterial radius, thickness, and modulus of elasticity [37,38]. The correlation difference is likely caused by drugs that affect elastic arteries differently than the muscular arteries [17]. Nitroglycerin, for example, produces a peripheral vascular effect by relaxing the smooth muscle. This insight supports the view that noninvasive sensors should be placed in as close proximity to an elastic artery as possible for *PWV* measures to avoid the modulation of *PWV* possible in the muscular arteries.

In this work, the correction coefficient was set to unity since the required measurements were not recorded in the referenced papers [15,16]. We recognize the physical properties of the aorta at SBP are different (less compliant) than those at DBP, causing a faster-moving pressure wave. To estimate the impact of the correction coefficient, referenced values [27] for both a canine and a human were substituted into equation (6.5). The pressure to PWV_f R^2 values improved from 0.70 to 0.92 and 0.75 to 0.94 for the Payne et al. and Ochiai et al. datasets, respectively. It is possible for future studies to perform per patient calibration as shown by equation (6.5) and to measure the required aortic wall information using ultrasound. A PWV_f can then be calculated from a foot-based *PWV* measure that is free from errors induced by reflected waves [25,26]. Additional studies are required to determine the advantage of this estimate and the associated improvement in SBP prediction.

Flow-corrected PWV significantly improves PWV correlation with SBP, which is important for continuous cuff-less blood pressure measures. Uncorrected data could potentially lead to unneeded treatments. For a single person tested in our laboratory, it was found that ignoring flow velocity leads to an underestimate of systolic blood pressure by $\sim 32\ mmHg$ for both normal and hypertensive conditions. A key limitation of this study is the lack of published data that includes both flow velocity and PWV. Additional studies are required that explicitly measure aortic flow velocity along with PWV and vessel characteristics across a broad age range, under varying physiological conditions.

6.6 Conclusion

Accounting for the flow contribution to *PWV* based on the fundamental physics of wave propagation in nonlinear elastic arteries improves blood pressure prediction. It was found that flow-corrected *PWV* correlates with SBP better than both uncorrected *PWV* and rPTT, based on analysis of prior published studies with pharmaceutically induced blood pressure shifts. We found that using peak flow velocity to correct PWV produces robust blood pressure to PWV_f correlation for peripheral ($R^2 = 0.70$) and aortic ($R^2 = 0.75$) *PWV* measurements across the full range of physiologic pressure. Flow correction of *PWV* unifies the correlation curves, enabling both SBP and DBP to be associated with the same physical *PWV* measure.

6.7 References

[1] World Health Organization, "A global brief on hypertension, silent killer, global public health crisis," WHO, Document number: WHO/DCO/WHD/2013.2 2013.

[2] "Measurement and clinical evaluation of blood pressure (JSH 2009)," *Hypertens Res*, vol. 32, pp. 11-23, 2009.

[3] Calhoun DA., Jones D.et al. , "Resistant hypertension: diagnosis, evaluation, and treatment. A scientific statement from the American Heart Association Professional Education Committee of the Council for High Blood Pressure Research.," *Hypertension*, vol. 51, no. 1403, 2008.

[4] Blacher J., Asmar R., Djane S., London GM., Safar ME., , "Aortic pulse wave velcity as a marker of cardiovascular risk in hypertensive patients," *Hypertension*, vol. 33, pp. 1111-17, 1999.

[5] Blacher, J., A. P. Guerin, B. Pannier, et al. , "Impact of aortic stiffness on survival in end stage renal disease," *Circulation*, vol. 99, no. 18, pp. 2434-2439, 1999.

[6] Nurnberger J.,A. Saez,S. Dammer,A. Mitchell,R. Wenzel,T. Philipp, R. Schafers , "Left Ventricular ejection time: a potential determinant of pulse wave velocity in young, healthy males," *J. Hypertens.*, vol. 21, no. 11, pp. 2125-2132, 2003.

[7] Kim EJ., CG Park, JD Park, SY Suh, CU Choi, JW Kim, SH Kim, HE Lim, SW Rha, HS Seo, DJ Oh , "Relationship between blood pressure parameters and pulse wave velocity in normotensive and hypertensive subjects: invasive study," *J Hum Hypertens*, vol. 21, pp. 141-148, 2007.

[8] J. D. Kortweg, "Uber die Fortpflanzungsgeschwindigkeit des Schalles in elastischen Rorren," *Ann. Phys. Und Chem., Neue Folge*, vol. 5, p. 225, 1878.

[9] V. Hardung, "Propagation of pulse waves in Visco-elastic tubings," *Handbook of Physiology*, vol. 2, no. 1, pp. 107-135, 1962.

[10] Hughes D., F. Babbs, C. Geddes , "Measurement of Young's modulus of elasticity of the canine aorta with ultrasound," *Ultrasound Imaging 1*, vol. 4, pp. 356-367, 1979.

[11] Hill A.V., J. C. Bramwell, "The velocity of the pulse wave in man," *Proc. Royal Society for experiments in Biology and Medicine*, vol. 93, pp. 298-306, 1922.

[12] Bramwell J.C., A.V. Hill , "The formation of breakers in the transmission of pulse wave," *J. Physiol*, vol. 57, no. lxxiii, 1923.

[13] Histand M., M. Anliker , "Influence of flow and pressure on wave propagation in the canine aorta," *Circ Res*, vol. 32, pp. 524-29, 1973.

[14] Kobayashi T, Ichikawa S, Takeuchi Y, and Togawa T. Chen W, "Continuous estimation of systolic blood pressure using the pulse arrival time and intermittent calibration," *Med Biol Eng Comput*, vol. 38, pp. 569-574, 2000.

[15] Payne R. A., Symeonides C., Webb D., Maxwell S. , "Pulse transit time measured from the ECG: an unreliable marker of beat-to-beat blood pressure," *J. Appl. Physiol.*, vol. 100, pp. 136-141, 2006.

[16] Ochiai R., J. Takeda, H. Hosaka, Y. Sugo, R. Tanaka, T. Soma , "The relationship between modified pulse wave transit time and cardiovascular changes in isoflourane anesthetized dogs," *J Clin Monit*, vol. 15, pp. 493-501, 1999.

[17] Smulyan H., S. Mookherjee, R.A. Warner , "The effect of nitroglycerin on forearm arterial distensibility," *Circ.*, vol. 76, no. 6, pp. 1264-1269, 1886.

[18] Lillie J.S., A.S. Liberson,D. Mix, K. Schwarz, A. Chandra, D.B. Phillips, S.W. Day, D.A. Borkholder, "Pulse wave velocity prediction and compliance assessment in elastic arterial segments.," *Cardiovasc Eng Tech*, vol. 6, no. 1, pp. 49-58, Dec 2014.

[19] Salvi P., C. Palombo, G. Salvl, C. Labat, G. Parati, A. Benetos, "Left ventricular ejection time, not heart rate, is an independent correlate of aortic pulse wave velocity," *J Appl Physiol*, Sept 2013.

[20] Lillie J.S., A.S. Liberson, D.A. Borkholder, "Pulse wave velocity prediction in multi-layer thick wall arterial segments," in *FFHMT*, Ottawa, 2015, p. Paper No. 163.

[21] Chen W., T. Kobayashi,S. Ichikawa,Y. Takeuchi,T. Togawa , "Continuous estimation of systolic blood pressure using the pulse arrival time and intermittent calibration," *Med Biol Eng Comput*, vol. 38, pp. 569-574, 2000.

[22] Chen Y., W. Changyun, T. Guocai, B. Min, G. Li , "Continuous and Noninvasive Blood Pressure Measurement: A Novel Modeling Methodology of the Relationship Between Blood Pressure and Pulse Wave Velocity," *Ann. Biomed. Eng*, vol. 37, no. 11, pp. 2222-2233, Nov 2009.

[23] Liberson A., J. S. Lillie, D.A. Borkholder , "Numerical Solution for the Boussinesq Type Models with Application to Arterial Flow," *JFFHMT*, vol. 1, pp. 9-15, 2014.

[24] O'Rourke M., J. Seward , "Central arterial pressure and arterial pressure pulse: New views entering the second century after Korotkov," *Mayo Clin Proc*, vol. 81, no. 8, pp. 1057-1068, Aug 2006.

[25] Lieber A., S. Millasseau, L. Bourhis, J. Blacher, A. Protogerou, B. Levy, M. Safar , "Aortic wave reflection in men and women," *Am J Physiol Heart Circ*, vol. 299, pp. H235-H242, April 2010.

[26] O'Rourke M., *McDonald's Blood Flow in Arteries: Theoretical, Experimental and Clinical Principles*, 5th ed. USA: Oxford University Press, 2005.

[27] Klabunde R. , *Cardiovascular Physiology Concepts*, 2nd ed. Philadelphia, USA: Lippincott Williams & Wilkins, 2011.

[28] Ottesen J.T., M. Danielsen, , *Mathematical Model in Medicine*. The Netherlands: IOS Press, 2000.

[29] Hsieh KS., CK. Chang, KC. Chang, HI. Chen , "Effect of loading conditions on peak aortic flow velocity and its maximal acceleration," *Proc Natl Sci* , vol. 15, no. 3, pp. 165-170, 1991.

[30] Hamzaoui O., JF Georger, X. Monnet, H. Ksouri, J. Maizel, C. Richard, JL Teboul , "Early administration of norepeniphrine increases cardiac preload and cardiac output in septic patients with life threatening hypotension," *Critical Care*, vol. 14, no. R142, pp. 1-9, 2010.

[31] Burgess C., "The hemodynamic effects of aminophylline and salbutamol alone and in combination," *Clin Pharm Ther*, vol. 40, no. 5, pp. 550-553, Nov 1986.

[32] Poole-Wilson P. A., G. Lewis, T. Angerpointer, A.D. Malcom, B.T. Williams , "Haemodynamic effects of salbutamol and nitroprusside after cardiac surgery," *Brit*

Heart J., vol. 39, pp. 721-725, 1977.

[32] Kawakami H., T. Sumimoto, M. Hamada, M. Mukai, Y. Shigematsu, H. MaTSUOKA, M. Abe, K. Hiwada , "Acute effect of glyceryl Trinitrate on systolic blood pressure and othe hemodynamic variables," *Angiology*, vol. 46, no. 2, pp. 151-156, Feb 1995.

[33] Jones E., M. Anliker,I. Chang , "Effects of viscosity and constraints on the dispersion and dissipation of waves in large blood vessels. II. Comparison of analysis and experiments," *J Biophys*, vol. 11, pp. 1121-1134, 1971.

[34] Raimund E., H. Eggebrecht , "Aortic Dimensions and the Risk od Disection," *Heart*, vol. 92, pp. 137-142, 2006.

[35] Pedley T.J., *The fluid mechanics of large blood vessels*., 2008.

[36] Tanaka H., M. Munakata et al. , "Comparison between carotid-femoral and brachial-ankle pulse wave velocity as measures of arterial stiffness," *J. Hypertens*, vol. 27, no. 10, pp. 2022-2027, 2009.

[37] YU WC., SY Chuang, YP Lin, CH Chen, , "Brachial-ankle vs. carotid-femoral pulse wave velocity as a determinant of cardiovascular structure and function," *J. Hum. Hypertens*, vol. 22, no. 1, pp. 24-31, 2008.

[38] Van Egmond, J., et al., “Accuracy and Reproducibility of 30 Devices for Self-Measurement of Arterial Blood Pressure,” American Journal of Hypertension, 6(10):873-9, 1993.

Chapter 7: Conclusions and Future Work

Study hard what interests you most, in the most undisciplined, irreverent and original manner possible.
- Richard Feynman, Physicist and Bongo player

7.1 Summary of Contributions

The overriding goal of this work was to create a continuous noninvasive blood pressure system. PWV and ECG are two of the physiological signals required. While today's wearables have integrated photoplethysmography as a way to measure heart rate, they have yet to extend and combine the necessary measures to extract PWV. Companies like AlivCor have created smartphone sensors that enable ECG measurement; however, the sensors are not yet in a wearable form. In addition to these measures, a measure of pre-ejection period and flow are required. Multiple approaches show promise, such as the ballistocardiogram (BCG), impedance plethysmography, inductive sensing, RF techniques such as dual-antenna nanosecond pulse near-field sensing (NPNS), and micro-ultrasound sensors. As of this writing, none of these techniques have been in a wearable form factor and validated across various physiological states against a gold standard (Doppler ultrasound). The combination of ECG, PWV, and flow measures is required in a wearable microsystem to allow for cuff-less continuous non-invasive blood pressure monitoring. To provide the missing insights in this area, we developed and validated a series of three models, each incorporating additional complexities and nonlinearities of the arterial system.

The first model, presented in Chapter 3, was a one-dimensional nonlinear model for pressure wave propagation in a compliant tube with a linear elastic wall filled with an incompressible fluid. It was recognized in a number of clinical studies that both pressure and LVET affected PWV. Using our first model and a physiologically based electromechanical hemodynamic simulator, we studied this effect. The results indicate an inverse quadratic relationship between ejection time and PWV, with ejection time

dominating the PWV shifts, over those observed with changes in peak pressure. The key insight provided by the model is that PWV is a superposition of flow velocity and a pressure-dependent term as seen in equation (3.16). Flow velocity can dominate the change in PWV under physiological conditions that cause a large change, such as digestion. In our study, PWV was substantially affected by average flow velocity (~10%) changes controlled within the physiological range of LVET. To a lesser extent, PWV was affected by peak pressure changes alone (~2%).

The second model, presented in Chapter 4, predicted the general relationship between PWV and BP with a rigorous account of nonlinearities in the fluid dynamics model, blood vessel elasticity, and finite dynamic deformation of a membrane type thin anisotropic wall. Pulse wave propagation in a compliant arterial segment is presented within the framework of pseudoelastic deformation of biological tissue undergoing finite deformation in thin-walled arterial segments. An essential ingredient is the dependence of results on nonlinear aspects of the model: convective fluid phenomena, hyperelastic constitutive relation, large deformation, and a longitudinal pre-stress load. An exact analytical solution for PWV is presented as a function of pressure, flow, and pseudoelastic orthotropic parameters. The key insight was that the entirely nonlinear model achieves the best match with the experimental data. To retrieve individual vascular information of a patient, the inverse problem of hemodynamics is presented, calculating local orthotropic hyperelastic properties of the arterial wall. The proposed technique can be used for non-invasive assessment of arterial elastance and blood pressure using direct measurement of PWV, accounting for hyperelastic orthotropic properties. This critical finding creates a non-invasive aortic calibration by using the

(pressure, PWV) curve to extract the associated material properties of the vessel (c, a_{11}, a_{12}, a_{22}). A similar calibration technique is also possible by measuring pressure and the corresponding change in aortic radius.

The final model, presented in Chapter 5, examined the impact of the thick arterial wall made up of three layers (intima, media, and adventitia) with different material properties in the radial direction. We examine the accuracy of PWV prediction based on a traditional homogeneous structural model for thin-walled arterial segments. In reality, arteries are described as composite heterogeneous hyperelastic structures, where the thickness dimension cannot be considered small compared to the cross-section size. The dependence of PWV on pressure for three vessels of different thicknesses is compared against that of a traditional thin wall model of a membrane shell interacting with an incompressible fluid. The key insight was that a single thick layer model is sufficient to predict PWV of an arterial segment and provides improved accuracy over the thin wall model. For a hypertensive subject, the thick wall model provides improved accuracy up to 8.4% in PWV prediction over its thin wall counterpart. This translates to nearly 20% improvement in blood pressure prediction based on a PWV measure.

In the linear and fully nonlinear model, flow velocity is additive to the classic pressure wave, as estimated by arterial material properties. This suggests that flow velocity correction may be important for cuff-less, non-invasive blood pressure measures. In Chapter 6, we examined the impact of systolic flow correction of a measure of PWV on systolic blood pressure prediction accuracy using data from two published *in vivo* studies. Both studies examined the relationship between PWV and blood pressure under pharmacological manipulation, one in mongrel dogs and the other in healthy adult males. Systolic flow correction of the measured PWV improves the R^2 correlation to systolic blood pressure from 0.81 to 0.92 for the mongrel dog study, and from 0.34 to 0.88 for the human subjects study. The key insight is the introduction of a flow-corrected *PWV* that improves correlation with systolic blood pressure over uncorrected *PWV*. For diastolic pressure prediction, *PWV* measured at the foot should be used. Flow-corrected *PWV* calculated using equation (6.5) allows correlation of *PWV* with SBP, with time point measurement at the diastolic foot of the waveform, a robust measurement point.

7.2 Future Work

The overriding goal of this work is to create a continuous noninvasive blood pressure system. While we have successfully advanced the science in this area, there are still exciting areas in which to work to achieve a truly wearable device with accurate calibration across all physiological states.

In the first linear model, we created and validated a model that shows that flow is additive to PWV and critical for SBP prediction. There are multiple approaches that show promise, such as the ballistocardiogram (BCG), impedance plethysmography (IPG), inductive sensing, RF techniques such as dual-antenna nanosecond pulse near-field sensing (NPNS), and micro-ultrasound sensors. As of this writing, none have been created in a wearable form factor and validated across various physiological states against a gold standard (Doppler ultrasound).

To create the complete microsystem capable of continuous monitoring of blood pressure, it is critical to accurately sense ECG, PEP, transit time, and aortic flow. ECG sensors are now commonly worn on the chest. Companies like MC10 have created systems that communicate the raw signal via Bluetooth low energy to handheld devices. Wrist-worn measures are also possible by having an electrode on the left wrist and touching the top plate electrode with one's right finger. Companies like AliveCor have demonstrated this technology on a handset. The final location that is ideal for a wearable is an ear-worn ECG [1]. This location is relatively free of motion artifacts and is ideal for BCG and PPG.

BCG is considered a noninvasive method to determine both aortic valve opening and stroke volume [1,2]. PEP is extracted as the time from the ECG R-wave to the J-wave of the BCG signal. Significant research is still required to understand this measure over various physiological states. Stroke volume can be estimated from the J-wave amplitude. A linearly proportional relationship between J-wave amplitudes and stroke volume is observed because the BCG recoil is directly related to the mass (or volume) of the pumped blood [1]. Stroke volume coupled with aortic radius and LVET would allow for flow velocity estimation.

A transit time measure is typically done from the aortic valve opening to a distal point on the body using a PPG sensor. He et al. successfully demonstrated an ear-mounted system that combined ECG, BCG, and PPG [1]. This approach allowed the extraction of transit time from the BCG J-wave to the foot of the PPG signal. Sola et al. have also demonstrated a transit time measure on the chest [3]. They used IPG to detect the aortic valve opening and a PPG sensor located at the aortic arch and brachiocephalic branch point.

The challenge is to develop a microsystem that can integrate the sensors and algorithms into a single device or devices that are accurate, discrete, and wearable. The location and system will depend heavily on the use case and frequency required for sampling the sensors. The system will then need to be refined and validated across numerous IRB studies.

For the first time in our history, wearable devices are collecting meaningful physiological data and digitally storing them to the Cloud. Our work has provided the

theoretical framework that may enable cuff-less noninvasive blood pressure (CNIBP) monitoring. This advancement is exciting because information like heart rate, ECG, CNIBP, activity level, and weight are continuously being stored for many people. The list of clinically meaningful and wearable sensors is constantly growing and improving. The ability to use this information for data mining, and look for health trends, I believe, will lead to medical breakthroughs never before possible. It is my hope that this will truly democratize medicine.

7.3 References

[1] D. He, Winokur E., Sodini C. , "An ear-worn vital signs monitor," *IEEE Trans Biomed Eng*, vol. 62, no. 11, Nov 2015.

[2] O'Rourke M., *McDonald's Blood Flow in Arteries: Theoretical, Experimental and Clinical Principles*, 5th ed. USA: Oxford University Press, 2005.

[3] Sola J., C. Sartori. et al. , "Noninvasive and Nonocclusive blood pressure estimation via a chest sensor," *IEEE Trans Biomed Eng*, vol. 60, no. 12, Dec 2013.

Appendix A: Noninvasive Blood Pressure – Phase I

IRB Study Proposal, for work conducted at Rochester General Hospital

Sreedevi Chennupati, MD (RGH), David Borkholder, PhD (RIT), Jeffrey Lillie, MS (RIT),

Stephen Silver, MD (RGH)

Social and Scientific Value

Hypertension is an important risk factor for cardiovascular diseases, such as cardiac failure, stroke and coronary artery disease. The incidence of hypertension in the United States was about 31% according to the NHANES data from 1999-2000.[1] The increase in prevalence beyond the expected rate is likely related to increasing incidence of obesity and the aging of the population.[1,2] The number of persons with hypertension worldwide was 972 million in 2000 and is anticipated to increase to 1.56 billion by the year 2025[3].

Adding to the burden of hypertension further are factors that confound office blood pressure readings, the data on which physicians mostly rely for making treatment decisions. White coat hypertension, where the office blood pressure readings are higher than ambulatory readings, is present in nearly 21% of the population.[4] Though overall, white coat hypertension causes less morbidity than sustained hypertension, it still needs to be treated, and may result in excess medication usage, given the erroneously high office blood pressure readings.[5]

Masked hypertension is a relatively new entity, where office blood pressure readings are deceptively low and ambulatory blood pressure readings are high. The incidence of masked hypertension is about 19% among adults when determined using self or ambulatory blood pressure readings. Their cardiovascular risk seems comparable to patients with recognized hypertension.[6] Failure to recognize the presence of masked hypertension may result in delayed diagnosis of hypertension and/or hypertension that is inadequately treated.

The gold standard for blood pressure measurement is the intra arterial measurement of blood pressure, whose invasive nature renders it impractical for routine use. The invention of aneroid sphygmomanometers has facilitated repetitive blood pressure measurements in ambulatory and outpatient settings. The current recommendation with this machine, is to check blood pressure in the same arm repeated at least twice, with additional readings if the difference is 5 mmHg or greater. Blood pressure readings are influenced by the condition of the machine and operator characteristics such as, but not limited to, proper method, end-digit preference and selective recording of desirable readings.[7] Optimal recording of blood pressure as described above is less often practiced than desired, given the time constraints of modern medical practice. A study in 2006 showed that aneroid blood readings were inaccurate when compared to intra arterial blood pressure readings performed at the same time, regardless of BMI.[8] An automated and more accurate method of blood pressure measurement that eliminates operator introduced error in measurement, and can be office based and ambulatory can potentially enhance treatment of hypertension.

There is a growing body of research on non-invasive, continuous blood pressure (BP) monitoring techniques that do not rely on an occlusive cuff. These techniques include external pressure sensors, near infrared imaging, ultrasound, and photoplethysmography (PPG). While all these methods have limitations, the photoplethysmographic (PPG) technique offers the greatest potential for true continuous monitoring of BP in a form that facilitates unrestricted ambulatory movement. The small

form factor is less cumbersome to carry, and facilitates use in outpatient and ambulatory settings. However, accuracy and calibration remain an issue.

Historically, the methods that used PPG for blood pressure measurement relied on the relationship between pressure and pulse wave velocity in the arteries. Frequently, the time period between the R-wave of an EKG recording and arrival of the resultant pulse at a peripheral point obtained via PPG are recorded. Based on this data, pulse wave velocity is calculated, and DBP and SBP are derived using a regression equation. The results from this approach show modest correlation to systolic blood pressure (SBP) but correlate poorly with diastolic blood pressure (DBP)[9].

It is hypothesized that this is due to

1. Difference in vascular compliance through out the vascular tree especially when using blood vessels of different caliber and physical characteristics

2. use of a single transit time measurement for determination of both SBP and DBP which are influenced and are dependent on different factors

3. and the inclusion of pre-ejection period (PEP) in the transit time calculation while this period precedes pulse transmission into the arteries. Since the fundamental equations are based on pulse wave velocity in the arteries, inclusion of PEP represents an error term.

An alternate approach utilizes two PPG measurements on a single artery (most commonly the radial artery). However, variable sensor coupling impacts the shape of the waveform there by making consistent measurement of time difference difficult.

The proposed work will examine two approaches to mitigate the challenges described above with non-invasive sensors. Data will be simultaneously collected for both approaches with occlusive-cuff BP measurements collected for comparison.

Approach 1: The Electrocardiogram (EKG), phonocardiogram (recording of heart sounds), and ear PPG will be used to allow determination of PEP and the true transit time. This true transit time will be correlated with DBP, while SBP will be correlated with PEP.

Approach 2: PPG signals will be measured on both ears, and waveforms recorded. The time difference between arrivals of the foot of the waveform at both ears will be correlated to DBP; and the time difference between the arrivals of the peak of the waveform at both ears will be correlated to SBP. This approach fundamentally relies on the fact that from the origin of the right brachiocephalic artery, the distance to left ear (via the aortic arch, left common carotid and then left external carotid arteries) is greater than the distance to right ear from the heart (via the brachiocephalic and right common carotid and then external carotid arteries) which then results in differences in pulse transit time, assuming the pulse velocity is the same in both branches. Since the pulse wave velocity is related to arterial elasticity, which in turn is correlated with pressure in the system, the time differences at the foot and peak of the PPG waveforms can be used to estimate DBP and SBP respectively. It may allow for beat to beat pressure readings to be accurately recorded.

During both approaches, participants will be asked to assume different positions, and recordings using the sphygmomanometer and PPG based method will be obtained in all these positions. The positions include—supine, head of bed elevated at 45 degrees, sitting and standing.

Public Dissemination of Trial Results

The results may be disseminated in summary form through conferences and/or journal publications.

Objective of the Study

This study will provide adequate data from a clinical population for preliminary validation of the two approaches described above. Subsequent work will involve development of a microelectrode based system with wireless sensor nodes for non-invasive, continuous, ambulatory monitoring of blood pressure without the use of an occlusive cuff.

Outcomes

Study results will be compared to blood pressure measures obtained with an aneroid sphygmomanometer and/or intra arterial measurements when available. BP accuracy will be compared against the Association for the Advancement of Medical Instrumentation (AAMI) standards for noninvasive arterial blood pressure measurement (maximal mean difference and standard deviation from at least 85 patients should not exceed 5±8 mmHg from a reference method).

Sample Size

Sample size was chosen to provide a reasonably large dataset for testing the current concept, as this is a pilot study, meant to calibrate the PPG based device. The sample size is not driven by statistics, as there is no base line data available to estimate variance.

We expect to have 3 groups of 50 participants each.

Group I: To be recruited from an outpatient setting from the Rochester General Health System (RGHS).

Group II: To be recruited from those scheduled for a cardiac stress test either at inpatient or outpatient units belonging to the RGHS.

Group III: To be recruited from those scheduled to have a coronary angiogram at the Rochester General Hospital.

Randomization – Sequence Generation

No randomization is required.

Randomization – Allocation Concealment

No randomization is required.

Randomization Implementation

No randomization is required.

Blinding

Blinding is not applicable to this study.

Statistical Methods

Group comparisons are not planned at this time since this is not the aim of the proposed study.

Fair Subject Selection – Recruitment of Participants

Participants will be recruited from outpatient or inpatient settings belonging to RGHS.

Exclusion criteria

Less than 18 years of age, pregnancy, severe cardiac disease, severe COPD, severe peripheral vascular disease, inability to tolerate change in position as described above, inability to follow instructions in English, impaired cognitive or functional status.

Favorable Risk-Benefit Ratio – Interventions Offering the Prospect of Health Related Benefit

Participants receive no direct benefit from participating in the study. But, an easier and accurate method of blood pressure measurement method may result in better BP control and resultant benefits accrue to society in general.

Interventions Performed Solely to Answer the Research Questions

1. Collection of EKG, phonocardiogram, two ear PPG, and cuff-based BP from individuals participating in the study in an out patient, non-stress test related setting. This data may be obtained on two separate occasions, and in different body positions as mentioned earlier in the protocol. This data is required to test the proposed approach for non-invasive, cuff-less blood pressure monitoring.
2. Collection of two ear PPG, EKG and phonocardiogram (wherever possible) data on patients undergoing cardiology stress testing. This data is required to test the proposed approach for non-invasive, cuff-less blood pressure monitoring under exercise conditions.

3. Collection of two-ear PPG, EKG and phonocardiogram (wherever possible) data on patients undergoing cardiac catheterization procedures. This data is required to test the proposed approach for non-invasive, cuff-less blood pressure monitoring.

Clinical Balance

There is no intervention performed as part of the study.

Respect for Potential and Enrolled Subjects – Trial Monitoring Plan

Not applicable, as the study involves only obtaining measurements and does not involve any intervention, medical or surgical.

Communication of Protocol Changes and Trial Monitoring

Not applicable, as the study involves only obtaining measurements and does not involve any intervention, medical or surgical.

References:

1. The burden of adult hypertension in the United States 1999 to 2000: a rising tide. Fields LE, Burt VL, Cutler JA, Hughes J, Roccella EJ, Sorlie, P. Hypertension. 2004 Oct; 44 (4): 398-404.
2. Trends in hypertension prevalence, awareness, treatment, and control rates in United States adults between 1988-1994 and 1999-2004. Cutler JA, Sorlie PD, Wolz M, Thom T, Fields LE, Roccella EJ. Hypertension 2008 Nov; 52 (5):818-827.
3. Global burden of hypertension: analysis of worldwide data. Kearney PM, Whelton M, Reynolds K, et al. *Lancet* 2005; 365:217-223.
4. How common is white coat hypertension? Pickering JG, James GD, Boddie C, Harshfield GA, Blank S, Laragh JH. JAMA 1988 Jan 8; 259(2): 225-228.
5. White coat hypertension: a clinical review. Celis H, Fagard RH. Eur J Intern Med 2005; 15: 348-357.
6. Prevalence, causes and consequences of masked hypertension: A meta-analysis. Werberk WJ, Kessels AGH, deLeeuw PW. Am J Hyperten. 2008; 21:969-975.
7. Does this patient have hypertension? How to measure blood pressure. Reeves RA. JAMA Apirl 19, 1995; Vol 273, No.15 pp1211-1218.
8. Comparison of oscillometric and intraarterial systolic and diastolic blood pressures in lean, overweight, and obese patients. Umana E, Ahmed W, Fraley MA, Alpert MA. Angiology. 2006, Jan-Feb; 57(1):41-45
9. Pulse transit time measured from the ECG: an unreliable marker of beat-to-beat blood pressure. Payne RA, et al. J Appl Physiol 2006; 100:136-41.

Appendix B: Noninvasive Blood Pressure Measurement on a Stationary Recumbent Bicycle

IRB Proposal, for work conducted at Rochester Institute of Technology

Social and Scientific Value

Hypertension is an important risk factor for cardiovascular diseases, such as cardiac failure, stroke and coronary artery disease. The incidence of hypertension in the United States was about 31% according to the NHANES data from 1999-2000.[1] The increase in prevalence beyond the expected rate is likely related to increasing incidence of obesity and the aging of the population.[1,2] The number of persons with hypertension worldwide was 972 million in 2000 and is anticipated to increase to 1.56 billion by the year 2025[3].

Adding to the burden of hypertension further are factors that confound office blood pressure readings, the data on which physicians mostly rely for making treatment decisions. White coat hypertension, where the office blood pressure readings are higher than ambulatory readings, is present in nearly 21% of the population.[4] Though overall, white coat hypertension causes less morbidity than sustained hypertension, it still needs to be treated, and may result in excess medication usage, given the erroneously high office blood pressure readings.[5]

Masked hypertension is a relatively new entity, where office blood pressure readings are deceptively low and ambulatory blood pressure readings are high. The incidence of masked hypertension is about 19% among adults when determined using self or ambulatory blood pressure readings. Their cardiovascular risk seems comparable to patients with recognized hypertension.[6] Failure to recognize the presence of masked hypertension may result in delayed diagnosis of hypertension and/or hypertension that is inadequately treated.

The gold standard for blood pressure measurement is the intra arterial measurement of blood pressure, whose invasive nature renders it impractical for routine use. The invention of aneroid sphygmomanometers has facilitated repetitive blood pressure measurements in ambulatory and outpatient settings. The current recommendation with this machine, is to check blood pressure in the same arm repeated at least twice, with additional readings if the difference is 5 mmHg or greater. Blood pressure readings are influenced by the condition of the machine and operator characteristics such as, but not limited to, proper method, end-digit preference and selective recording of desirable readings.[7] Optimal recording of blood pressure as described above is less often practiced than desired, given the time constraints of modern medical practice. A study in 2006 showed that aneroid blood readings were inaccurate when compared to intra arterial blood pressure readings performed at the same time, regardless of BMI.[8] An automated and more accurate method of blood pressure measurement that eliminates operator introduced error in measurement, and can be office based and ambulatory can potentially enhance treatment of hypertension.

There is a growing body of research on non-invasive, continuous blood pressure (BP) monitoring techniques that do not rely on an occlusive cuff. These techniques include external pressure sensors, near infrared imaging, ultrasound, and photoplethysmography (PPG). While all these methods have limitations, the photoplethysmographic (PPG) technique offers the greatest potential for true continuous monitoring of BP in a form that facilitates unrestricted ambulatory movement. The small

form factor is less cumbersome to carry, and facilitates use in outpatient and ambulatory settings. However, accuracy and calibration remain an issue.

Historically, the methods that used PPG for blood pressure measurement relied on the relationship between pressure and pulse wave velocity in the arteries. Frequently, the time period between the R-wave of an EKG recording and arrival of the resultant pulse at a peripheral point obtained via PPG are recorded. Based on this data, pulse wave velocity is calculated, and DBP and SBP are derived using a regression equation. The results from this approach show modest correlation to systolic blood pressure (SBP) but correlate poorly with diastolic blood pressure (DBP)[9].

The proposed work will examine an approach to mitigate the challenges described above with non-invasive sensors. Data will be collected necessary to measure BP using the new approach and compared with occlusive-cuff BP measurements.

During this approach, participants will be asked to ride a stationary recumbent bicycle for 35 minutes with the difficulty level increased every 5 minutes for the first 25 minutes, followed by 2 cool down steps where the level is decreased. Recordings using the sphygmomanometer and PPG based method will be obtained each time after 3 minutes at a particular resistance level. The participants will remain on the stationary recumbent bicycle for the complete length of the test, approximately 45 minutes. Participants will be asked back to repeat the study in approximately 1 week.

Resistance level 1 feels like you are riding on a flat surface with no head wind. Resistance level 5 feels like you are riding up a moderate incline or into a 15-20 MPH head wind. Resistance levels 2-4 are linearly increasing in difficulty between these two extremes. In general it will cause your heart rate to increase, as it would during moderate aerobic exercise. You should be able to carry on a conversation at all of the levels of this testing.

Public Dissemination of Trial Results

The results may be disseminated in summary form through conferences and/or journal publications.

Objective of the Study

This study will provide adequate data from a clinical population for preliminary validation of the approach described above. Subsequent work will involve development of a microelectrode based system with wireless sensor nodes for non-invasive, continuous, ambulatory monitoring of blood pressure without the use of an occlusive cuff.

Outcomes

Study results will be compared to blood pressure measures obtained with an aneroid sphygmomanometer. BP accuracy will be compared against the Association for the Advancement of Medical Instrumentation (AAMI) standards for noninvasive arterial blood pressure measurement (maximal mean difference and standard deviation from at least 85 patients should not exceed 5±8 mmHg from a reference method).

Sample Size

Sample size was chosen to provide a reasonably large dataset for testing the current concept, as this is a pilot study, meant to calibrate the PPG based device. The sample size is not driven by statistics, as there is no base line data available to estimate variance. We expect to have 1 group of 30 participants. Group I: To be recruited from Rochester Institute of Technology students or faculty. (RIT).

Randomization – Sequence Generation

No randomization is required.

Randomization – Allocation Concealment

No randomization is required.

Randomization Implementation

No randomization is required.

Blinding

Blinding is not applicable to this study.

Statistical Methods

Group comparisons are not planned at this time since this is not the aim of the proposed study.

Fair Subject Selection – Recruitment of Participants

Participants will be recruited from students or faculty on the Rochester Institute of Technology Campus

Exclusion criteria

Less than 18 years of age, pregnancy, severe cardiac disease, severe COPD, severe peripheral vascular disease, inability to tolerate change in position as described above, inability to follow instructions in English, impaired cognitive or functional status.

Favorable Risk-Benefit Ratio – Interventions Offering the Prospect of Health Related Benefit

Participants receive no direct benefit from participating in the study. But, an easier and accurate method of blood pressure measurement method may result in better BP control and resultant benefits accrue to society in general.

Interventions Performed Solely to Answer the Research Questions

4. Collection of EKG, phonocardiogram, two ear PPG, and cuff-based BP from individuals participating in the study in an out patient, non-stress test related setting. This data may be obtained on two separate occasions, and in different body positions as mentioned earlier in the protocol. This data is required to test the proposed approach for non-invasive, cuff-less blood pressure monitoring.

Clinical Balance

There is no intervention performed as part of the study.

Respect for Potential and Enrolled Subjects – Trial Monitoring Plan

Not applicable, as the study involves only obtaining measurements and does not involve any intervention, medical or surgical.

Communication of Protocol Changes and Trial Monitoring

Not applicable, as the study involves only obtaining measurements and does not involve any intervention, medical or surgical.

Monitoring Equipment Approved for Use with Humans

The biopac system will be used to measure PPG and ECG on the subjects. Biopac systems provided an EC declaration of conformity with the equipment.

References:

1. The burden of adult hypertension in the United States 1999 to 2000: a rising tide. Fields LE, Burt VL, Cutler JA, Hughes J, Roccella EJ, Sorlie, P. Hypertension. 2004 Oct; 44 (4): 398-404.
2. Trends in hypertension prevalence, awareness, treatment, and control rates in United States adults between 1988-1994 and 1999-2004. Cutler JA, Sorlie PD, Wolz M, Thom T, Fields LE, Roccella EJ. Hypertension 2008 Nov; 52 (5):818-827.
3. Global burden of hypertension: analysis of worldwide data. Kearney PM, Whelton M, Reynolds K, et al. *Lancet* 2005; 365:217-223.
4. How common is white coat hypertension? Pickering JG, James GD, Boddie C, Harshfield GA, Blank S, Laragh JH. JAMA 1988 Jan 8; 259(2): 225-228.
5. White coat hypertension: a clinical review. Celis H, Fagard RH. Eur J Intern Med 2005; 15: 348-357.
6. Prevalence, causes and consequences of masked hypertension: A meta-analysis. Werberk WJ, Kessels AGH, deLeeuw PW. Am J Hyperten. 2008; 21:969-975.
7. Does this patient have hypertension? How to measure blood pressure. Reeves RA. JAMA Apirl 19, 1995; Vol 273, No.15 pp1211-1218.
8. Comparison of oscillometric and intraarterial systolic and diastolic blood pressures in lean, overweight, and obese patients. Umana E, Ahmed W, Fraley MA, Alpert MA. Angiology. 2006, Jan-Feb; 57(1):41-45
9. Pulse transit time measured from the ECG: an unreliable marker of beat-to-beat blood pressure. Payne RA, et al. J Appl Physiol 2006; 100:136-41